An Investigation of Notch-Dependent Expression of the Drosophila gene *hindsight* using CRISPR/Cas9 Genome Editing

by

Richard Do

A thesis
presented to the University of Waterloo
in fulfillment of the
thesis requirement for the degree of
Doctor of Philosophy
in
Biology

Waterloo, Ontario, Canada, 2026

© Richard Do 2026

Examining Committee Membership

The following served on the Examining Committee for this thesis. The decision of the Examining Committee is by majority vote.

External Examiner	Dr. Andrew Swan Associate Professor, Department of Biomedical Sciences, University of Windsor
Supervisor(s)	Dr. Bruce Reed Associate Professor, Department of Biology, University of Waterloo
Internal Member	Dr. Mungo Marsden Associate Professor Emerit and Adjunct Professor, Department of Biology, University of Waterloo
Internal Member	Dr. Bernard Duncker Professor, Department of Biology, University of Waterloo
Internal-external Member	Dr. Joe Quadrilatero Professor, Department of Kinesiology and Health Sciences, University of Waterloo

AUTHOR'S DECLARATION

I hereby declare that I am the sole author of this thesis. This is a true copy of the thesis, including any required final revisions, as accepted by my examiners.

I understand that my thesis may be made electronically available to the public.

Abstract

The Drosophila gene *hindsight* (*hnt*) encodes a large (1894 AAs) C_2H_2 zinc-finger transcription factor that is expressed in a tissue specific manner and is essential for Drosophila development. Also known as *pebbled, hnt* is a functional homolog of the mammalian gene *Ras Responsive Element Binding Protein-1* (*RREB-1*), the mis-regulation of which is associated with several types of cancer in humans. In some contexts, *hnt* is transcriptionally upregulated by Notch-dependent activation of the transcription factor Suppressor of Hairless (Su(H)). Given the broad developmental expression of *hnt* and given that *hnt* has been identified as a direct target of Notch signalling in specific contexts, additional contexts in which *hnt* functions as a downstream target of Notch signalling may represent novel models for studying Ras-related human pathologies.

In order to investigate novel *in vivo* contexts in which *hnt* functions downstream of Notch activation, CRISPR/Cas9 genome editing was used to dissect the extensive 5' regulatory region of the *hnt* gene, which is ~40 kb in size, with the aim of further defining and characterizing Notch-dependent cis-regulatory elements (NREs). Using a CRISPR/Cas9 knockout technique based on homology-directed repair (HDR), four transgenic mutant lines were recovered, each associated with a ~5 kb deletion within the *hnt* upstream regulatory region. Each deletion line was designed to remove a putative NRE and was marked by a *3xP3-DsRed* insertion generated by HDR. Unexpectedly, each insertion/deletion line was found to function as an enhancer trap - showing DsRed expression in subsets of the endogenous *hnt* expression pattern. Only one of these four deletions, named $hnt^{\Delta N4}$, which is located ~38 kb upstream of the transcription start site of

hnt, was associated with a phenotype. $hnt^{\Delta N4}$ mutants complete embryogenesis but display defects in tracheal development, including collapse of the dorsal trunks, ultimately resulting in early larval lethality. In addition, further analysis of the $hnt^{\Delta N4}$ mutant tracheal phenotype revealed a disorganization of F-actin and consequential defects in taenidial fold formation and patterning.

hnt expression during embryogenesis was characterized using immunostaining as well as reporter gene expression and the newly generated DsRed enhancer trap lines. This analysis revealed a distinct up-regulation of *hnt* expression in a subset of tracheal cells referred to as "transverse connection junctional cells" (TCJs), as well as a specific cell type of the PNS. This elevated expression of *hnt* in the TCJs and PNS cells was abrogated in the $hnt^{\Delta N4}$ mutant. Changes in *hnt* expression were also observed in embryos in which Notch signalling was either reduced or activated. *hnt* expression and tracheal phenotypes were also observed in a conditional N^{ts} background, and a shift to restrictive conditions following initial tracheal development resulted in a striking phenocopy of the $hnt^{\Delta N4}$ mutant, including reduced TCJ and PNS cell expression and tracheal phenotypes.

The Su(H) consensus binding sequence that is deleted in the $hnt^{\Delta N4}$ mutant was also targeted using CRISPR/Cas9 mutagenesis, which involves error-prone non-homologous end-joining (NHEJ). While not lethal, mutations recovered by NHEJ showed that deletions specific to this consensus Su(H) sequence are associated with defective tracheal development in late-stage embryos and some reduced *hnt* expression, although these effects occurred with reduced penetrance relative to the $hnt^{\Delta N4}$ mutant.

Overall, this work reinforces the concept that the gene *hnt* is a target of Notch signalling during Drosophila development. In this work, I find the response to Notch signalling involves increased *hnt* expression in the developing tracheal system, and this is most evident for one particular cell type – the TCJ cells. This Notch-dependent up-regulation of *hnt* expression may be required for organization and structure of tracheal cells through an indirect downstream regulation or remodelling of the actin cytoskeleton.

Acknowledgments

Many thanks to my supervisor Dr. Bruce Reed for his support and guidance over the years and for encouraging the growth of my professional skills. I would like to thank the members of my advisory committee, Dr. Mungo Marsden and Dr. Bernard Duncker, for their valuable insight and both Dr. Joe Quadrilatero and Dr. Andrew Swan for participating as examiners of my thesis.

I am incredibly appreciative of the support of my friends and family, without which, I would not be where I am today. Finally, to my fiancée Vivian - thank you for your unwavering support, constant companionship, endless laughs, and bringing a deeper meaning to my life.

Table of Contents

Examining Committee Membership ii

AUTHOR'S DECLARATION iii

Abstract iv

Acknowledgments vii

List of Figures xi

List of Tables xii

List of Abbreviations xiii

Chapter One: General Introduction 1

1.1 Hindsight 2

1.1.1 Developmental functions of Hnt 3

1.2 RREB-1 6

1.3 Notch 7

1.4 Roles of Hnt downstream of Notch 8

1.5 Developing Tracheal System 11

1.5.1 Branching 12

1.5.2 Tracheal Cell Fusion and Organization 16

1.5.3 Cuticle and Taenidial Folds 20

1.5.4 Functions of Notch and Hnt in the Developing Trachea 21

1.6 CRISPR/Cas9 Mutagenesis 25

1.7 Research Objectives 27

1.8 Thesis Overview 30

Chapter Two: Materials and Methods 31

2.1 Generation of CRISPR/Cas9 genome edited strains 32

2.1.1 Identifying suitable CRISPR/Cas9 targets 32

2.1.2 Construction of gRNA expression vectors for injection 32

2.1.3 Construction of homology-directed repair donor vectors for injection 33

2.1.4 CRISPR mix microinjections 35

2.1.5 CRISPR mutated stock genetics and screening 35
2.1.5.1 ΔNRE deletion mutants 35
2.1.5.2 Co-CRISPR NRE-4 Su(H) mutants 36
2.2 Primers and Oligonucleotides 37
2.3 Genomic DNA extraction and PCR screening of putative CRISPR alleles 42
2.4 Long-range PCR 43
2.5 Embryo Collection & Dechorionation 44
2.6 Embryonic Lethality & Viability Assays 44
2.7 Anti-Hnt immunostaining & rhodamine phalloidin staining 45
2.8 N^{ts} Temperature Shift Protocols 47
2.9 Imaging 47
2.9.1 Embryo Hanging Drop Preparation 48
2.9.2 Larvae Immobilization 49
2.9.3 Larvae Dissections 49
2.9.4 Pupal Case Dissections 50
2.10 Fly Stocks 51
Chapter Three: Generation, Verification, and Initial Characterization of CRISPR/Cas9 Mutants 54
3.1 Overview 55
3.2 Results 56
3.2.1 Generation of CRISPR/Cas9 mutated *hnt* stocks 56
3.2.2 PCR verification of ΔNRE *hnt* stocks 60
3.2.3 *3xP3-DsRed* insertions function as enhancer traps in the *hnt* regulatory region 63
3.2.4 Spurious *3xP3-DsRed* insertions are expressed in typical *hnt* expression patterns 66
3.2.5 Complementation test cross of $hnt^{\Delta N4}$ allele to hnt^{XE81} allele 69
3.2.6 $hnt^{\Delta N4}$ phenotype is not associated with embryonic lethality 72
3.2.7 $hnt^{\Delta N4}$ mutants exhibit lethal larval tracheal phenotypes 77
Chapter Four: In the Context of the Developing Tracheal System, Hnt is Required for Subcellular Organization of Actin and is Downstream of Notch Signalling 81
4.1 Overview 82

4.2 Results 84
4.2.1 *Peb1* gene reporter constructs are expressed in the developing tracheal system and a single cell type of the PNS 84
4.2.2 *Peb1* and NRE-4 sequence contain specific tracheal enhancer elements 89
4.2.3 NRE-4 deletion reduces embryonic expression of Hnt in the developing trachea 93
4.2.4 *hnt* is required for apical organization of F-actin in the DT 96
4.2.5 Increased actin expression partially rescues $hnt^{\Delta N4}$ tracheal phenotypes 99
4.2.6 NRE-4 Su(H) consensus binding sequence mutation causes tracheal phenotypes 103
4.2.7 Notch signalling regulates *hnt* expression in some cell types 111
Chapter Five: Discussion and Future Directions 121
5.1 Overview 122
5.2 DsRed insertions into the regulatory region of *hnt* function as tissue specific enhancer traps 124
5.2.1 Spurious DsRed insertions are also expressed in *hnt* patterns 125
5.3 Specific enhancer elements map to NRE-4 sequence 127
5.4 Hnt is required for actin organization in the embryonic trachea 129
5.4.1 Increased expression of actin partially rescues $hnt^{\Delta N4}$ actin phenotypes 131
5.5 Hnt operates downstream of Notch activity 133
5.5.1 *hnt* mechanisms downstream of Notch signalling in the developing trachea 135
5.5.2 Su(H) likely interacts with other enhancer elements to regulate *hnt* expression in the trachea 137
5.5.3 N^{ts} disruption of Notch activity generates similar tracheal *hnt* phenotypes 139
5.5.4 TCJ cells and PNS cells are sites of robust Notch-dependent *hnt* expression 140
5.5.4.1 PNS cell with strong expression of *hnt* is likely an extrasensory organ socket cell 142
5.6 Conclusions 144
5.7 Future Directions 145
References 147
Appendices 155

List of Figures

Figure 1.1 Embryonic tracheal system. 15

Figure 1.2 Tracheal cell architecture. 19

Figure 1.3 Notch responsive element candidates in the *hnt* regulatory region. 29

Figure 3.1 CRISPR/Cas9 deletion mutant generation. 58

Figure 3.2 CRISPR/Cas9 ΔNRE mutant verification. 62

Figure 3.3 DsRed insertions into the *hnt* regulatory region function as enhancer traps. 65

Figure 3.4 DsRed expression patterns of spurious CRISPR mutations. 68

Figure 3.5 $hnt^{\Delta N4}$ fails to complement hnt^{XE81}. 71

Figure 3.6 Punnett square diagrams of crosses used to identify $hnt^{\Delta N4}$ mutants. 74

Figure 3.7 Embryonic Lethality and Viability Assay of CRISPR/Cas9 induced mutants. 76

Figure 3.8 $hnt^{\Delta N4}$ mutants exhibit lethal tracheal phenotypes. 80

Figure 4.1 Embryonic expression of the *Peb1* reporter construct. 87

Figure 4.2 NRE-4 DsRed insert does not co-express with *Peb1-eGFP* in TCJ cells, single PNS cells, and the posterior DT. 92

Figure 4.3 $hnt^{\Delta N4}$ embryos exhibit reduced expression levels of Hnt. 95

Figure 4.4 The late-stage 17 $hnt^{\Delta N4}$ mutant tracheal system displays a disorganized F-actin phenotype. 98

Figure 4.5 Increased expression of actin5C partially rescues the $hnt^{\Delta N4}$ phenotype. 102

Figure 4.6 $hnt^{N4\text{-}F42.2}$ embryos exhibit variable levels of Hnt expression. 107

Figure 4.7 Direct mutation of NRE-4 causes visible tracheal phenotypes. 110

Figure 4.8 TCJ cells and PNS cells are sites of Notch activity. 113

Figure 4.9 *Peb1* reporter expression is reduced in a Notch loss-of-function background and is increased in a Notch gain-of-function condition. 116

Figure 4.10 A subset of embryonic expression of Hnt is downstream of Notch signalling. 120

List of Tables

Table 2.1 PCR primers used to screen genomic DNA of *y*^{1} *w*^{1118}*; attP2{nos-Cas9}/TM6C, Sb, Tb* for SNPs. 37

Table 2.2 Oligonucleotides used to generate gRNA targets. 38

Table 2.3 PCR primers used to clone homology arms. 39

Table 2.4. PCR primers used to verify homology arm cloning into pDsRed-attP2. 40

Table 2.5 PCR primers used to verify CRISPR/Cas9 mutant alleles. 40

Table 2.6 PCR primers used for long-range PCR amplification of *hnt* regulatory sequence. 41

Table 2.7 PCR primers used to screen NRE-4 Su(H) sites in prospective indel mutants 41

Table 2.8 List of Drosophila stocks used in this study and their sources. 51

List of Abbreviations

AS	amnioserosa
BO	Bolwig's organ
Cas	CRISPR associated
ChIP	chromatin immunoprecipitation
CNS	central nervous system
CRISPR	clustered regularly interspaced short palindromic repeats
DB	dorsal branch
DIC	differential interference contrast
DT	dorsal trunk
EGFR	epidermal growth factor receptor
F-actin	filamentous actin
GB	ganglionic branch
GBR	germ-band retraction
HDR	homology-directed repair
JNK	Jun-kinase
LB	lysogeny broth
LHA	left homology arm
LT	lateral trunk
NGS	normal goat serum
NHEJ	non-homologous end-joining
NICD	Notch intracellular domain
NRE	Notch responsive elements
OE	oenocyte
PAM	protospacer adjacent motif
PBS	phosphate buffered saline
PCR	polymerase chain reaction
PNS	peripheral nervous system
PS	posterior spiracle
RHA	right homology arm
SNP	single nucleotide polymorphism
SOP	sensory organ precursor
TC	transverse connective
TCJ	transverse connective junction
TSS	transcription start site
UAS	upstream activating sequence
VB	visceral branch

Chapter One:

General Introduction

1.1 Hindsight

The gene *hindsight* (*hnt*) - also known as *pebbled* (*peb*) - encodes a transcription factor that contains 14 C_2H_2 zinc finger domains and is located on the *X*-chromosome of *Drosophila melanogaster* (Yip et al., 1997). During embryogenesis, *hnt* is expressed in several different tissues having widely different functions. In addition to the amnioserosa (AS), where *hnt* is required for the morphogenetic process of germ band retraction and to prevent premature cell death of this extraembryonic tissue, embryonic tissues that express *hnt* include the anterior and posterior midgut primordia, the developing tracheal system, clusters of cells known as oenocytes (hepatocyte-like cells involved in lipid metabolism), and components of the peripheral nervous system (PNS) (Yip et al., 1997; Wilk et al., 2000; Pickup et al., 2002). In adult Drosophila *hnt* is also widely expressed in several disparate tissues including absorptive enterocytes of the midgut, sensory organ precursor cells (SOPs) of both micro- and macrochaetae, ovarian follicle-cells and a subset of migratory follicle cells known as border cells. In addition, *hnt* is expressed in adult glutamatergic sensory neurons, reproductive gland secretory cells in the ovary, and spermathecae (Baechler et al., 2016; Reeves & Posakony, 2005; Sun & Deng, 2007; Deady et al., 2017; Farley et al., 2018; Sun & Spradling 2013).

As a transcription factor, *hnt* is expected to target and regulate the expression of specific genes. Anti-Hnt immunohistochemical staining of the larval salivary gland polytene chromosomes, a technique that can be used to identify transcription factor binding sites, revealed over 50 potential Hnt binding sites; these results include a strong signal at the cytological location of the *hnt* gene itself (4C10), suggesting that *hnt* is self-targeting, potentially undergoing negative autoregulation (Ming et al., 2013). In addition, ChiP-Seq

analysis of *hnt* in the GM2 embryonic cell line revealed several target genes potentially regulated by *hnt*. However, with the exception of *nvy,* many of these potential targets have remained unexplored at the molecular level (Farley et al., 2018; Ming et al., 2013). Likewise, many candidate genetic pathways and interactors of *hnt* were identified through an autosomal-dosage modifier screen using the hypomorphic alleles hnt^{308} and hnt^{peb}. This screen identified over 60 loci that showed genetic interactions with *hnt*; these loci can be classified into groups of genes associated with several biological functions, including transcriptional regulation, actin binding, signal transduction, and extracellular matrix composition and function (Wilk et al., 2004).

1.1.1 Developmental functions of Hnt

hnt is required for maintenance of epithelial integrity and microfilament organization in several contexts, including the extraembryonic amnioserosa, the embryonic tracheal system, and the R cells (photoreceptor associated neurons) of the developing ommatidia in the pupal eye imaginal disc (Reed et al., 2004; Wilk et al., 2000; Pickup et al., 2002; Oliva et al., 2015). For example, in the developing trachea, Hnt is expressed in all embryonic tracheal cells and *hnt* mutant embryos exhibit loss of epithelial integrity in the trachea, resulting in the aberrant formation of epithelial sacs (Wilk et al., 2000).

Hnt is also expressed in the larval eye imaginal disc, where it promotes apical F-actin organization in the eight presumptive R cells of each of the 750-800 ommatidial units within the developing compound eye. *hnt* mutant R cells exhibit reduced F-actin in their apical tips and, based on mosaic analysis, will delaminate if 5/8 R cells in a cluster fail to

express *hnt*, demonstrating an inability to meet a threshold of required apical F-actin to establish sufficient contact with the overlaying cone cells (Pickup et al., 2002). In addition, *hnt* is required to properly guide photoreceptor axons by regulating downstream transcriptional targets involved in regulating actin cytoskeleton organization, such as the filamin homolog *jitterbug* (*jbug*) (Oliva et al., 2015; Oliva & Sierralta, 2010). *hnt* mutant photoreceptor axons display guidance defects, migrating in improper directions and forming ectopic bundles on the medulla surface, indicating a defect in axon repulsion. In contrast, photoreceptor axons having increased levels of Hnt erroneously overshoot their normal target and extend into the wrong medulla layer and sometimes lobula (Oliva & Sierralta, 2010). In this context, *jbug* function is required downstream of Hnt to properly guide photoreceptor axon targeting (Oliva et al., 2015).

In the extra-embryonic membrane known as the amnioserosa, Hnt is required for the downregulation of Jun-kinase (JNK) signalling; and as mentioned above, strong (nullomorphic) *hnt* mutants fail to complete the morphogenetic process of germ band retraction (GBR). Weaker (hypomorphic) *hnt* mutants, however, can complete GBR but fail in the subsequent and related morphogenetic process of dorsal closure. JNK signalling is active in the amnioserosa and the dorsal leading edge prior to dorsal closure where it promotes assembly of focal adhesion complexes in adjacent epithelial cells (Reed et al., 2001). In this model, JNK signalling must be downregulated in the amnioserosa by Hnt, and reduced Hnt function results in persistent JNK signalling and defective focal complexes in the leading edge – ultimately resulting in dorsal closure defects (Reed et al. 2001).

In oogenesis, Hnt also plays a role in regulating levels of adhesion proteins in the follicle cells of developing egg chambers. In addition, Hnt is expressed in a subset of migratory follicle cells known as border cells, which play a role in the formation of the structure known as the micropyle. In a genetic mosaic situation, anterior follicle cell *hnt* mutant clonal patches show increased expression of the cell adhesion molecules Armadillo (β-catenin) and DE-cadherin. These *hnt* mutant clonal patches of follicle cells also fail to undergo typical movements, indicating that *hnt* is required to reduce cell-cell adhesion and is required for border cell motility by attenuating adhesion protein levels (Melani et al., 2008).

hnt has been linked to several cell signalling pathways in varying contexts. These include promoting Epidermal Growth Factor Receptor (EGFR) signaling and the downregulation of the JNK signaling pathway both during embryogenesis and in the developing pupal eye (Kim et al., 2020; Reed et al., 2001; Pickup et al., 2002). In addition, *hnt* regulates the differentiation and specification of stem cells in the developing midgut through both the Notch and EGFR signaling pathways (Baechler et al., 2016). Based on these findings, it has been suggested that the specific function of *hnt* is highly context dependent – but it may serve a general function in facilitating cross-talk between these major signaling pathways.

Despite a wealth of information regarding tissue expression, there is little information regarding a general function for *hnt*, and how it regulates cellular and developmental processes during embryonic development as a transcription factor (Oliva et al., 2015; Pickup et al., 2009; Sun & Deng, 2007; Wilk et al., 2000).

1.2 RREB-1

Ras Responsive Element Binding protein-1 (RREB-1) is the mammalian homologue of *hnt* and is a known downstream effector of Ras/MAPK signalling. Like Hnt, RREB-1 can function as either a transcriptional activator or repressor (Liu et al., 2009; Chen et al., 2010; Kent et al., 2010; Thiagalingam et al., 1996; reviewed in Deng et al., 2020). The consensus binding motif sequence of *hnt* is very similar to that of RREB-1 (Ming et al., 2013; Thiagalingam et al., 1996), and the expression of RREB-1 can rescue both GBR failure and axon death defects in *hnt* mutants, suggesting that there is functional conservation between Hnt and RREB-1 (Ming et al., 2013; Farley et al., 2018). Additionally, like *hnt*, RREB-1 has also been implicated in regulating cell adhesion. In embryonic mouse epiblast cells, RREB-1 acts as a repressor of several different genes related to cytoskeletal actin and adherens junctions. Knockout of RREB-1 causes cardiovascular defects, resulting in ectopic punctate organization of actin, E-cadherin, and β-catenin in epiblast cells (Morgani et al., 2021).

RREB-1 has been linked to different human diseases such as pancreatic, thyroid, and colorectal cancer (Kent et al., 2013; Zhang et al., 2003; Zou et al., 2011). Drosophila is an ideal *in vivo* model system to study the transcriptional regulation of *hnt*, and any discoveries made may be relevant to understanding the relationship of RREB-1 to human diseases. Overall, a better understanding of the regulation and function of *hnt* may shed light on the regulation and role of RREB-1 in the onset and progression of specific types of cancer in humans – ultimately with the hope of developing new therapeutic strategies.

1.3 Notch

The Notch protein is a transmembrane receptor. In Drosophila the receptor can bind two ligands, Delta (Dl) and Serrate (Ser), that are also transmembrane proteins. In general, this type of cell signaling is known as juxtacrine signaling or contact-dependant signaling. Upon interaction of ligand and receptor, proteolytic cleavage of the Notch receptor is initiated, which releases the Notch intracellular domain (NICD) in the cell receiving the ligand signal. The NICD is then imported into the nucleus where it interacts with the DNA-binding CSL protein, also known as Suppressor of Hairless (Su(H)) in Drosophila. In the absence of Notch signalling, Su(H) functions as a transcriptional repressor, but it switches to an activator when bound to NICD (Furriols & Bray, 2001; Morel & Schweisguth, 1999; Fortini & Artavanis-Tsakonas, 1994). Once activated by NICD, the co-activator Mastermind and other transcription factors are recruited to the transcription factor complex while co-repressors such as Hairless and SMRTR are released, culminating in the formation of the Su(H) activator complex that functions to upregulate target genes (reviewed in Bray, 2006; Artavanis-Tsakonas et al., 1995).

The Notch signaling pathway is highly conserved and plays important roles in the development of most metazoans. In general, Notch signalling is often involved in the early stages of binary cell fate decisions as well as boundary formation and is activated reiteratively in many different developmental events (reviewed in Radtke & Raj, 2004; Kooh et al., 1993; Kavaler et al., 1999; Haberman et al., 2003). In addition, Notch signaling has also been implicated in both the promotion and suppression of tumorigenesis depending on the cellular context (reviewed in Radtke & Raj, 2004). As such, the outcome of activation of the Notch signaling pathway is highly context dependent.

Notch is required in a wide variety of Drosophila developmental processes. For example, Notch is required for proper PNS cell differentiation (Kavaler et al., 1999). PNS cells arise from a series of asymmetric cell divisions that are mediated by Notch and Numb signalling to prevent sister cells from adopting the same cell fate (Guo et al., 1996; Kavaler et al., 1999). In the salivary gland duct, Notch interaction with Ser is required to specify imaginal ring cells from salivary gland cells (Haberman et al., 2003; Yang & Deng, 2018). Notch signalling has also been studied extensively in the development of the wing imaginal disc. Here, Notch is modulated by the glycosyltransferase Fringe, causing a ligand sensitivity switch from Dl to Ser, and this process defines a row of border cells that divide the dorsal and ventral compartments (Couso et al., 1995; Panin et al., 1997).

1.4 Roles of Hnt downstream of Notch

hnt has been identified in the literature as a direct transcriptional target of Notch signalling in at least four developmental contexts. This includes Drosophila Kc tissue culture cells, which are hemocyte-like in character, where *in vitro* Notch activation results in direct upregulation of *hnt* transcription. In this system ChIP assays also identified several upstream regulatory regions of *hnt* as significant regions bound by Su(H) following Notch activation (Terriente-Felix et al., 2013). Additionally, in crystal cell precursors (a hemocyte lineage), Notch activity is required *in vivo* to direct crystal cells into a specific cell fate, and expression of *hnt* in this context requires Su(H) interaction downstream of Notch, which in turn, requires binding of the transcription factor Lozenge at sites near to the Su(H) motifs (Terriente-Felix et al., 2013).

In addition to the hemocyte lineage, and representing a second example, Notch signalling also operates upstream of *hnt* expression in the adult ovarian follicle cells. In this context Hnt functions as a mediator between the two antagonistic Notch and Hedgehog signalling pathways that regulate a mitotic to endocycle switch. Hnt is activated downstream of Notch signalling and represses the expression of *string* (*cdc25* homolog) and the transcription factor *cut*, and co-operates with the *tram-track* transcription factor to downregulate Hedgehog signalling. This action is required to arrest cell proliferation and promote follicle cell differentiation, and misexpression of Hnt in the follicle cells is sufficient to promote premature entry into the endocycle (Sun & Deng, 2007).

In a third developmental context, Hnt operates downstream of Notch signalling in the adult female reproductive gland where it is required to form reproductive gland secretory cells. Secretions produced by these cells function as lubricant for the uterus, stabilizing and recruiting sperm to the spermathecae for storage (Schnakenberg et al., 2011; Sun & Spradling, 2013). Knockdown of either Hnt or Notch signalling during pupal development results in reproductive glands deficient in secretory cells. Such adult females are poorly fertile due to an inability to store sperm within the spermathecae, and show less frequent ovulation and egg deposition (Sun & Spradling, 2013).

In the last of four reported contexts*, hnt* has also been identified as a direct target of Notch signalling in DmD8 cells. Likewise, in the adult muscle progenitor cells, which are the DmD8 cell line's *in vivo* correlate, Hnt functions downstream of Notch in what has been described as an "incoherent feed-forward loop", where Notch activity simultaneously activates expression of both the cell cycle regulator *string* and its repressor: Hnt. This

function is thought to generate a transient wave of expression of the repressed gene (in this case the gene *string*). Overexpression of Hnt in this context phenocopies Notch overexpression, resulting in flightless adults, while premature expression of Hnt or Notch RNAi in the myoblasts inhibits mitosis, resulting in fewer myoprogenitors (Krejcí et al., 2009).

Given that *hnt* is often a downstream effector of Notch in a variety of developmental contexts and given that *hnt* is expressed in numerous developmental processes, suggests that there are likely additional undiscovered contexts in which *hnt* functions downstream of Notch signalling during Drosophila development.

1.5 Developing Tracheal System

The Drosophila tracheal system provides a powerful model for studying epithelial tube formation, cell migration, and branching morphogenesis during development. This highly organized network of epithelial tubes delivers oxygen throughout the organism and arises from a series of developmental events regulated by conserved signalling pathways (Manning & Krasnow, 1993; Samakovlis et al., 1996a). All tracheal cells express the transcription factor gene *trachealess* (*trh*), which specifies the tracheal cell fate during early embryogenesis (Wilk et al., 1996). The tracheal system first appears at embryonic stage 10 as ten paired placodes, one per hemisegment, spanning thoracic segment 2 to abdominal segment 8 (Campos-Ortega & Hartenstein, 1985). During placode invagination, the tracheal cells undergo a final round of mitosis, reaching ~50 cells per placode and arrest at the G1 phase for the rest of embryogenesis. During the larval stage, tracheal cells resume the cell-cycle and become somatically polyploid through the endocycle. Tracheal cells are not predetermined in either position or fate but instead respond dynamically to local signalling cues (Samakovlis et al., 1996a). As such, the developing tracheal system is an interesting model to study genetic and cell-cell interactions as no cell division occurs; the complexity of the tracheal system is shaped through a series of genetic programs that specify cell fates and roles, which in turn, govern crucial morphogenetic events such as branch migration, expansion, and fusion (Beitel & Krasnow, 2000; Ribeiro et al., 2004; Samakovlis et al., 1996a; reviewed in Hayashi & Kondo, 2018).

1.5.1 Branching

Tracheal placodes, which are ectodermal in origin, invaginate to form the tracheal primordium. This process requires apical actin enrichment and apical cell constrictions driven by EGFR signalling through the ligand Spitz (Spi) and the activator Rhomboid (Rho) as well as Rho-1 GTPase (*crossveinless-c*) activity (Wilk et al., 1996; Llimargas & Casanova, 1999; Brodu & Casanova, 2006). Following formation of the tracheal primordium, tracheal cells initiate expression of the FGF receptor Breathless (Btl), which is required for processing the FGF ligand Branchless (Bnl) (Sutherland et al., 1996; Ohshiro et al., 2002). These activities facilitate the primary tracheal branching event.

Each primary branch (Fig. 1.1A') has a unique identity determined in part by expression of developmental genes, such as the homeotic gene *spalt* (*sal*), and the gap gene *knirps* (*kni*) which function to assign the dorsal and lateral identities of the primary branches (Franch-Marro & Casanova, 2002; Chen et al., 1998). The DB migrates towards the dorsal midline while the lateral trunks (LTa and LTp) migrate laterally and form both the ganglionic branch (GB), that travels to the central nervous system (CNS), and the lateral trunks (LT) that connect adjacent metameres. The dorsal trunk (DTa) primary branch migrates along the antero-posterior axis, fusing with neighbouring DTp, connecting all the tracheal metameres and forming the largest and only multicellular tube in the tracheal system.

Tip cell identity and migration of the primary branches is dependent on dynamic non-tracheal cell secretion of the chemoattractant Bnl. Upon binding and processing of the Bnl ligand, the group of cells closest to the signal activate a signalling cascade that

determines the tip cell identity. The presumptive tip cells upregulate expression of the Notch ligand Delta (Chihara & Hayashi, 2000) and activate ERK/MAPK signalling (Reichman-Fried et al., 1994), resulting in expression of the transcription factor Pointed (Pnt) (Samakovlis et al., 1996a). Through Notch-mediated lateral inhibition, a single presumptive tip cell expressing high levels of Dl suppresses Dl expression in neighbouring cells, causing them to adopt stalk-cell identities, while assuming the tip cell identity itself (Ikeya & Hayashi, 1999; Llimargas, 1999). The tip cell subsequently begins migrating, guided by dynamic sources of Bnl expression, directing branch outgrowth (Sutherland et al., 1996; Du et al., 2017). In addition to Bnl, migration guidance is encouraged by additional branch specific signals that refine branch positioning. For example, Hedgehog signalling in a striped pattern confines dorsal branches (DB) to a specific metamere compartment while Dpp signalling from the epidermis of the dorsal leading-edge inhibits dorsal elongation of terminal cells, promoting migration away from the dorsal midline (Kato et al., 2004).

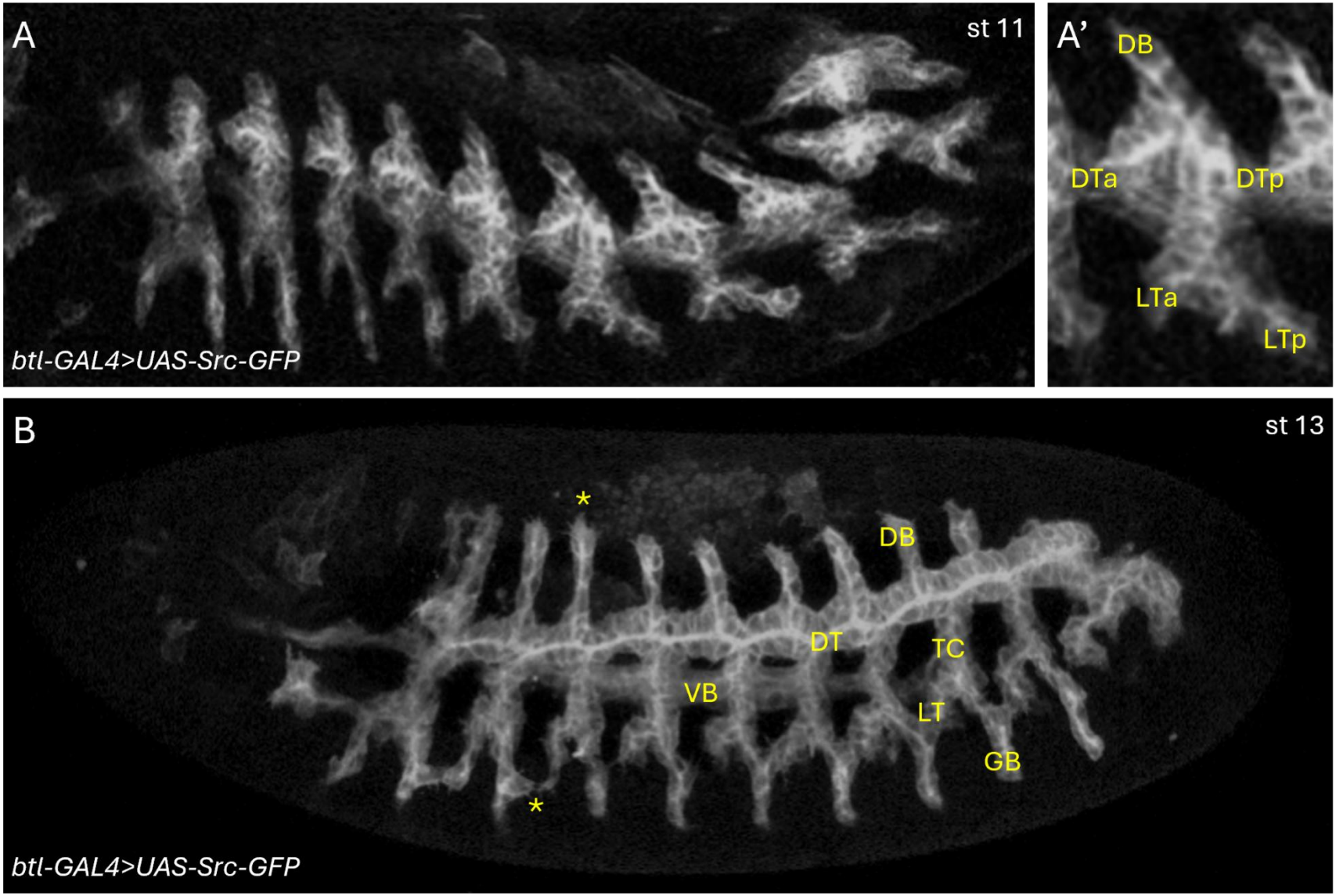

A
st 11
btl-GAL4>UAS-Src-GFP
A'
DB
DTa
DTp
LTa
LTp
B
st 13
*
DB
DT
TC
VB
LT
GB
*
btl-GAL4>UAS-Src-GFP

Figure 1.1 Embryonic tracheal system. Confocal live imaging of embryos expressing *btl-GAL4>UAS-Src-GFP* to visualize the developing tracheal system. (A) Lateral view of stage 11 tracheal primordium undergoing primary branching migration patterns – sometimes referred to as the "dancing man pattern". (A') Magnified inset of a single tracheal metamere (a dancing man) in (A) with labelled nascent primary branches. (B) Lateral view of stage 13 tracheal system. Tracheal tip cells exposed to Bnl/FGF ligand extend filopodia (asterisk). The dorsal trunk (DT) is the largest tracheal branch in length and diameter and joins all tracheal segments into a vast network, eventually connecting the anterior and posterior spiracles. Dorsal branches (DB) migrate to the dorsal midline. The transverse connective (TC) branch extends laterally from the DT. The visceral branch (VB) extends internally towards the intestine, and the lateral trunks (LT) migrate towards other neighbouring LT branches and fuse to form a continuous branch. The ganglionic branch (GB) extends towards the ventral nerve cord and CNS. DTa = dorsal trunk anterior, DTp = dorsal trunk posterior, LTa = lateral trunk anterior, LTp = lateral trunk posterior.

1.5.2 Tracheal Cell Fusion and Organization

Beginning at approximately embryonic stage 14, tracheal development proceeds as secondary branching is initiated when tip cells receive additional cues such as Wingless (Wg). These tip cells then become specialised fusion cells that express the fusion markers and transcription factors Escargot (Esg) and Dysfusion (Dys) (Llimargas, 2000; Samakovlis et al., 1996b; Tanaka-Matakatsu et al., 1996; reviewed in Caviglia & Lushnig, 2014; Jiang & Crews, 2003). Esg suppresses ERK/MAPK expression in the nascent fusion cell and promotes ERK/MAPK signalling in the neighbouring cell which then assumes the terminal cell fate (Miao & Hayashi, 2016). Towards the end of embryogenesis, terminal cells ramify and extend several thin cytoplasmic extensions towards target tissues and facilitate gas exchange. During larval life stages, the terminal cells extensively branch and grow to cover larger areas as the larva dramatically increases in size.

Three major fusion events occur within the tracheal system: the DT and LT fusion events connect tracheal segments of neighbouring metameres, while DB fusion connects opposing branches across the dorsal midline. Notably, DT fusion differs from the other fusion events, as it does not require Esg function, despite being expressed in fusion cells, and instead relies on a mesodermal “bridge cell” that is required to facilitate branch connection (Tanaka-Matakatsu et al., 1996; Wolf & Schuh, 2000; Wolf et al., 2002).

As migrating tracheal branches approach their fusion targets, fusion cells extend filopodia-like extensions to establish contact (Uemura et al., 1996). At these contact sites, fusion cells upregulate and accumulate DE-cadherin, encoded by *shotgun* (*shg*), and form stable adherens junctions that appear as small ring-shaped structures (Uemura et al., 1996;

Tanaka-Matakatsu et al., 1996). Subsequently, actin-rich tracks develop at the contact site, mediated by actin-regulatory molecules such as Formin3 (Form3), and extend toward the pre-existing lumen in anticipation of *de novo* lumen formation between the two fusion cells and thus connecting the two branches (Kato et al., 2016; Tanaka-Matakatsu et al., 1996; Tanaka et al., 2004). Following successful fusion, the paired fusion cells adopt a distinct toroidal shape through a process involving plasma membrane fusion, differentiating them from other tracheal cells (Jiang et al., 2007).

The cellular architecture of the tracheal epithelium consists of a monolayer sheet of polarized cells surrounded by a basal lamina, composed of collagen type IV and laminin, and apically supported by a rigid cuticle structure, known as the taenidial folds, lining the lumen (Fig. 1.2A) (reviewed in Fessler & Fessler, 1989; Tepass & Hartenstein, 1994; Samakovlis et al., 1996a). The tracheal cells in the larger DT are composed of a multicellular layer that forms intercellular junctions to surround the lumen. Other branches such as the DBs or LTs consist of single-cell layers that form autocellular adherens junctions to surround the lumen (Fig. 1.2B) (Tepass & Hartenstein, 1994; Ribeiro et al., 2004). The DT adjacent TC branch is populated by tracheal cells that form a mixture of both intercellular and autocellular adherens junctions except for the transverse connective junction cell (TCJ cell) which always forms an autocellular adherens junction (Ribeiro et al., 2004).

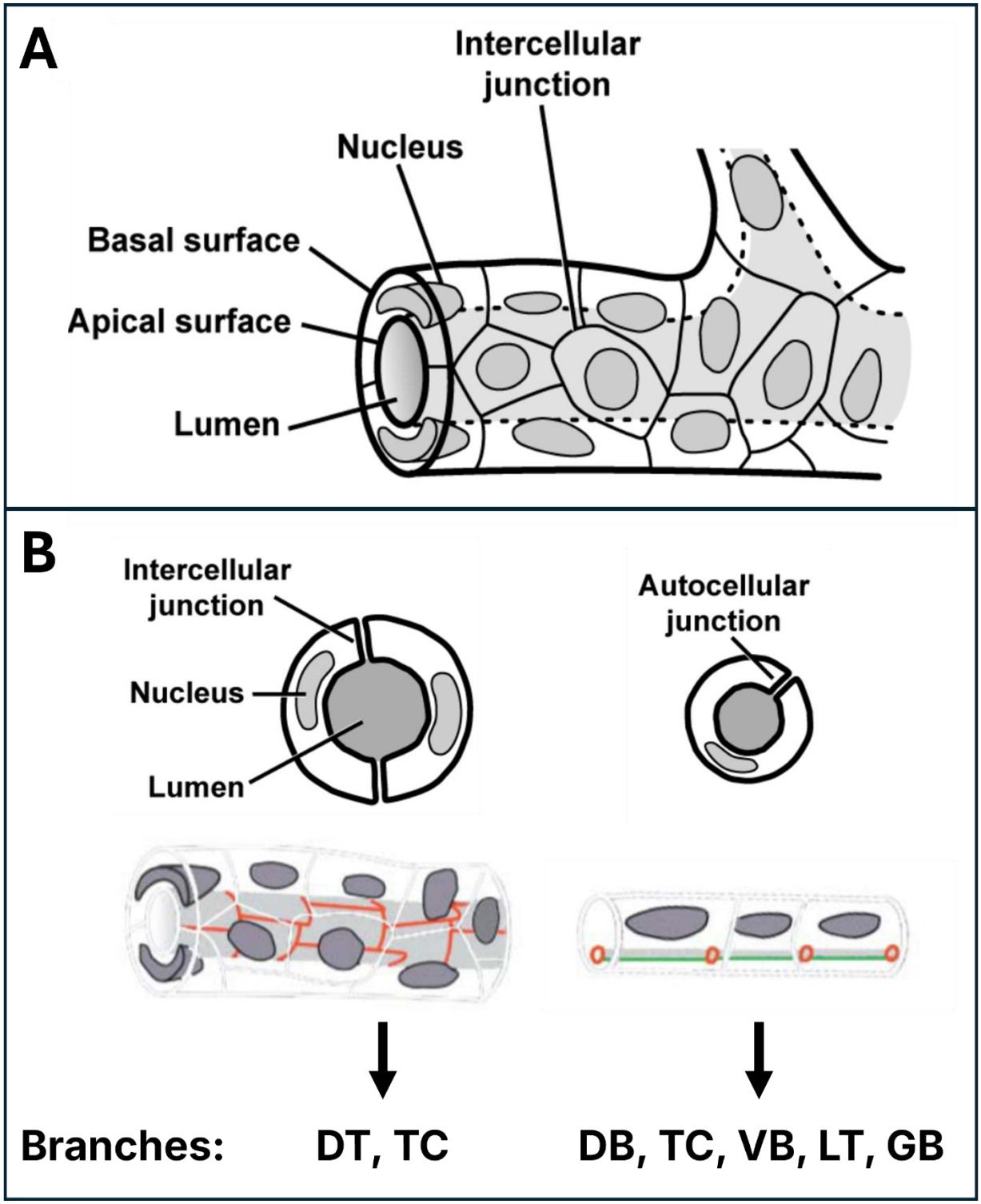

A
Intercellular junction
Nucleus
Basal surface
Apical surface
Lumen
B
Intercellular junction
Nucleus
Lumen
Autocellular junction
Branches:
DT, TC
DB, TC, VB, LT, GB

Figure 1.2 Tracheal cell architecture. (A) Late stage embryonic tracheal cells are organized in a monolayer sheet of epithelial cells. The apical surface of tracheal cells faces the tracheal lumen while the basal surface of cells interacts with the basement membrane. (B) Only the larger dorsal trunk (DT) is formed exclusively by multiple tracheal cells forming intercellular junctions. Other finer branches such as the dorsal branch (DB), visceral branch (VB), lateral trunks (LT), and ganglionic branch (GB) are composed of cells forming autocellular junctions. The transverse connective branch (TC) is populated by cells forming a mixture of both intercellular and autocellular junctions, with the exception of the TC/DT junction cell (TCJ) which regularly forms autocellular junctions. (Adapted from Samakovlis et al., 1996a and Ribeiro et al., 2004)

1.5.3 Cuticle and Taenidial Folds

Mature taenidial folds, or just taenidiae, are parallel rings of chitin that encompass the tracheal lumen providing structural strength and flexibility. By analogy, this tubular structure can be compared to a vacuum cleaner hose. Interestingly, the precursors of the taenidiae, known as the taenidial ridges, are continuous across multiple cells that encircle the tracheal lumen (reviewed in Öztürk-Çolak et al., 2016a). During taenidial formation the apical plasma membrane of tracheal cells corrugates at regular intervals. These corrugations are associated with F-actin cables and chitin synthase complexes, which predetermine the spatial deposition of chitin, resulting in the distinct taenidial fold shape (reviewed in Moussian, 2010; Öztürk-Çolak et al., 2016b). This F-actin arrangement is organized in part by Myosin-II contractions (Hannezo et al., 2015) and is also regulated by the formin DAAM and the non-receptor tyrosine kinases encoded by *Src42A* and *Tec29* (Matusek et al., 2006). Notably, disruptions to the apical F-actin organization are reflected in the pattern of the future mature taenidial folds (Matusek et al., 2006; Öztürk-Çolak et al., 2016b). Src42A has been shown to regulate the actin bundles and accumulates at the junctions between tracheal cells. A two-way feedback mechanism between the taenidial folds and actin bundles has been proposed whereby Src42A activity is used to communicate and regulate tracheal lumen formation (Öztürk-Çolak et al., 2016b).

Taenidial folds are redeposited and reassembled at each molt as larvae transition from one larval instar stage to the next. Despite the vast increase in tracheal size and length between each instar stage, taenidial folds of each instar stage are formed equidistant and undergo structural rearrangements, a process mediated by Matrix metalloproteinase 1

(Mmp1), in-between molts. This gradually widens the distance between each fold during larval growth (Glasheen et al., 2010).

1.5.4 Functions of Notch and Hnt in the Developing Trachea

Notch signalling is required for proper tracheal morphogenesis, and zygotic Notch mutants form underdeveloped branches while some of the tracheal cells inappropriately adopt neuroblast fates (Hartenstein et al., 1992). As a result, previous studies have extensively studied the effects of Notch signalling in early tracheal morphogenetic events (Ikeya & Hayashi, 1999; Llimargas, 1999).

Notch activity is well known to regulate the tip/fusion cell identity in migrating branches by lateral inhibition, thus limiting the tip cell identity to a single cell by suppressing expression of the Notch ligand Dl and activating signalling pathways to specify stalk-cell identity in adjacent cells (Ikeya & Hayashi, 1999; Llimargas, 1999). Due to the Notch requirements in tip cell specification, Notch mutants typically exhibit fusion failure (Ikeya & Hayashi, 1999; Llimargas, 1999). This context is dynamic and regulated by several signals and pathways that co-operate to determine either the fusion, terminal, or stalk cell identity; and Notch defects in both timing and variety result in different phenotypes. Knockdown of Notch in the nascent trachea results in fusion defects in the DT and DB, resulting in several DB cells ectopically adopting the fusion cell fate, resulting in ectopic fusions between adjacent branches (Ikeya & Hayashi, 1999; Llimargas, 1999).

During late embryogenesis, the Notch ligands Dl and Ser are expressed along the length of the DT shortly after the completion of DT fusion (Llimargas, 1999; Ikeya &

Hayashi, 1999). In thoracic tracheal segments of third instar larvae, Dl and Notch interactions at the TC and DB junctions adjacent to the DT define a boundary used to segregate the DT (Rao et al., 2015). Dl expression is linked to the DT identity as ectopic expression of Sal in TC branch cells results in downstream expression of Dl, and ectopic expression of Dl in DB cells causes a local increase in branch diameter (Rao et al., 2015). Interestingly, preliminary studies in the trachea have not been able to define a role for the Notch ligand Serrate, despite its broad expression in the DT (Haberman et al., 2003; Ikeya & Hayashi, 1999).

Notch signalling has also been implicated to control differentiation of adult tracheal cells. In late larval/pupal stages, the Drosophila trachea is re-organized as several populations of tracheoblasts, clusters of dormant imaginal cells, re-enter mitosis and rapidly proliferate and use the pre-existing trachea as a framework to expand. During metamorphosis these cells gradually replace all larval tracheal cells, forming the adult tracheal system (Whitten, 1957). In late larvae and nascent pupae, Notch signalling is promoted by protein glycosylation and thought to regulate the differentiation of imaginal cells to adult tracheal cells (Li et al., 2024). It is of some interest that *hnt* is strongly expressed in the spiracular branch tracheoblasts (Pitsouli & Perrimon, 2010; Pitsouli & Perrimon, 2013; Li et al., 2024) and responds to Notch activity in these imaginal cells (Li et al., 2024).

hindsight is expressed in all embryonic tracheal cells and, by immunostaining, Hnt is first detected at stage 11 in the newly specified invaginating tracheal placodes. As embryogenesis continues, *hnt* is expressed in all tracheal branches (Yip et al., 1997; Wilk et

al., 2000). Previous studies have linked *hnt* to different tracheal functions such as maintenance of epithelial integrity, and possibly both temporally regulating differentiation of adult tracheal cells and luminal maturation and expansion (Wilk et al., 2000; Li et al., 2024; Öztürk-Çolak et al., 2018).

hnt has also been identified as a putative transcriptional target of Blimp-1 through an *in silico* analysis. Blimp-1 is a transcription factor that regulates genes related to tracheal lumen maturation and more specifically, chitin deposition and F-actin organization, by regulating the temporal control of cuticle deposition (Öztürk-Çolak et al., 2018).

The *hnt* alleles hnt^{XE81}, hnt^{1142} and the $Df(1)rb^{(1)}$ deficiency were previously used to investigate *hnt* loss of function tracheal phenotypes. In *hnt* mutants, early events such as placode invagination, primary branching and fusion of the DT occur as expected. However, the tracheal epithelium eventually breaks down, as late fusion events fail and DT metameres expand into individual sac-shapes (Wilk et al., 2000). Apico-basal polarity is still maintained in *hnt* mutants and taenidial folds of first instar larvae are collapsed and irregular in both diameter and organization (Wilk et al., 2000). $Df(1)rb^{(1)}$ mutants are deficient for tracheal enhancers of *hnt* and thus eliminate all tracheal expression of *hnt* while leaving the coding sequence intact, and $Df(1)rb^{(1)}$ embryos also exhibit loss of tracheal integrity (Wilk et al., 2000). As such, Hnt is required for epithelial integrity and assembly of taenidial folds, but the mechanism behind these identified functions remains unknown. In this chapter, I present novel evidence that identifies *hnt* as a requirement for

tracheal actin organization, providing missing context for the role and mechanism of *hnt* in taenidial fold assembly.

1.6 CRISPR/Cas9 Mutagenesis

CRISPR/Cas (Clustered Regularly Interspaced Short Palindromic Repeats/CRISPR associated) is an adaptive defense system that evolved in bacteria and archaea to defend against invading viruses and plasmids. There are three types of CRISPR/Cas systems (Type I-III). The type II systems are unique, in that they employ a single large multi-domain Cas protein (Cas9) to bind and cleave target DNA sequences using an RNA template (known as the crRNA) to direct endonuclease activity. Cas9 endonuclease activity requires that base-pair complementation between the crRNA and target DNA be followed by a PAM sequence (protospacer adjacent motif, NGG consensus sequence). The PAM motif is essential for distinguishing between endogenous (self) and foreign (non-self) DNA. The Type II system of *Streptococcus pyrogenes* has been adapted for widespread applications of genome editing; it has been successfully modified by combining the two RNA molecules required for Cas9 activity, known as the crRNA and the tracrRNA, into a single chimeric guide-RNA molecule (gRNA) (Jinek et al., 2012). Techniques and constructs for designing and expressing gRNAs are now routine, and hundreds of transgenic stocks designed to express specific gRNAs, either ubiquitously or under GAL4 control, are publicly available from Drosophila stock centres.

CRISPR/Cas9 mutagenesis is an effective method that has been used to modify the genome of Drosophila and other organisms for over a decade (Yu et al., 2014; Hwang et al., 2013; Kane et al., 2017; Jinek et al., 2012; Gratz et al., 2013). In Drosophila, the CRISPR/Cas9 system has become a powerful tool that is routinely used to induce targeted double stranded breaks (DSBs). The ability to create DSBs at a target site can be used to recover mutations at a site of interest through the error prone process of non-homologous

end-joining (NHEJ); it can also be used to recover engineered knock-in or knock-out modifications of target genes by providing a template for endogenous homology-directed repair mechanisms (HDR). Until the advent of CRISPR/Cas9 genome editing technology, such homologous recombination techniques were possible but extremely limited and labour-intensive for Drosophila researchers. These days, Drosophila researchers can design CRISPR/Cas9 engineered genomic modifications that are easily recovered through the germline to create stable genetic strains; the recovery and maintenance of such strains relies on the well-established resources and techniques of classical Drosophila genetics (Ewen-Campen et al., 2017; Gratz et al., 2013; Gratz et al., 2014; Kane et al., 2017; Gratz et al., 2015).

1.7 Research Objectives

Given the various developmental contexts in which *hnt* functions downstream of Notch (Terriente-Felix et al., 2013; Sun & Deng, 2007; Sun & Spradling, 2013; Krejcí et al., 2009), and given that *hnt* is expressed in an assortment of developmental contexts (Yip et al., 1997; Wilk et al., 2000), I asked if it is possible to discern a novel *in vivo* role for *hnt* as a downstream target of Notch signalling by mutating Su(H) consensus binding sequences found in the upstream regulatory region of *hnt*.

Hypothesis: I hypothesize that there are unidentified roles for Hnt in regulating tissue specific functions downstream of Notch signalling during Drosophila development.

Objectives:

1. **Use CRISPR/Cas9 techniques to mutate the upstream regulatory region of *hnt*, targeting previously identified Notch responsive elements (NREs) and candidate Su(H) consensus binding sequences.**
2. **Examine and explore the phenotypes of mutations induced by objective 1.**
3. **Determine if *hnt* is a target gene of Notch signalling in novel developmental contexts.**

My initial strategy to generate mutants was to use CRISPR/Cas9 to delete large areas of the *hnt* regulatory region that encompass candidate Su(H) consensus binding sequences and surrounding enhancer elements (see Fig. 1.3). I screened key upstream

regulatory regions of *hnt*, previously identified as sites bound by Su(H) following Notch activation (Terriente-Felix et al., 2013), for candidate Su(H) sequences to manipulate, and found four putative targets. The candidates were chosen based on similarity to the Su(H) consensus binding sequence and relative distance to one another, to avoid deletion overlap. Of the four candidates, three (NRE-1, NRE-3, NRE-4) were a perfect match to the core Su(H) consensus sequence (GTG(G/A)GAA) while the one remainder (NRE-2) contained a single mismatch (Morel & Schweisguth, 1999). NRE-1, NRE-2, and NRE-4 were identified in previously published work (Terriente-Felix et al., 2013), while NRE-3 was identified as a candidate NRE by myself, based on my finding of a perfect Su(H) consensus binding sequence at this location.

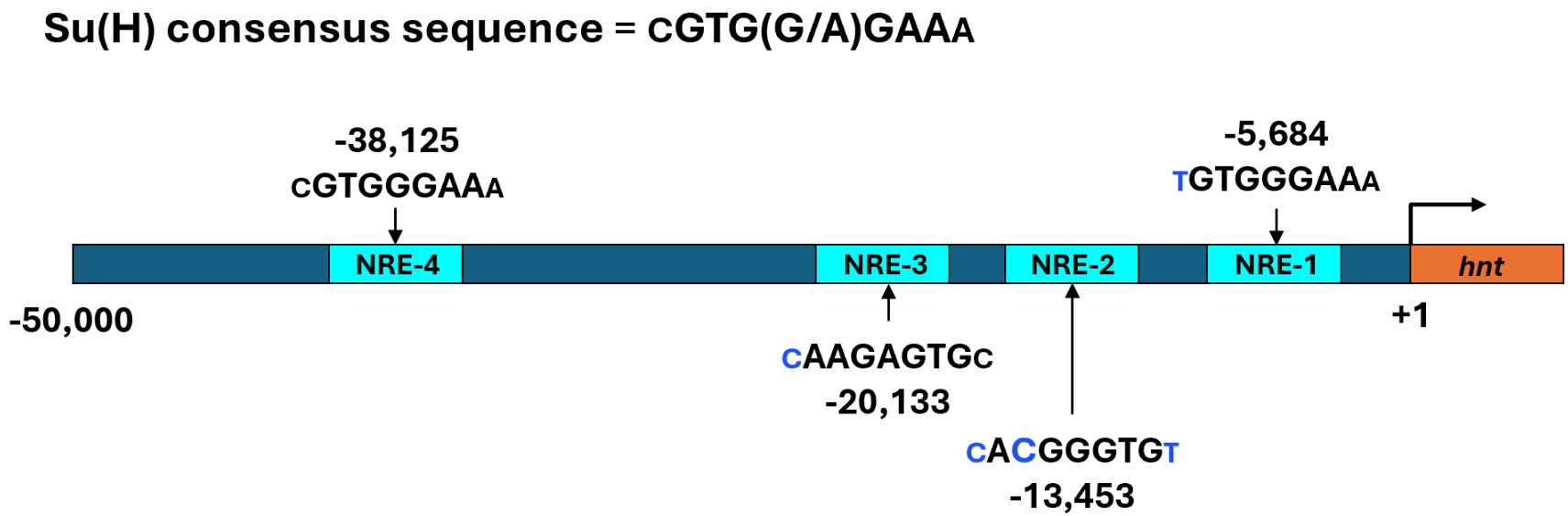


Figure 1.3 Notch responsive element candidates in the *hnt* regulatory region. Schematic of the upstream regulatory region of *hnt*. The *hnt* 5' untranslated region is represented in orange, and the transcription start site is denoted as +1. The Su(H) consensus sequences targeted for deletion are indicated by arrows. ~5 kb NRE deletions are represented in cyan. Consensus sequences listed above the DNA map are found on the sense strand and sequences below are found on the antisense strand and are shown in reverse order. Mismatches between the NRE sequence and the consensus Su(H) sequence are colored in blue. Sequences flanking the core sequence in smaller case represent residues that are less conserved (Morel & Schweisguth, 1999).

1.8 Thesis Overview

In Chapter Three of this thesis, I describe the generation and recovery of the CRISPR/Cas9 mutants outlined above and their initial characterization as alleles of *hnt*. I showed that the recovered allele $hnt^{\Delta N4}$ is associated with lethality and is a verified allele of *hnt*. In addition, I also investigated an unexpected observation of the *3xP3-DsRed* gene cassette functioning as an enhancer trap in both PCR verified deletion mutants and spurious deletion mutants.

In Chapter Four, I investigate the lethal tracheal collapse phenotypes exhibited by $hnt^{\Delta N4}$ mutants. Rhodamine phalloidin staining of these mutants showed evidence of a novel role for *hnt* in the regulation of actin organization in tracheal cells. Furthermore, I establish that *hnt* expression and function lies downstream of Notch signalling in the PNS and tracheal settings by mutating the Su(H) consensus sequence in NRE-4 using a co-CRISPR technique and performing temperature shift experiments using the temperature-sensitive Notch allele, N^{ts}, to knockdown Notch signalling.

In Chapter Five, I discuss the notable findings of my thesis and suggest future experiments and areas to investigate.

Chapter Two:

Materials and Methods

2.1 Generation of CRISPR/Cas9 genome edited strains

2.1.1 Identifying suitable CRISPR/Cas9 targets

For ΔNRE targets, two putative gRNA target regions approximately 2.5 kb upstream and 2.5 kb downstream of the NRE were PCR amplified from genomic DNA of *y* w^{1118}*;; attP2{nos-Cas9}/TM6C, Sb Tb* using the primers listed in Table 2.1 and screened for single nucleotide polymorphisms (SNPs) against the *Drosophila melanogaster* reference genome 6 (release FB2021_04; Öztürk-Çolak et al., 2024). flyCRISPR Optimal Target Tool (Gratz et al., 2014) was used to generate appropriate gRNA targets adjacent to protospacer adjacent motif sequences (NGG) within target regions and simultaneously screened the putative gRNA target sites against the *Drosophila melanogaster* reference genome 6 (release FB2021_04; Öztürk-Çolak et al., 2024) to avoid off-target sites. This method was also used to identify the gRNA target used to mutate the NRE-4 Su(H) consensus sequence site.

2.1.2 Construction of gRNA expression vectors for injection

The following methods were used to synthesize the gRNA expression vectors: gRNA-ΔNRE-1-Up, gRNA-ΔNRE-1-Dn, gRNA-ΔNRE-2-Up, gRNA-ΔNRE-2-Dn, gRNA-ΔNRE-3-Up, gRNA-ΔNRE-3-Dn, gRNA-ΔNRE-4-Up, gRNA-ΔNRE-4-Dn, and gRNA-NRE-4-Su(H). gRNA expression vectors were created as previously described (Gratz et al., 2015).

Complementary oligonucleotides were designed to represent the gRNA target sequences identified in section 2.1.1 (Table 2.2) and annealed by mixing 1 µL of 100 µM stock of both the top and bottom strands, 1 µL of T4 DNA ligase buffer (10X), 6 µL of dH_2O, and 1 µL of T4 Polynucleotide Kinase (NEB, Cat #M0201S). The mixture was incubated for

30 minutes at 37°C, 5 minutes at 95°C, followed by a gradual decrease to 25°C at a rate of -5°C/min.

The annealed gRNA target insert was ligated into the *BbsI* (NEB, Cat #R0536S) digested pU6-BbsI-chiRNA (gift from Melissa Harrison & Kate O'Connor-Giles & Jill Wildonger; Addgene plasmid #45946) by combining 50 ng of digested plasmid, 1 µL of annealed gRNA target insert, 1 µL of T4 DNA ligase (NEB, Cat #M0202S), 1 µL of T4 DNA ligase buffer (10X), and enough dH_2O to bring the mixture to 10 µL total, then incubated for 1 hour at 25°C. Ligation reactions were transformed into 100 µL of competent XL-1 Blue *Escherichia coli* cells (Stratagene; La Jolla, CA).

300 µL of lysogeny broth medium (LB; 1% tryptone (w/v), 0.5% yeast extract (w/v), 1% NaCl (w/v)) was added to the cells and incubated at 37°C for 30 minutes. 200 µL of the cells were streaked onto LB-agar plates (LB with 1.5% agar (w/v)) containing 100 µg/mL ampicillin and incubated overnight at 37°C. Individual colonies were inoculated in 2.5 mL LB medium containing 50 µg/mL ampicillin and incubated with agitation overnight at 37°C. Plasmids were isolated using Monarch® Spin Plasmid Miniprep Kit (NEB, Cat #T1110S) and screened by Sanger sequencing using T7 and T3 sequencing primers.

2.1.3 Construction of homology-directed repair donor vectors for injection

The following methods were used to synthesize the HDR donor vectors: pDsRed-ΔNRE-1, pDsRed-ΔNRE-2, pDsRed-ΔNRE-3, and pDsRed-ΔNRE-4. HDR donor plasmids were generated as previously described (Gratz et al., 2015).

For each unique NRE-deletion, the 5' "left homology arm" (LHA) was generated by amplifying ~1 kb of homology sequence upstream of NRE-deletion targets from *y w FRT-19A* gDNA (section 2.1.5) using primers listed in Table 2.3. Both the LHA PCR product and pDsRed-attP2 (gift from Melissa Harrison & Kate O'Connor-Giles & Jill Wildonger; Addgene plasmid #51019) were digested using *PaqCI* restriction enzyme following manufacturer protocols (NEB, Cat #R0745S). LHA was ligated into *PaqCI* digested pDsRed-attP2 with a 3:1 insert to vector molar ratio using 1 µL of T4 DNA ligase, 1 µL of T4 DNA ligase buffer (10X), and enough dH_2O to bring the mixture to 10 µL total, and incubated for two hours at 25°C. The ligation reaction was then used to transform XL-1 Blue *Escherichia coli* cells and subsequently recovered as described in section 2.2.2 to generate the intermediate LHA-pDsRed-attP2 vector.

The 3' "right homology arm" (RHA) was generated by amplifying ~1 kb of homology sequence downstream of NRE-deletion targets from *y w FRT-19A* gDNA (section 2.1.5) using primers listed in Table 2.3. Both the RHA PCR product and LHA-pDsRed-attP2 were digested using *SapI* restriction enzyme following manufacturer protocols (NEB, Cat #R0569S). RHA was ligated into the *SapI* digested LHA-pDsRed-attP2 vector as described above and subsequently transformed into XL-1 Blue *Escherichia coli* cells and recovered as described in section 2.2.2 to generate the final HDR donor vector used for injection.

This method was used to generate NRE-2, NRE-3, and NRE-4 donor vectors. With exception, the NRE-1 donor vector was constructed using the same methods described above but using the *EcoRI* (NEB, Cat# R3101S) and *NotI* (NEB, Cat# R0189S) restriction enzymes in place of *PaqCI* with respect to the LHA and the *PstI* (NEB, Cat# R0140S) and

XhoI (NEB, Cat# R0146S) restriction enzymes in place of *SapI* with respect to the RHA (Table 2.3) to clone homology arms into the MCS of pDsRed-attP2. Final HDR donor vectors were screened by Sanger sequencing using pHD-BB-2 and pHD-SV40-F sequencing primers (Table 2.4).

2.1.4 CRISPR mix microinjections

To generate ΔNRE CRISPR/Cas9 deletion mutants, 300 nos-Cas9 embryos (*y^1 w^{1118}; attP2{nos-Cas9}/TM6C, Sb, Tb*) were microinjected by BestGene Inc. (Chino Hills, CA) with an injection mix of a pDsRed-ΔNRE-X HDR donor vector, and the two respective gRNA expression vectors, gRNA-ΔNRE-X-Up and gRNA-ΔNRE-X-Dn, at concentrations of 100-500 ng/μL of the donor plasmid and 75-250 ng/μL of each gRNA expressing plasmid.

To generate NRE-4 Su(H) indel mutants, 400 vas-Cas9 embryos (*w[1118]; PBac{y[+mDint2]=vas-Cas9}VK00027*) were microinjected by Genome ProLab (Sherbrooke, QC) with an injection mix of pCFD3-ebony, (gift from Richard Padgett, Addgene plasmid #83380), and gRNA-NRE-4-Su(H) expression vector at concentrations of 150 ng/μL.

2.1.5 CRISPR mutated stock genetics and screening

2.1.5.1 ΔNRE deletion mutants

For ΔNRE deletion mutants, the following steps were performed by BestGene Inc. Surviving adult G-0 individuals were crossed to a *y w* background and F1 progeny were screened for DsRed in adult eyes and balanced with *FM7i* by crossing to *FM7i/C(1)DX, y f* to

produce balanced *X*-isogenic ΔNRE deletion mutants. Full crossing scheme is described in the Appendix.

2.1.5.2 Co-CRISPR NRE-4 Su(H) mutants

For NRE-4 Su(H) mutants, a modified version of protocols outlined in Kane et al., 2017 was followed. G-0 injected larvae were received from Genome Prolab following injection and surviving G-0 adult virgin females were crossed to either *FM7h, w/Y*; *tub-Gal80^{ts}, w^{+}/+*; *TM2*, *e/+* males for homozygous *ebony* screening methods, or to *FM7h, w/Y* males for heterozygous *ebony* screening methods. G-0 adult males were crossed to either *FM7h, w/w*; *tub-Gal80^{ts}, w^{+}/+*; *TM2*, *e/+* or *hnt^{308}/FM7h, w* for the same purposes described above. All G-0 crosses were single-pair matings.

F1 progeny from each single-pair mating were screened for *ebony* body color in homozygous screening methods or for the semi-dominant *ebony* expression in heterozygous screening methods. Individual males and virgin females were crossed to either *hnt^{308}/FM7h, w* or *FM7h, w/Y* as a source of the *X* balancer *FM7h, w* to establish *X*-isogenic lines. Balanced isogenic lines so established no longer needed to be screened for *ebony*. Full crossing schemes for both methods are described in the Appendix.

2.2 Primers and Oligonucleotides

All primers and oligonucleotides were ordered from Sigma-Aldrich (Oakville, ON) and used as indicated in section 2.1.

Table 2.1 PCR primers used to screen genomic DNA of *y¹ w¹¹¹⁸; attP2{nos-Cas9}/TM6C, Sb, Tb* for SNPs.

Primer Sequence
NRE-1 downstream target FWD
5' – TAAACGACTGATATGCAGCACC – 3'
NRE-1 downstream target REV
5' – CAATAACCTTTATCAGGTGGGTG – 3'
NRE-1 upstream target FWD
5' – AGTTTCAGCAATGTTCTTGCG – 3'
NRE-1 upstream target REV
5' – CACCCATCGTTACTCCCACC – 3'
NRE-2 downstream target FWD
5' – TTTTCAAGGGGTGGGTGTGC – 3'
NRE-2 downstream target REV
5' – GGTGGAAGTATTTGTGGGCA– 3'
NRE-2 upstream target/NRE-3 downstream target FWD
5' – TCAGATTCATGGCTTTGCTTGT – 3'
NRE-2 upstream target/NRE-3 downstream target REV
5' – AGGTCGTCACAGCCACATAA– 3'
NRE-3 upstream target FWD
5' – TGGGTTGCCGGTAATGATCT – 3'
NRE-3 upstream target REV
5' – ATCTCACGGTTTTGGCCATG – 3'
NRE-4 downstream target FWD
5' – GTCCGCATTGTCAAGCCATTT – 3'
NRE-4 downstream target REV
5' - TTTGTCGATGGCCAACTGCATC – 3'
NRE-4 upstream target FWD
5' – GTCTGCCCAAAGAGATCCCAG– 3'
NRE-4 upstream target REV
5' - CACATCGCATCCCCATCAAG – 3'

Table 2.2 Oligonucleotides used to generate gRNA targets. Underlined sequence represents overhangs present after annealing that are compatible for cloning into *BbsI* restriction enzyme digested vectors. All targets are adjacent to PAM sequence.

Oligonucleotide Sequence
NRE-1 downstream gRNA target
5’ – CTTCTGTTTTCTGCACTATTATTC – 3’
5’ - AAACGAATAATAGTGCAGAAAACA – 3’
NRE-1 upstream gRNA target
5’ – CTTCGCGTAGCTTTATCTCAACGA – 3’
5’ - AAACTCGTTGAGATAAAGCTACGC – 3’
NRE-2 downstream gRNA target
5’ – CTTCGGGCGCGCACATTACGAACT – 3’
5’ - AAACAGTTCGTAATGTGCGCGCCC – 3’
NRE-2 upstream gRNA target
5’ – CTTCGCGATGGTGCTTACAAGAGT – 3’
5’ - AAACACTCTTGTAAGCACCATCGC – 3’
NRE-3 downstream gRNA target
5’ – CTTCGCACAGGTGAGTCGCTGCGA – 3’
5’ - AAACTCGCAGCGACTCACCTGTGC – 3’
NRE-3 upstream gRNA target
5’ – CTTCGCTGCCCGCCTGATCATTAA – 3’
5’ - AAACTTAATGATCAGGCGGGCAGC – 3’
NRE-4 downstream gRNA target
5’ – CTTCGAAAGAGGCAAGACGCGTCG – 3’
5’ - AAACCGACGCGTCTTGCCTCTTTC – 3’
NRE-4 Su(H) consensus binding site gRNA target
5’ – CTTCGCAGCTGCACATCGTGGGAAA– 3’
5’ - AAACTTTCCCACGATGTGCAGCTGC – 3’

Table 2.3 PCR primers used to clone homology arms. Underlined and italicized sequence represents restriction enzyme recognition sites. Bolded sequence represents overhangs created by digestion through *AarI* or *SapI* restriction enzyme digestion. Primers designed with alternative restriction enzymes found in the MCS are indicated by asterisks.

Primer Sequence	Length
NRE-1 RHA Forward* (*PstI*) 5' – GACGCA*CTGCAG*TTTCTGCACTATTATTC – 3' Reverse* (*XhoI*) 5' - GGCCAC*CTGGAG*GTGTTAAATATACATT – 3'	*1017 bp*
NRE-1 LHA Forward* (*EcoRI*) 5' – CGCGAA*GAATC*GTTACGATCTGCATATAC – 3' Reverse* (*NotI*) 5' - TAACAA*GCGGCCGC*TTGAGATAAAGCTAC – 3'	*1047 bp*
NRE-2 RHA Forward 5' – GTAA*GCTCTTC*ATATACTTGGGATTCGGTTGGCAG – 3' Reverse 5' - TTAA*GCTCTTC*AGACCTGTGGGAAGAATCGTGTTG – 3'	*1042 bp*
NRE-2 LHA Forward 5' – TAAT*CACCTGC*TAATTCGCCTGAGCCAGAGACGATGAC – 3' Reverse 5' - AATT*CACCTGC*TATACTACAGTGGGAGGTGGCTGCGTTG – 3'	*1104 bp*
NRE-3 RHA Forward 5' – GTAA*GCTCTTC*ATATCAGCGACTCACCTGTGCACC – 3' Reverse 5' - TTAA*GCTCTTC*AGACGAGGCAACGACGACGTGGCC – 3'	*1021 bp*
NRE-3 LHA Forward 5' – TAAT*CACCTGC*TTAATCGCCTTGGCATCGGTTGGCATCG – 3' Reverse 5' - AATT*CACCTGC*TATACTACTAATGGTGCATTCAAAATGC – 3'	*1038 bp*
NRE-4 RHA Forward 5' – GATT*GCTCTTC*ATATCGCGTCTTGCCTCTTTCTTG – 3' Reverse 5' - GAGA*GCTCTTC*AGACTGGCTATGTTGGCTATATAG – 3'	*1185 bp*
NRE-4 LHA Forward 5' – TTGG*CACCTGC*TATATCGCCAAGTAGTCAAGTATCTACA – 3' Reverse 5' - TAAA*CACCTGC*TATACTACTGCTGGTCGTAAAGCCCATG – 3'	*1001 bp*

Table 2.4. PCR primers used to verify homology arm cloning into pDsRed-attP2.

Primer Sequence
pHD-BB-1 5′- ACGAAAGGCTCAGTCGAAAG - 3′
pHD-BB-2 5′- TGATATCAAAATTATACATGTCAACG - 3′
pHD-HSP70-R 5′- CGGTCGAGGGTTCGAAATCGATAAG - 3′
pHD-SV40-F 5′- GGCCGCGACTCTAGATCATAATC - 3′

Table 2.5 PCR primers used to verify CRISPR/Cas9 mutant alleles. These primers were also used in combination with pHD-SV40F and pHD-HSP70-R (Table 2.4) to confirm mutant alleles as described in section 3.2.2.

Primer Sequence	Expected Product Size
ΔNRE-1 gDNA Forward 5’ – TGGTTGCCAACTGCGTAACG – 3’ Reverse 5’ – TTGAGTTGGTTGCGCATGCG – 3’	*3705 bp*
ΔNRE-2 gDNA Forward 5’ – CATTGAGGGTGGAACATGCGT – 3’ Reverse 5’ – AACGGGCAGGCATCAAAATC – 3’	*3765 bp*
ΔNRE-3 gDNA Forward 5’ – CCGCACAACATCCGTCATCT – 3’ Reverse 5’ – GCGTCTGCCCATCAAACATC – 3’	*4003 bp*
ΔNRE-4 gDNA Forward 5’ – TCATCGATGGCACCTTGGTG – 3’ Reverse 5’ – AATCCCCGCCAGAGACAAAG – 3’	*3866 bp*

Table 2.6 PCR primers used for long-range PCR amplification of *hnt* regulatory sequence.

Primer Sequence	Expected Product Size
ΔNRE-1 gDNA Forward 5' – ACTGGAAATCGGAACTGGG – 3' Reverse 5' – GTTCTCCCTCGCTCACTGAT – 3'	*7887 bp*
ΔNRE-2 gDNA Forward 5' – ACAAGGACAGCGAACAGGTA – 3' Reverse 5' – ACGGGTTCTCAAAGGGGAAT – 3'	*9662 bp*
ΔNRE-3 gDNA Forward 5' – AACTGGAAATCGGAACTGGG – 3' Reverse 5' – AAACATGCGAACGAGAGAGC – 3'	*11302 bp*
ΔNRE-4 gDNA Forward 5' – ATCAATTAAGCGCGACACCC – 3' Reverse 5' – TGGCAGGGACATTCTTCAGA – 3'	*15579 bp*

Table 2.7 PCR primers used to screen NRE-4 Su(H) sites in prospective indel mutants.

Primer Sequence	Expected Product Size
NRE-4 Su(H) consensus binding sequence site Forward 5' – AACCGCCCACTGATAACTGA – 3' Reverse 5' - ATTGCTGCGCCACATTATGT – 3'	*487 bp*

2.3 Genomic DNA extraction and PCR screening of putative CRISPR alleles

10 mL of buffer for homogenizing whole flies ("squishing" buffer, SB) was prepared by combining 100 µL of 1 M Tris-HCl, 20 µL of 0.5 M EDTA, 50 µL of 5 M NaCl and dH_2O up to 10 mL, for a final concentration of 10 mM Tris-HCl pH 8.0, 1 mM EDTA, and 25 mM NaCl. SB was balanced to pH 8.5 and stored at room temperature.

To extract genomic DNA from putative ΔNRE deletion alleles, single adult males from homozygous viable lines or an L2 larva from homozygous lethal lines were isolated in 1.5 mL microfuge tubes and frozen at -80°C for 15 minutes and then homogenized in a mixture of 49.5 µL of SB and 0.5 µL of fresh Proteinase K (20 mg/mL, NEB Cat #P8107S) using a glass microfuge pestle. The tube was then vortexed and incubated at 37°C for 30 minutes in thermomixer (Eppendorf ThermoMixer® C, Sigma-Aldrich) with slight agitation. The mixture was transferred to a 95°C heat block and incubated for three minutes to inactivate Proteinase K, then centrifuged at 13,000 g for one minute. The supernatant was then transferred to a clean 1.5 mL microfuge tube and stored at -20°C.

Genomic DNA was used as a template for PCR reactions by combining 1 µL of gDNA, 2.5 µL of 10X ThermoPol Reaction Buffer (NEB, Cat #B9004S), 0.5 µL 10 mM dNTPs (NEB, Cat #N0447S), 0.5 µL of 10 mM FWD primers (Table 2.5), 0.5 µL of 10 mM REV primers (Table 2.5), 0.125 µL of *Taq* DNA polymerase (NEB, Cat #M0267S) and dH_2O up to 25 µL. Thermocycling conditions of the PCR reaction was an initial three minutes at 94°C, followed by 32 amplification cycles of 15 seconds at 94°C, 20 seconds at 50-60°C depending on primers, 30 seconds at 68°C, and a final extension duration of 5 minutes at 68°C at the end of the last cycle. 2 µL of PCR reactions were run on a 1.0% agarose gel using electrophoresis

and analyzed to confirm the presence of bands representing PCR products only possible through the intended CRISPR/Cas9 modification and HDR DNA repair mechanisms.

For the NRE-4 Su(H) indel mutants, genomic DNA was extracted from single adult *Bar*$^{+}$ males and used as a template for PCR amplification of the putative mutation site as described above using the primers listed in Table 2.7. 2 µL of PCR reactions were run on a 1.5% agarose gel using electrophoresis and analyzed to confirm the presence of a band representing a PCR product approximately 487 bp in size. Once confirmed, the remaining PCR reaction was cleaned using Monarch® Spin PCR & DNA Cleanup Kit (NEB, Cat #T1130S) and sequenced by Sanger sequencing using the forward primer (Table 2.7).

2.4 Long-range PCR

For long-range PCR amplification of *hnt* regulatory regions, genomic DNA was extracted from single adult males of homozygous viable lines or an L2 larva from homozygous lethal lines using Monarch® Spin gDNA Extraction Kit (NEB, Cat # T3010S). Extracted gDNA was used as a template for long-range PCR by combining 3 µL of gDNA, 5 µL of 10X LongAmp *Taq* Reaction Buffer (NEB, Cat #E5200S), 0.75 µL 10 mM dNTPs (NEB, Cat #N0447S), 1 µL of 10 mM forward primers (Table 2.6), 1 µL of 10 mM reverse primers (Table 2.6) 1 µL of LongAmp *Taq* DNA Polymerase (NEB, Cat #E5200S) and dH_2O up to 25 µL. Thermocycling conditions of the PCR reaction was an initial three minutes at 94°C, followed by 30 amplification cycles of 15 seconds at 94°C, 30 seconds at 50-60°C depending on primers, 50 seconds/kb at 65°C, and a final extension duration of 10 minutes at 65°C at the end of the last cycle.

1 µL of the PCR reaction was run on a 0.5% agarose gel using electrophoresis and analyzed to confirm the presence of expected bands. The remaining PCR reaction was gel extracted using Monarch® Spin DNA Gel Extraction Kit (NEB, Cat #T1120S) and Oxford Nanopore sequenced by Plasmidsaurus (South San Francisco, CA), who also assembled the consensus sequences. The consensus sequences were analyzed to confirm the intended CRISPR modifications had taken place and that the DsRed had been inserted through HDR.

2.5 Embryo Collection & Dechorionation

Adults were reared at 25°C on fresh food with a small dab of freshly prepared yeast paste to encourage egg-laying. Appropriately staged embryos were collected using an automated Drosophila embryo collector (Flymax Scientific) or by hand using filtration baskets made of nylon mesh and modified 50 ml screw-cap Falcon tubes (Reed et al., 2001).

Embryos were dechorionated using a 50% bleach solution mixed with a few drops of 1X PBT (PBS w/ 0.1% Triton X-100), incubated with slight agitation for approximately 2-5 minutes, and gently rinsed with deionized water.

2.6 Embryonic Lethality & Viability Assays

Embryonic lethality assays were performed as previously described (Reed et al., 2001). Embryos were collected as described in section 2.5, rinsed with deionized water and gently moved to grape juice-agar plates. Embryos were placed in grids of 10 embryos, up to 250 embryos per plate, and incubated with a dab of freshly prepared yeast paste placed

away from eggs at 25°C for 48 hours. Next, the remaining unhatched embryos were scored as unfertilized embryos (underdeveloped and white) or lethal embryos (brown), and embryonic lethality percentage was calculated as (lethal embryos/(total eggs - unfertilized eggs)) X 100%.

For larval viability assays, late-stage embryos and newly hatched first instar larvae were selected and reared on grape juice-agar medium with a dab of yeast paste at 25°C for 72 hours. The remaining viable third instar larvae were scored and larval viability percentage was calculated as (third instar larvae/starting population) X 100%.

2.7 Anti-Hnt immunostaining & rhodamine phalloidin staining

Embryos were collected and dechorionated as described in section 2.5. Embryos were then fixed for 20 minutes in 10 mL of heptane, 9 mL of PBS, and 1 mL of 37% wt. in H_2O formaldehyde solution (Sigma-Aldrich, Cat #F1635) in a clean scintillation vial.

For immunostaining, the following solutions were prepared:

BSA blocking solution was prepared by combining 25 mL of 100 mM Glycine (BioShop Canada Inc., Cat #GLN001), 250 µL of 10% Tween-20, 500 µL of 10% Triton X-100, 5 mL of 10X PBS, 0.05 g of bovine serum albumin (Sigma-Aldrich, Cat #A7906), and dH_2O up to 50 mL.

PBS-GlyX20H solution was prepared by combining 5 mL 10X PBS, 5 mL of 100 mM Glycine (BioShop Canada Inc., Cat #GLN001), 250 µL of 10% Tween-20, 500 µL of 10% Triton X-100, 50 µL of H_2O_2, and dH_2O up to 50 mL.

For immunostaining, embryos were dehydrated with 100% methanol and then rehydrated by transferring through a solution series of 25% PBS/75% methanol, 50% PBS/50% methanol, and 75% PBS/25% methanol, followed by two washes in 1X PBS, three washes in PBT, and then two washes in PBS-GlyX20H solution. Embryos were blocked for 1-2 hours at room temperature in 380 µL of BSA blocking solution and 20 µL of Normal Goat Serum (NGS) and then stained with 40 µL of mouse monoclonal anti-Hindsight (Hnt) 27B8 1G9 (1:10; from H. Lipshitz, University of Toronto) in 340 µL of PBS-GlyX20H and 20 µL of NGS, overnight at 4°C.

The following day, embryos were washed three times in PBS-GlyX20H, blocked as previously described, then incubated in 1.5 µL of Alexa Fluor 488 goat anti-mouse secondary antibody 1:1000 (Cedarlane Labs), 380 µL of PBS-GlyX20H, and 20 µL of NGS for 1-2 hours at room temperature in the dark. Embryos were washed three times in PBS-GlyX20H, followed by another three washes in PBS, and transferred through a glycerol series of 25% glycerol/75% PBS, 50% glycerol/50% PBS, 75% glycerol/25% PBS. The last solution was replaced with antifade mountant (1% DABCO (Sigma), in 90% glycerol/10% PBS) and then embryos were mounted on standard microscope slides and imaged.

For rhodamine phalloidin staining, embryos were dechorionated and fixed as described above and dehydrated with 80% ethanol in PBS, followed by three washes in 80% ethanol in PBS. The embryos were rehydrated by transferring through a PBT/ethanol series of 25% PBT/75% ethanol, 50% PBT/50% ethanol, 75% PBT/25% ethanol. Embryos were then rinsed twice in PBT for 1 hour total and then rinsed twice in 1X PBS, followed by addition of rhodamine phalloidin (Molecular Probes, Cat #R415) to a final concentration of

1 µg/mL. The mixture was incubated in the dark for 30 minutes and then washed three times in 1X PBS and transferred through a glycerol solution series as described above. Embryos were mounted on standard microscope slides with antifade mountant and imaged using confocal microscopy.

2.8 *N^{ts}* Temperature Shift Protocols

For the following *N^{ts}* temperature-shift protocol, the *y w FRT-19A* stock was used as a control and underwent matching conditions. Adults were reared at 18°C and embryos were collected over a two-hour interval using an automated Drosophila embryo collector (Flymax Scientific). Embryo collections were incubated at the permissive temperature (18°C) for 22-24 hours to allow embryos to reach stage 14 and then shifted to the restrictive temperature (29°C) for either two hours, in which case they were immediately fixed and immunostained with anti-Hnt as described in section 2.7, or for approximately 12 hours, after which they were immobilized on double-sided tape as described (section 2.9.2) and analyzed as first instar larvae using DIC brightfield imaging.

2.9 Imaging

Confocal microscopy was performed using a Nikon Eclipse 90i microscope fitted with a Nikon D-eclipse C1 scan head as previously described (Cormier et al., 2012). To accommodate readers with protanopia (red-green colour blindness), and unless otherwise noted, the GFP/FITC, and the TRITC/mCherry emission colours were custom set as yellow

and blue, respectively, using the Nikon Elements EZ-C1 3.70 software. To enhance contrast, some single channel images were similarly set as grayscale. DIC images were also collected using the same confocal microscope system, utilizing a polarized bright field detector in the 488 nm (GFP/FITC) excitation channel. Unless otherwise stated, most confocal micrograph images are Z-stack projections, where the step size was set to 0.5-2 μm for a total of 15-30 steps. Z-stack projections used the maximum pixel setting of the Nikon EZ-C1 3.70 software. In some instances, single step images (i.e. not Z-stack projections) were used to better demonstrate certain morphological features and are described as such. Unless stated otherwise, images are presented in conventional orientation with anterior to the left and dorsal up.

2.9.1 Embryo Hanging Drop Preparation

For live imaging of embryos, the hanging drop method developed for use with upright microscopes was used as previously described (Reed et al., 2009). Briefly, halocarbon oil mix was prepared by combining halocarbon oil viscosity series 700 and viscosity series 56 in equal ratios. Embryos were collected and dechorionated as described in section 2.5 and gently transferred onto a drop of halocarbon oil (~ 20-40 μL) placed on a wide (22 X 50 mm) coverslip. After the embryos were oriented in the desired position, the coverslip was carefully and quickly inverted, placed over a live imaging humidity chamber fitted with a damp piece of tissue to maintain humidity, and secured in place using tape. Embryos were then live-imaged using confocal microscopy.

2.9.2 Larvae Immobilization

To live-image the larval ventral PNS and tracheal branches, larvae were immbolized using heat treatment or double-sided tape. For heat treatment, larvae were rinsed in 1X PBS, blot dried using a kimwipe and transferred to a microscope slide. After immersing in halocarbon oil (section 2.9.1), larvae were exposed to 70°C heat for approximately 7-10 seconds until movement ceased and then oriented for imaging (Zhou et al., 2016; Wingen et al., 2017). Larvae were then gently covered using coverslips held up with Vaseline, to prevent excessive pressure, and imaged using confocal microscopy. For double-sided tape immobilization, slides were prepared by attaching a piece of double-sided tape onto a microscope slide and removing the back of the tape. Larvae were rinsed in 1X PBS, blot dried using a kimwipe and then transferred onto the tape. The larvae were secured onto tape by applying gentle pressure using a fine paintbrush, followed by immediate immersion in halocarbon oil mixture (section 2.9.1). Larvae were then covered with coverslips held up with Vaseline and imaged using confocal microscopy.

2.9.3 Larvae Dissections

Posterior midgut and tracheal dorsal trunks from a late third instar larva were dissected on a standard microscope slide. Larvae were rinsed in 1X PBS and blot dried using a kimwipe. To isolate the midgut, larvae heads were removed and bodies were everted to remove internal organs. Midgut was carefully separated, covered with a few drops of halocarbon oil, and imaged using confocal microscopy. For tracheal branches, larvae heads were removed and bodies were filleted ventrally. After the internal organs

were removed, the exposed trachea was isolated, covered with a few drops of halocarbon oil (section 2.9.1) and imaged using confocal microscopy.

2.9.4 Pupal Case Dissections

To mount and perform microscopy of late pupae (48-72 hours post pupariation), pupae were dislodged from cultures with water and a fine paint brush. After drying, fine jeweller's forceps (Dumont No. 5) were used to grasp pupae by their anterior spiracles and place them ventral side down onto double-sided tape applied to a microscope slide. The pupal case peeling procedure involved carefully removing the operculum using the forceps, and gently rupturing the pupal case longitudinally between the notum and wing bud. Once enough of the pupal case had been peeled by pulling strips of casing from the cut and adhering to the sticky tape, eventually exposing the abdomen, a small amount of halocarbon oil mixture (as described above in 2.9.1) was applied with a fine paint brush and the pupae were dislodged from their pupal cases using gentle pressure applied with the paint brush. Pupae were then transferred onto a coverslip in a small drop of halocarbon oil and prepared for confocal microscopy in a manner similar to the embryo hanging drop procedure described above (2.9.1).

2.10 Fly Stocks

All fly stocks and genetic crosses were raised on standard Drosophila media under conditions of 25°C and 12 light/12 dark hours unless otherwise specified.

Table 2.8 List of Drosophila stocks used in this study and their sources.

Stock	Source
y $N^{l1N\text{-}ts1}$g f/C(1)DX, y f	Bloomington Stock 2533
y $N^{l1N\text{-}ts1}$g f/FM7h, w	New stock recovered in this study
y w^{1118} P{ry[+t7.2]=neoFRT}19A	Bloomington Stock 1744. "*P{ry[+t7.2]=neoFRT}19A" is further abbreviated as "FRT19A"*.
w;; pebBAC[CH321-46J02, attP2]	Marc Freeman, University of Oregon. "*pebBAC[CH321-46J02, attP2]"* is further abbreviated as "peb^{BAC}".
y w hnt^{XE81}FRT19A;; peb^{BAC}/ TM6C, Sb	Reed Lab Stock Collection
w; Peb1-eGFP (*ZH-attP51D*, II)	Sarah Bray, University of Cambridge, UK
w;; Peb1-mCherry (*ZH-attP86Fb*, III)	Sarah Bray, University of Cambridge, UK
w^{1118};; PBac{y[+mDint2]=vas-Cas9}VK00027	Genome Prolab, Chino Hills, CA
y w^{1118};; attP2{nos-Cas9}/TM6C, Sb Tb	BestGene Inc., Sherbrooke, QC
FM7i/C(1)DX, y f	Bloomington Stock 5263
w; $GAL80^{ts}$; TM2, Ubx^{130} e^{s}/TM6B, Hu e Tb	Bloomington Stock 7108. "*$GAL80^{ts}$"* is abbreviation for *"P{w[+mC]=tubP-GAL80[ts]}10"*
FM7h, w/ w; *$GAL80^{ts}$/+*; *TM2*, *Ubx^{130} e/+*	Reed Lab Stock Collection. Not a true stock – requires selection – used as source of *FM7h, w/w ;; TM2,e / +* females or *FM7h, w ;; TM2, e* males for "jackpot line crosses" described in section 4.2.6.
w hnt^{308} FRT19A/FM7h, w	Reed Lab Stock Collection
y w; Tl{Tl}shg^{GFP}	Bloomington Stock 60584
w;; DPax2[B1]-DsRed	Josh Kavaler, Colby College, Maine, USA. Described in (Kim et al., 2020).

N^{55e11} FRT19A/FM7c	Bloomington Stock 28813
N^{55e11} FRT19A/FM7h, TwiG	Reed Lab Stock Collection - "*TwiG*" is abbreviation for *twist-GAL4 > UAS-GFP*.
$oc^{otd\text{-}XC86}$/FM7c, 2xTb-RFP	Bloomington Stock 36337 – "*FM7c, 2xTb-RFP"* is abbreviation for "*P{w[+mC]=2xTb[1]-RFP}FM7c, sn[+]"*.
y w P{w[+mW.hs]=GawB}NP3312/FM7c	Kyoto Stock 113216. "*P{w[+mW.hs]=GawB}NP3312" is further* abbreviated as "*Hnt-GAL4*" or "*NP3312*".
y w^{67c23}; P{w[+mC]=GAL4-btl.S}2	Kyoto Stock 109128. "*P{w[+mC]=GAL4-btl.S}2"* is abbreviated as "*btl-GAL4*".
w btl-GAL4>UAS-Act5C-GFP/CyO, P{lacZ.w^{+}}276	Bloomington Stock 8807. "*btl-GAL4>UAS-Act5C-GFP"* is abbreviation for *"P{GAL4-btl.S}2, P{UASp-Act5C.T:GFP}2"*.
UAS-Src-GFP (II)	Antonio Jacinto, Nova University Lisbon, Portugal. A truncated version of *Src64B* that localizes to cell membranes cloned upstream of GFP reporter (Kaltschmidt et al., 2000).
w; If/CyO; da-GAL4	Bloomington Stock 55850. "*da-GAL4*" is abbreviation for "*P{w[+mW.hs]=GAL4-da.G32}UH1".*
w; UAS-$N^{\Delta 34a}$	Steven Hou, Fudan University, China. Originally made in 1990 by Ed Griniger, NIH, Bethesda, Maryland, USA. A constitutively active (ligand independent) truncated version of the Notch receptor. Also known as "*P{UAS-$Notch^{\Delta E}$}*". On 2nd chromosome. (Fuerstenburg & Giniger, 1998).
y $w^{1118}$$hnt^{\Delta N1}$	New stock recovered in this study. *Bona fide* ΔNRE-1 deletion mutant. *Drosophila melanogaster* (R6.67) (release FB2026_01; Öztürk-Çolak et al., 2024) chrX:4,609,116…4,614,633
y $w^{1118}$$hnt^{\Delta N2}$	New stock recovered in this study. *Bona fide* ΔNRE-2 deletion mutant. *Drosophila melanogaster* (R6.67) (release FB2026_01; Öztürk-Çolak et al., 2024) chrX:4,601,567…4,606,674

y w^{1118}hnt^{ΔN3}	New stock recovered in this study. *Bona fide* ΔNRE-3 deletion mutant. *Drosophila melanogaster* (R6.67) (release FB2026_01; Öztürk-Çolak et al., 2024) chrX:4,595,611…4,601,404
y w^{1118}hnt^{ΔN4}/FM7i	New stock recovered in this study. *Bona fide* ΔNRE-4 deletion mutant. *Drosophila melanogaster* (R6.67) (release FB2026_01; Öztürk-Çolak et al., 2024) chrX:4,576,880…4,581,697
y w^{1118}hnt$^{ΔN1-5}$	New stock recovered in this study. Spurious ΔNRE-1 deletion mutant.
y w^{1118}hnt$^{ΔN4-1}$	New stock recovered in this study. Spurious ΔNRE-4 deletion mutant.
y w^{1118}hnt^{ΔN4}/FM7h, TwiG	New stock recovered in this study. "*TwiG*" is abbreviation for *twist-GAL4 > UAS-GFP*.
y w^{1118}hnt^{ΔN4}/FM7c, 2xTb-RFP	New stock recovered in this study. *"2xTb-RFP"* is abbreviation for *"P{w[+mC]=2xTb[1]-RFP}FM7c, sn[+]"*.
w; P{y[+t7.7] GFP[3xP3.cUa]=white-eraser}attP2	Bloomington Stock 90371. Abbreviated as "*3xP3-GFP*". Used as a control for 3xP3 promoter activity.

Chapter Three:

Generation, Verification, and Initial Characterization of CRISPR/Cas9 Mutants

3.1 Overview

hnt is an essential transcription factor that is expressed in a wide range of developmental contexts and tissues. However, despite extensive characterization of *hnt* expression patterns, the regulatory mechanisms driving *hnt* expression in many of these contexts remains unclear (Yip et al., 1997; Wilk et al., 2000). In some cases, *hnt* has been shown to be a downstream responder of Notch signalling (Terriente-Felix et al., 2013; Sun & Deng, 2007; Sun & Spradling, 2013; Krejcí et al., 2009), which raises the question of whether there are unidentified developmental contexts in which Notch signalling regulates *hnt* expression. To investigate this possibility, I used CRISPR/Cas9 techniques to excise candidate Su(H) consensus binding sequences located in previously identified Notch responsive regions (NREs) of the upstream regulatory region of *hnt* (Gratz et al., 2015; Terriente-Felix et al., 2013). Through homology directed repair (HDR), *3xP3-DsRed* reporter gene cassettes were inserted at deletion sites to aid in identifying mutants but were incidentally found to function as enhancer traps.

The recovered deletion lines ($hnt^{\Delta N1}$, $hnt^{\Delta N2}$, $hnt^{\Delta N3}$, and $hnt^{\Delta N4}$) were confirmed through PCR analysis and subsequently screened for hemizygous lethality. Of the four mutant lines, only $hnt^{\Delta N4}$ produced a lethal phenotype, which was associated with tracheal defects such as complete collapse of the larval tracheal system and distorted taenidial fold structures. Given that *hnt* has been previously associated with tracheal defects (Wilk et al., 2000), these preliminary findings provide initial evidence that *hnt* expression in the developing tracheal system may be regulated by Notch signalling.

3.2 Results

3.2.1 Generation of CRISPR/Cas9 mutated *hnt* stocks

Based on previously published work that identified *hnt* as a direct downstream target of the Notch signalling pathway in certain contexts (Terriente-Felix et al., 2013; Krejcí et al., 2009; Sun & Deng, 2007), I used CRISPR/Cas9 to generate ~5 kb deletions that would remove Su(H) consensus binding sites within the 5' upstream regulatory region of the *hnt* gene (Fig. 3.1). It was the hope that such deletions would further elucidate the relationship between Notch signalling and *hnt* expression. For each of the four previously defined NRE target sites (Fig. 3.1B), I designed two gRNA expressing plasmids and a complementary HDR donor vector. Here, the strategy was that the two gRNAs would guide Cas9 to target sites generating double-stranded breaks on either side of the NRE target sequence and thereby excise the NRE site (Fig. 3.1A). Genomic DNA distal and proximal to these gRNA target sequences was PCR amplified and cloned into a HDR donor vector, which, in turn, flanked a *3xP3-DsRed* gene cassette. Following deletion of the NRE target site, it was expected that endogenous HDR mechanisms using the donor vector as a template, would result in the insertion of the *3xP3-DsRed* cassette as a marker of a successfully generated NRE deletion at a relatively common frequency (Fig. 3.1A). The 3xP3 insect promoter is well-known to drive DsRed expression in the adult eye and ocelli, allowing for effortless screening of CRISPR mutagenesis events using fluorescence stereomicroscopy (Horn et al., 2000).

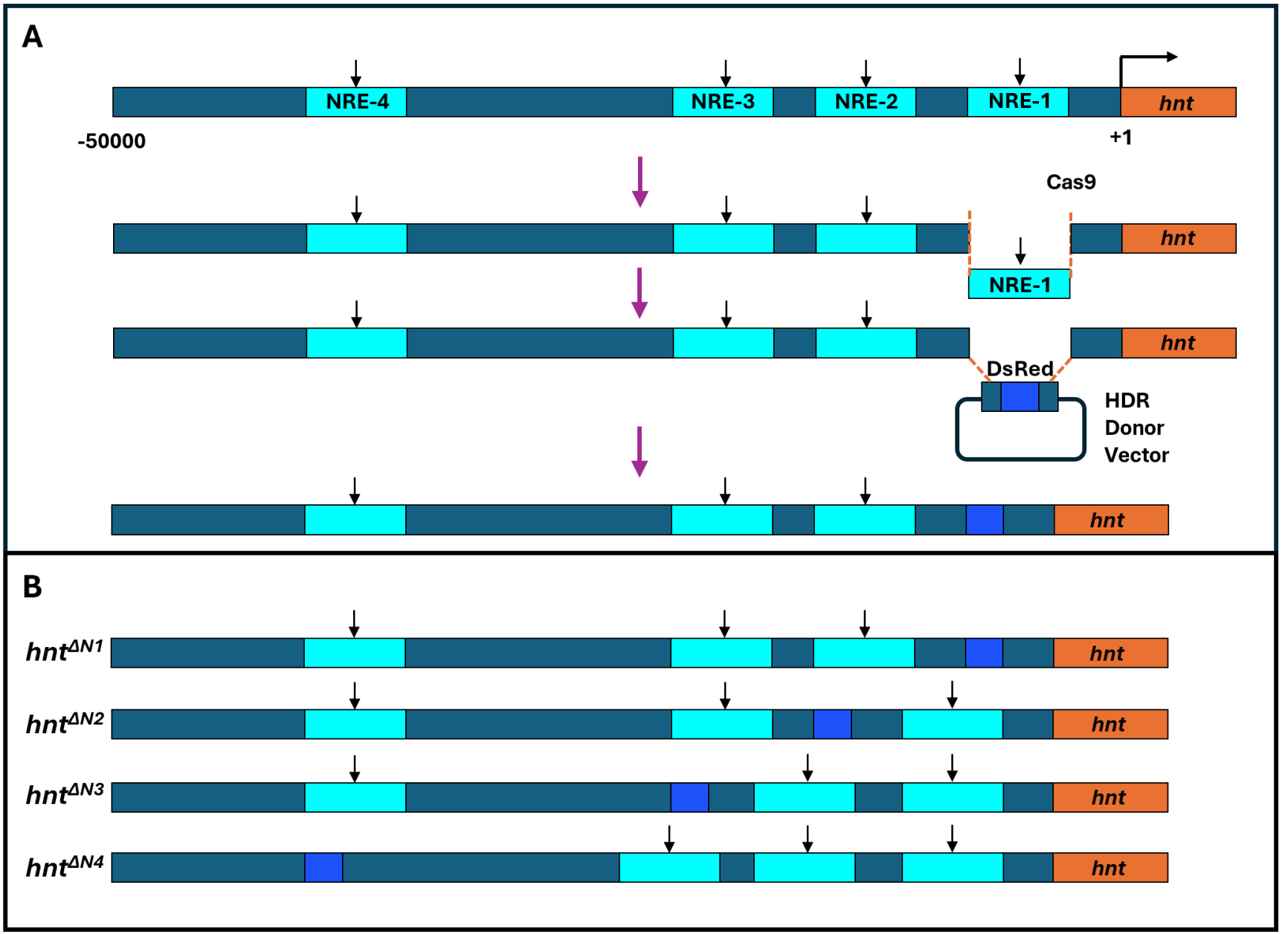

A
NRE-4
NRE-3
NRE-2
NRE-1
hnt
-50000
+1
Cas9
NRE-1
DsRed
HDR
Donor
Vector
B
hntΔN1
hntΔN2
hntΔN3
hntΔN4

Figure 3.1 CRISPR/Cas9 deletion mutant generation. (A) Schematic illustrating example approach to generate wide NRE deletions in the germline. Designated ~5 kb NRE sites (cyan) surround a central Su(H) consensus binding sequence (black arrow). gRNAs direct Cas9 to induce double-stranded breaks at upstream and downstream targets to excise the NRE site and delete the internal Su(H) binding sequence. DNA repair mechanisms will initiate HDR, and use provided HDR donor vectors with cloned homology arms flanking a *3xP3-DsRed* gene cassette to incorporate a screenable marker. (B) Schematic of the 5' upstream regulatory region of *hnt* showing the four deletion mutants expected to be recovered.

The CRISPR injection components were formulated and sent to BestGene Inc., where the mix was injected into ~300 embryos of genotype *y* w^{1118}*; attP2{nos-Cas9}/TM6C, Sb Tb*. In this stock the *nos*-regulatory sequences drive expression of Cas9 within the female germline stem cells, and this results in strong maternal loading of Cas9 protein within the germplasm/germline of the G-0 injected embryos. Subsequently, injected embryos will contain both Cas9 protein and gRNA molecules within their posterior pole plasm – resulting in the formation of an active Cas9 complex within the progenitor cells of the germline, known as pole cells. Surviving G-0 adults, whose germlines were expected to possibly carry the deletions and associated DsRed insertions, were backcrossed to a *y w* background and the resulting progeny were subsequently screened for the DsRed marker. NRE transformants, so identified, were crossed to the balancer chromosome *FM7i* to generate *X*-isogenic sibling lines generated from single female crosses (described in Appendix, Fig. A4).

In total, 28 ΔNRE deletion lines were generated and balanced over *FM7i*, consisting of: seven ΔNRE-1 lines, six ΔNRE-2 lines, seven ΔNRE-3 lines, and eight ΔNRE-4 lines (Fig. 3.2A). Once obtained, these *X*-isogenic lines were screened for lethality in adults by scoring for male progeny not carrying the *FM7i* balancer chromosome (Bar^+ progeny = viable) (Fig. 3.2A). Much to my surprise, all ΔNRE-1, ΔNRE-2, and ΔNRE-3 lines were observed as homozygous and hemizygous viable (blue, Fig. 3.2A), while all but one of the ΔNRE-4 lines were found to be lethal (yellow, Fig. 3.2A).

3.2.2 PCR verification of ΔNRE *hnt* stocks

All 28 new *hnt* alleles generated by CRISPR/Cas9 genome editing were analyzed by PCR with 8/28 alleles confirmed (checkmarks, Fig. 3.2A). In brief, primers were designed to amplify the flanking genomic DNA and elements internal to the DsRed cassette insertion. Alleles were considered verified (checkmark, Fig. 3.2A) if three PCR products representing the LHA, RHA, and FL were produced and matched the expected size (Fig. 3.2B). Following PCR confirmation, one representative line was kept from each NRE deletion, and named $hnt^{\Delta N1}$, $hnt^{\Delta N2}$, $hnt^{\Delta N3}$, and $hnt^{\Delta N4}$ (Fig. 3.1B). Long-range PCR was performed on the representative lines, and the products were sequenced using Oxford Nanopore sequencing to confirm recovery of the intended NRE deletions. Each line recovered and named above represents a *bona fide* deletion carrying the *3xP3-DsRed* cassette inserted at the NRE target sites, NRE1-NRE4, as described. The specific co-ordinates, with respect to the reference genome sequence, for each deletion line, are annotated in Table 2.8 (Fly Stocks). Other lines that did not pass the PCR screening and did have DsRed expression, were also subject to further analysis – but not being considered "*bona fide*", these lines were considered as "spurious".

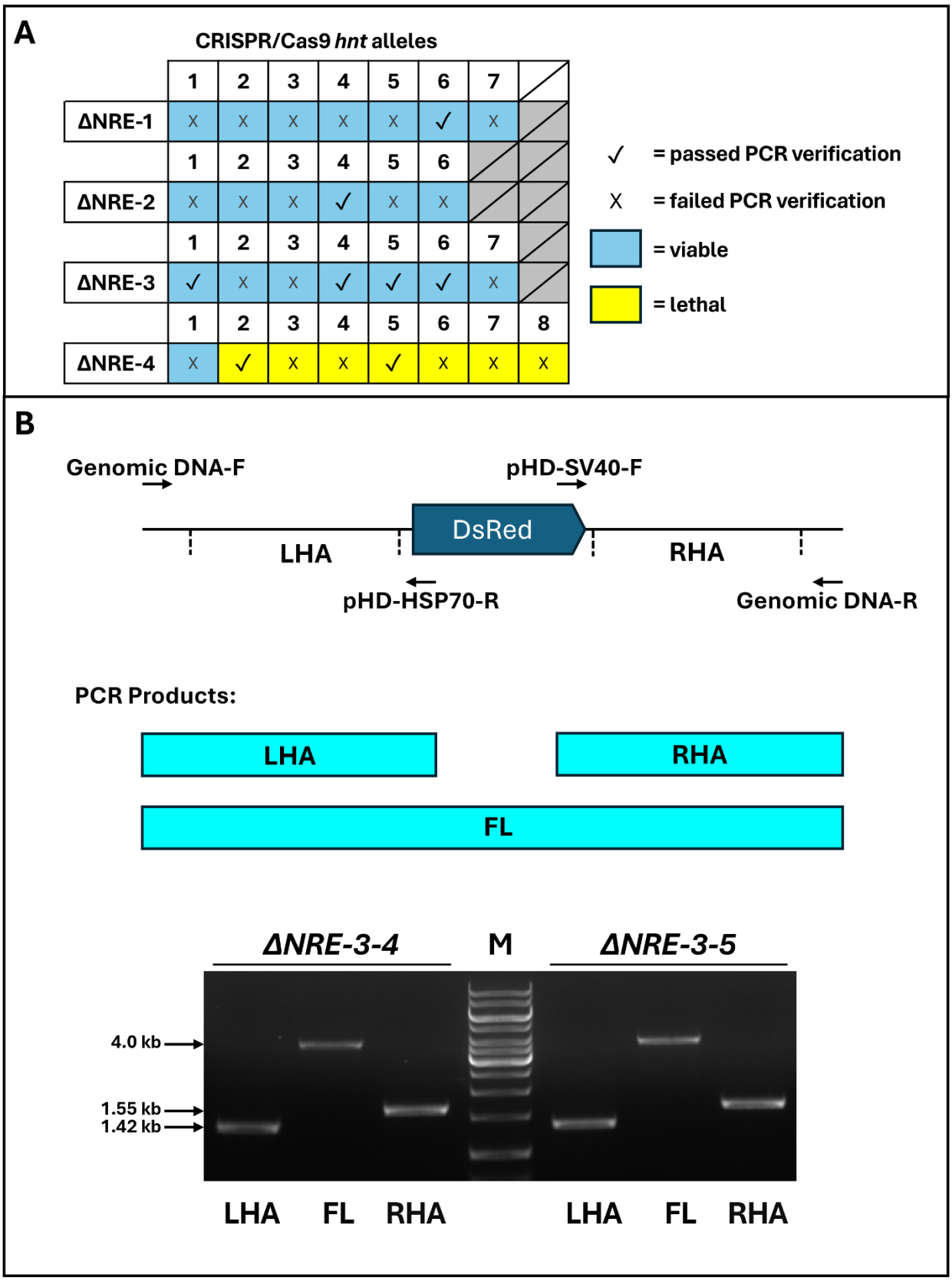

A
CRISPR/Cas9 hnt alleles
1 2 3 4 5 6 7
ΔNRE-1 X X X X X ✓ X
1 2 3 4 5 6
ΔNRE-2 X X X ✓ X X
1 2 3 4 5 6 7
ΔNRE-3 ✓ X X ✓ ✓ ✓ X
1 2 3 4 5 6 7 8
ΔNRE-4 X ✓ X X ✓ X X X
✓ = passed PCR verification
X = failed PCR verification
= viable
= lethal
B
Genomic DNA-F
pHD-SV40-F
DsRed
LHA
RHA
pHD-HSP70-R
Genomic DNA-R
PCR Products:
LHA
RHA
FL
ΔNRE-3-4
M
ΔNRE-3-5
4.0 kb
1.55 kb
1.42 kb
LHA FL RHA
LHA FL RHA

Figure 3.2 CRISPR/Cas9 ΔNRE mutant verification. (A) Table summarizing all isogenic *FM7i* balanced potentially mutant stocks (28 in total) received from BestGene Inc. injection services (NRE1 = 7 stocks; NRE2 = 6 stocks; NRE3 = 7 stocks; NRE4 = 8 stocks). Based on the presence or absence of hemizygous males lacking the *FM7i* balancer chromosome (*Bar*$^{+}$), stocks were scored as viable (blue boxes) or lethal (yellow boxes), respectively. Stocks that were confirmed as *bona fide* by PCR analysis are shown by checkmarks within their boxes and stocks that did not pass the PCR analysis are marked with an (x) inside their boxes. (B) Illustration of the PCR strategy (adapted from Gratz et al., 2015) used to confirm *hnt* mutant alleles showing data from analysis of *ΔNRE-3-4* and *ΔNRE-3-5* as examples. The two outermost primers were designed based on genomic DNA sequence on either side of the left and right homology arms sequences, while the two other innermost primers were designed based on sequences within the HDR donor vector. Alleles were considered verified if PCR products (cyan) representative of the left homology arm (LHA), right homology arm (RHA), and full length (FL) were produced and matched the expected sizes. Successful PCR amplification of the LHA and RHA indicates successful insertion of the *3xP3-DsRed* marker at the target site, while the FL product is only expected as a PCR product (here ~4 kb in size) if the ~5 kb target sequence has been successfully deleted.

3.2.3 *3xP3-DsRed* insertions function as enhancer traps in the *hnt* regulatory region

In the embryo, the 3xP3 promoter normally drives expression in Bolwig's organ and some PNS neurons (Fig. 3.3E) (Horn et al., 2000). To confirm correct function of the *3xP3-DsRed* insertion in the newly generated mutant lines, I screened embryos for DsRed expression in Bolwig's organ and PNS neurons. I found that DsRed was expressed as expected in those tissues, but surprisingly, I also observed DsRed expression in additional patterns that resembled subsets of known endogenous *hnt* expression (Fig. 3.3A,F) (Yip et al., 1996; Wilk et al., 2000). This observation suggested that the inserted DsRed was functioning as an enhancer trap and was being expressed under the regulatory control of not only the 3xP3 insect promoter, but also *hnt* enhancer elements. The ability of *3xP3-DsRed* to function as an enhancer trap has been reported previously in *Bombyx mori* (silkworms), but this effect, to the best of my knowledge, has not been reported for Drosophila (Tsubota et al., 2014).

The expression patterns of DsRed in $hnt^{\Delta N1}$, $hnt^{\Delta N2}$, and $hnt^{\Delta N3}$ embryos commonly overlapped, where DsRed was observed in the amnioserosa (Fig. 3.3B-D), oenocytes, and chordotonal organs (Fig. 3.3H-J). In the case of $hnt^{\Delta N4}$, DsRed was observed predominantly in the tracheal system (Fig. 3.3K). The overlapping expression patterns between $hnt^{\Delta N1}$, $hnt^{\Delta N2}$, and $hnt^{\Delta N3}$embryos could indicate a redundancy in tissue specific enhancer elements, so-called shadow enhancers (Hong et al., 2008).

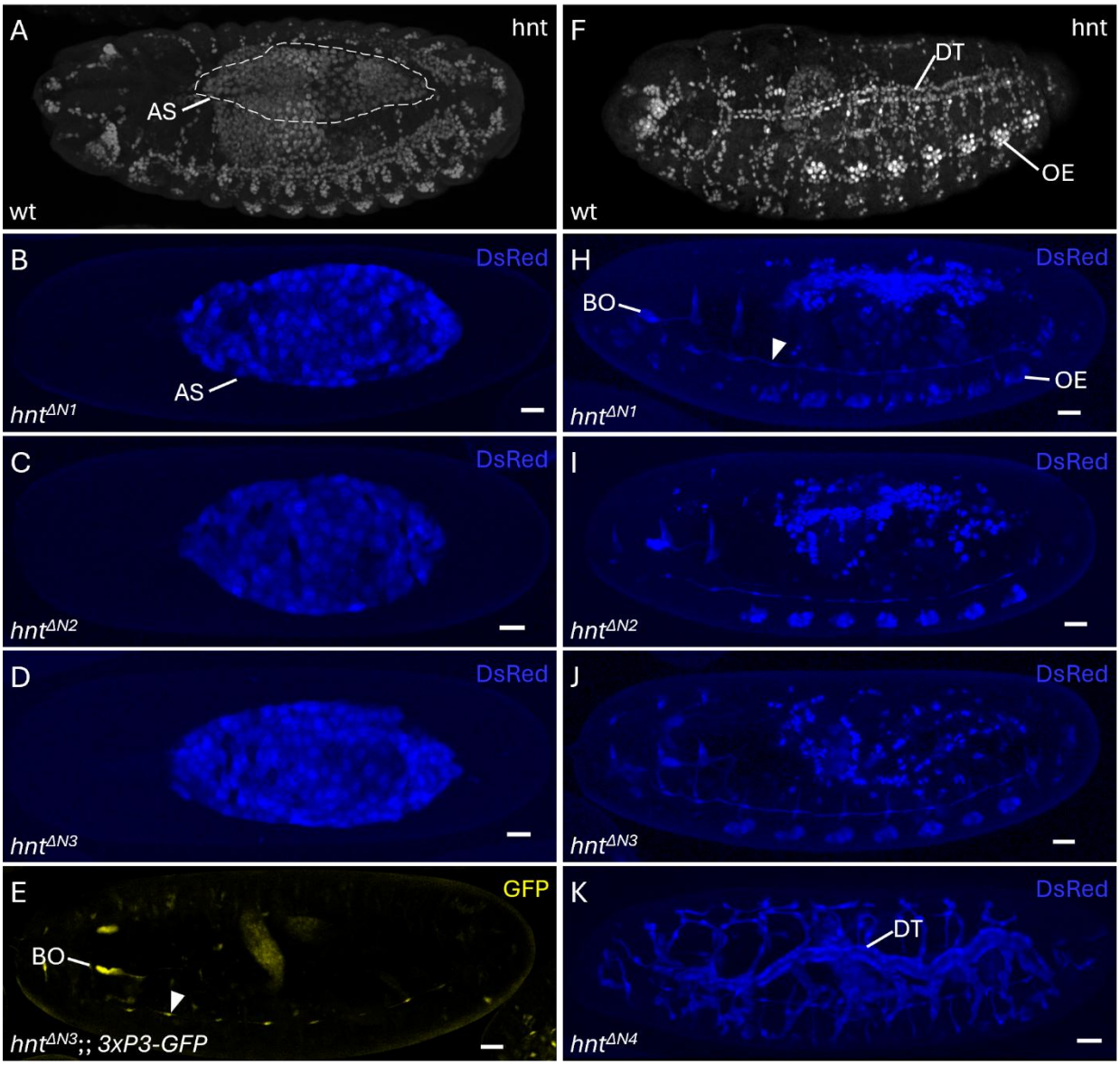

A
hnt
AS
wt
F
hnt
DT
OE
wt
B
DsRed
AS
hntΔN1
H
DsRed
BO
OE
hntΔN1
C
DsRed
hntΔN2
I
DsRed
hntΔN2
D
DsRed
hntΔN3
J
DsRed
hntΔN3
E
GFP
BO
hntΔN3;; 3xP3-GFP
K
DsRed
DT
hntΔN4

Figure 3.3 DsRed insertions into the *hnt* regulatory region function as enhancer traps. (A) Dorsal view of control wildtype embryo immunostained using anti-Hnt showing endogenous *hnt* expression in the amnioserosa (AS), as well as the trachea, developing midgut, and oenocytes. (B-D) Dorsal view of $hnt^{\Delta N1}$, $hnt^{\Delta N2}$, and $hnt^{\Delta N3}$ embryos showing presence of DsRed expression in the amnioserosa (AS) and lack of DsRed in other tissues where *hnt* is normally expressed, such as the tracheal system. $hnt^{\Delta N4}$ did not express DsRed in the amnioserosa at this stage and is not shown. (E) Dorsolateral view of late-stage $hnt^{\Delta N3}$ embryo that also carried a control *3xP3-GFP* insert on the 3^{rd}-chromosome showing the expected GFP expression under control of the 3xP3 promoter in Bolwig's organ (BO) and a group of PNS neurons (arrowhead). (F) Lateral view of late-stage control wildtype embryo immunostained using anti-Hnt showing endogenous *hnt* expression in the tracheal system (DT = dorsal trunk), and robust expression in the oenocytes (OE) as well as many other cell types. (H-J) Lateral view of late-stage $hnt^{\Delta N1}$, $hnt^{\Delta N2}$, and $hnt^{\Delta N3}$ embryos showing the expected DsRed expression in BO and lateral neurons (arrowhead) as well as the unexpected expression in the degenerating amnioserosa, the PNS, and the OE. Tracheal expression in these lines was not observed. (K) Lateral view of late-stage $hnt^{\Delta N4}$ embryo showing prominent DsRed expression throughout the tracheal system and PNS, but not in the amnioserosa or oenocytes. All scale bars represent 20 μm.

3.2.4 Spurious *3xP3-DsRed* insertions are expressed in typical *hnt* expression patterns

Two sibling lines of the selected deletion mutants, $hnt^{\Delta N1\text{-}5}$ and $hnt^{\Delta N4\text{-}1}$, did not pass the PCR allele screen, suggesting that the insertion of the *3xP3-DsRed* cassette had not gone according to plan (Fig. 3.1B). Curiously, these spurious lines were found to express DsRed so vibrantly as to be visible to the naked eye in adults and some larval stages (Fig. 3.4E). Embryos, larvae, and pupae from these two spurious lines, $hnt^{\Delta N1\text{-}5}$ and $hnt^{\Delta N4\text{-}1}$, were examined for DsRed expression (summarized in Fig. 3.4).

The spurious $hnt^{\Delta N4\text{-}1}$ allele was found to express DsRed in the developing adult oenocytes, developing indirect flight muscles, and sensory organ cells (arrowheads, Fig. 3.4A-B), areas in which *hnt* expression has been detected independently using both GAL4 enhancer trap lines as well as immunostaining (Reedlab, unpublished observations). In both early (dorsal closure stage) and late-stage $hnt^{\Delta N4\text{-}1}$ embryos, DsRed was also observed in many endogenous *hnt* expression patterns, including the tracheal system, embryonic oenocytes, chordotonal organs, and PNS (Fig. 3.4D). Uniquely, the spurious $hnt^{\Delta N4\text{-}1}$ allele was found to express DsRed in the embryonic amnioserosa (Fig. 3.4C), whereas the *bona fide* $hnt^{\Delta N4}$ allele did not, as mentioned above, show any amnioserosa expression.

Similarly, $hnt^{\Delta N1\text{-}5}$ was found to express DsRed in the posterior midgut of the 3rd larval instar (Fig. 3.4E-F) whereas the sibling line $hnt^{\Delta N1}$ did not display this pattern of expression.

An explanation for these spurious inserts and their expression patterns is discussed in Chapter 5 (see section 5.2.1).

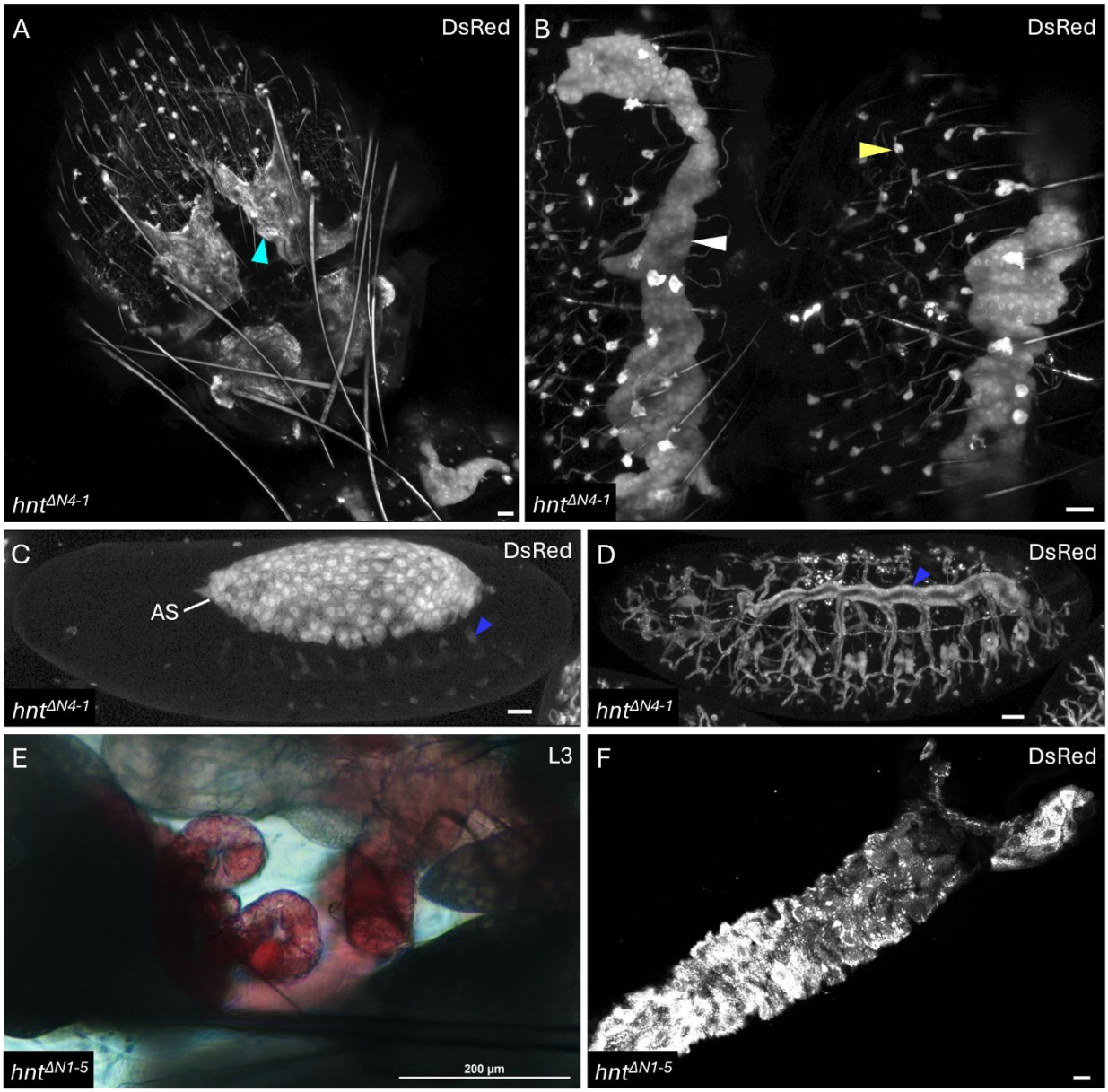

A
DsRed
hntΔN4-1
B
DsRed
hntΔN4-1
C
DsRed
AS
hntΔN4-1
D
DsRed
hntΔN4-1
E
L3
hntΔN1-5
200 µm
F
DsRed
hntΔN1-5

Figure 3.4 DsRed expression patterns of spurious CRISPR mutations. Confocal images of *3xP3-DsRed* expression patterns in spurious ΔNRE lines. (A) Dorsal view of late $hnt^{\Delta N4\text{-}1}$ pupa dissected from pupal case showing DsRed expression in areas of the notum and scutellum, including the developing indirect flight muscles (cyan arrowhead) and the sensory organ precursors (SOP) of microchaetae and macrochaetae. Signal within the developing bristle shafts is associated with autofluorescence. (B) Dorsal view of developing abdominal segments of late $hnt^{\Delta N4\text{-}1}$ pupa showing SOP expression (yellow arrowhead) and expression in the developing adult oenocytes (white arrowhead). (C) Lateral view of a dorsal closure stage $hnt^{\Delta N4\text{-}1}$ embryo showing strong DsRed expression in the amnioserosa (AS) that was not observed in embryos of its sibling line $hnt^{\Delta N4}$ and developing tracheal system (blue arrowhead). (D) Lateral view of a late-stage $hnt^{\Delta N4\text{-}1}$ embryo showing strong DsRed expression in many tissues and cell types associated with endogenous *hnt* expression, including the tracheal system (blue arrowhead), oenocytes, as well as many cell types of the PNS. (E) Dorsal brightfield image of a wandering $hnt^{\Delta N1\text{-}5}$ third instar larva showing extremely strong DsRed expression in the midgut that is frequently visible to the naked eye without fluorescence microscopy. Dorsal trunk of trachea is out of focus in the foreground. (F) Dissected posterior midgut of third instar larval $hnt^{\Delta N1\text{-}5}$ showing extremely strong DsRed expression. All scale bars represent 20 μm, except as indicated in (E).

3.2.5 Complementation test cross of $hnt^{\Delta N4}$ allele to hnt^{XE81} allele

Since $hnt^{\Delta N4}$ was the only lethal NRE deletion mutant recovered, I performed a complementation cross with hnt^{XE81} as previously described (Ng et al., 2020) in order to genetically verify $hnt^{\Delta N4}$ as a *hnt* allele, and to confirm the PCR results. In Drosophila genetics, a complementation test of an *X*-linked lethal mutation requires the availability of an *X;autosome* duplication (i.e. *Dp(1;2)*, *Dp(1;3)*, or *Dp(1;4)*). The hnt^{XE81} allele is characterized as a strong hypomorphic embryonic lethal (Yip et al., 1997) and is completely rescued by a *Dp(1;3)* associated with $peb^{BAC\text{-}CH321\text{-}46J02}$ (peb^{BAC}). Briefly, peb^{BAC} represents a duplication (*Dp(1;3)*) of a ~97 kb genomic fragment (co-ordinates X:4,551,841…4,648,822) cloned into a BAC vector, which carries the *mini-white* marker gene ([w^+]) in a white-eye background, and is inserted into the *attP2* site on the 3^{rd}-chromosome. $Dp(1;3)peb^{BAC}$ complements all *hnt* alleles tested so far, including hnt^{XE81}.

I performed a complementation test by crossing $y\ w^{1118}\ hnt^{\Delta N4}/FM7i,\ B$ virgin females to $y\ w^{1118}\ hnt^{XE81}/Y;;\ peb^{BAC}/\ TM6C,\ Sb$ males and scoring (inner box, Fig. 3.5) the resulting F1 progeny. Presence of $B^+\ Sb^+$ [w^+] males (yellow box, Fig. 3.5) indicated that peb^{BAC} complemented and rescued $hnt^{\Delta N4}$ hemizygous lethality. The absence of $y\ w^{1118}$; $B^+\ Sb$ females (blue box, Fig. 3.5) signified that $hnt^{\Delta N4}$ failed to genetically complement hnt^{XE81}, providing further evidence that $hnt^{\Delta N4}$, which is a ~5 kb deletion 38 kb upstream of the *hnt* transcription start site, behaves as a loss-of-function *hnt* allele.

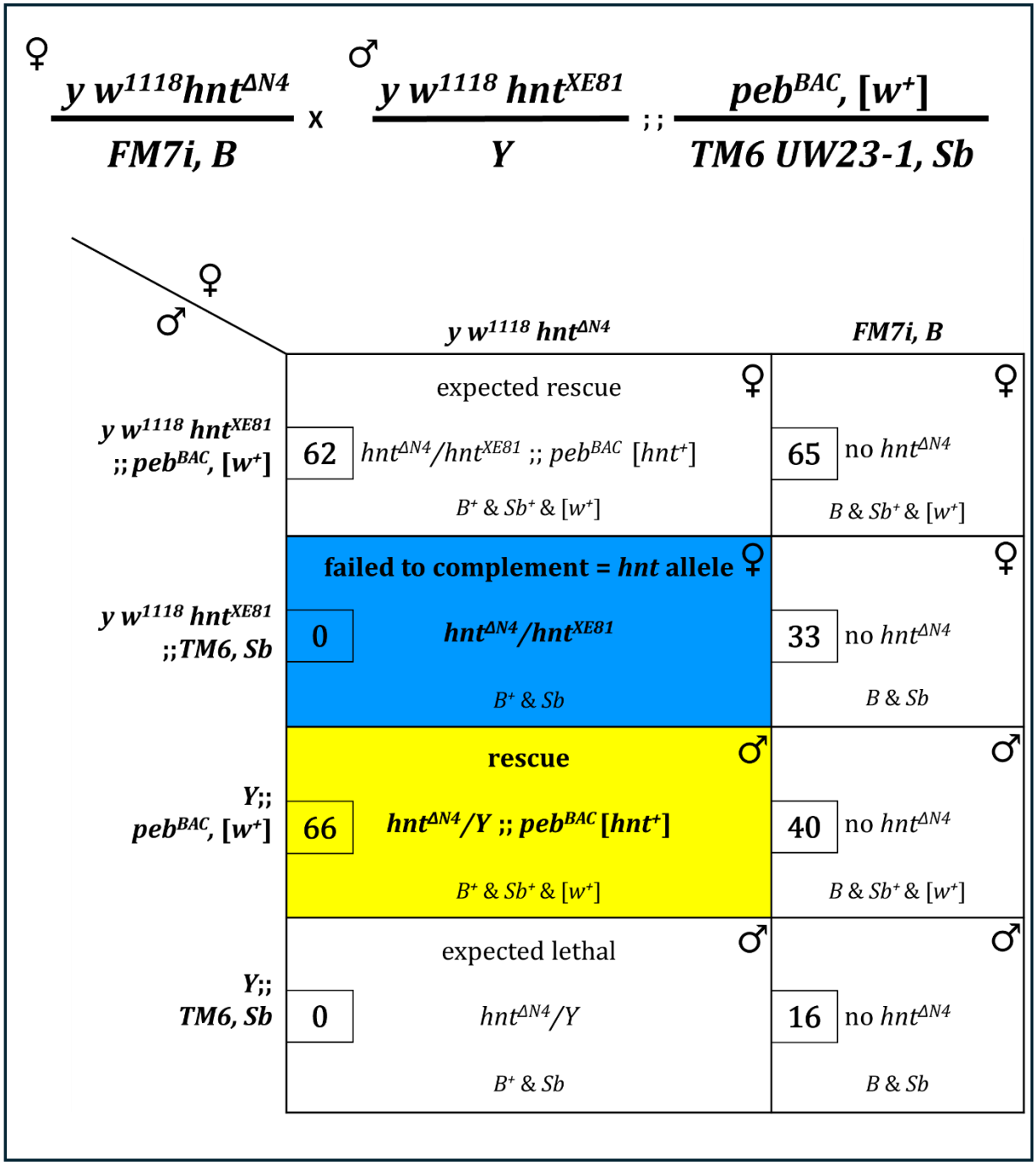

♀ y w1118 hntΔN4 / FM7i, B x ♂ y w1118 hntXE81 / Y ;; pebBAC, [w+] / TM6 UW23-1, Sb
♀
♂
y w1118 hntΔN4
FM7i, B
y w1118 hntXE81 ;; pebBAC, [w+]
y w1118 hntXE81 ;;TM6, Sb
Y;; pebBAC, [w+]
Y;; TM6, Sb
expected rescue
62
hntΔN4/hntXE81 ;; pebBAC [hnt+]
B+ & Sb+ & [w+]
65
no hntΔN4
B & Sb+ & [w+]
failed to complement = hnt allele
0
hntΔN4/hntXE81
B+ & Sb
33
no hntΔN4
B & Sb
rescue
66
hntΔN4/Y ;; pebBAC [hnt+]
B+ & Sb+ & [w+]
40
no hntΔN4
B & Sb+ & [w+]
expected lethal
0
hntΔN4/Y
B+ & Sb
16
no hntΔN4
B & Sb

Figure 3.5 $hnt^{\Delta N4}$ fails to complement hnt^{XE81}. A Punnett square is shown outlining the genetic complementation test that was performed to verify $hnt^{\Delta N4}$ as an allele of *hnt*. $hnt^{\Delta N4}$ virgin females were crossed to males carrying the strong hypomorphic embryonic lethal hnt^{XE81} allele on the *X*-chromosome in the background of peb^{BAC}, a duplication whereby a 97 kb *X*-chromosome hnt^{+} fragment is carried on the 3^{rd}-chromosome. F1 progeny were scored and tallied (inner boxes) by sex and inherited dominant markers for the *X* and 3^{rd} balancer chromosomes (*B* and *Sb,* respectively) as well as the peb^{BAC} [w^{+}] marker. peb^{BAC} was shown to complement and rescue the $hnt^{\Delta N4}$ allele (presence of hemizygous males, yellow box) and $hnt^{\Delta N4}$ failed to complement hnt^{XE81} (absence of $hnt^{\Delta N4}/hnt^{XE81}$ trans-heterozygous females, blue box). $hnt^{\Delta N4}$ is, therefore, genetically defined as a mutant allele of *hnt*.

3.2.6 *hnt$^{\Delta N4}$* phenotype is not associated with embryonic lethality

Of the NRE deletions that were recovered and confirmed, only the *hnt$^{\Delta N4}$* allele was associated with lethality and failed to complement *hnt^{XE81}* (Fig. 3.5). Since the classical phenotype of *hnt* embryonic lethal alleles is failure in GBR (Yip et al., 1997), I re-balanced *hnt$^{\Delta N4}$* over *FM7h, twi-GAL4 + UAS-GFP* to incorporate an embryonic fluorescent screening marker (Fig. 3.6A) and examined *hnt$^{\Delta N4}$* mutant embryos, identified by absence of GFP expression, for similar embryonic phenotypes. The *hnt$^{\Delta N4}$* mutant showed no evidence of failure in GBR and was found to successfully complete embryogenesis with no observed difference of hatching rates in mutants (Fig. 3.7A). However, occasional *hnt$^{\Delta N4}$* L1 larval mutants displayed a mild "tail-up" phenotype (data not shown), where the posterior segment of the animal is fixed in a vertical position instead of the usual posterior position, a phenotype that has been observed in hypomorphic *hnt* alleles and GBR mutants (Yip et al., 1997; Frank & Rushlow, 1996).

Given that there is no difference between mutant and control embryonic hatching rates (Fig. 3.7A), I concluded that the lethal phase of *hnt$^{\Delta N4}$* must be associated with the larval/pupal stages. To test this hypothesis, I rebalanced the mutant *hnt$^{\Delta N4}$* allele over an *FM7c, 2x-RFP, Tb* balancer (Fig. 3.6B). The *Tubby* (*Tb*) dominant marker manifests as a cuticle phenotype generating short and stocky larvae and pupae, therefore, hemizygous *hnt$^{\Delta N4}$* mutants (*Tb^{+}*) are easily identified by a wildtype cuticle and body length (Guan et al., 2006). I observed that *Tb^{+}* mutants were largely growth arrested or dead at early larval stages, and appeared small, largely immobile, and dispersed away from food sources, a behaviour observed in larvae under hypoxic conditions (Wingrove & O'Farrell, 1999).

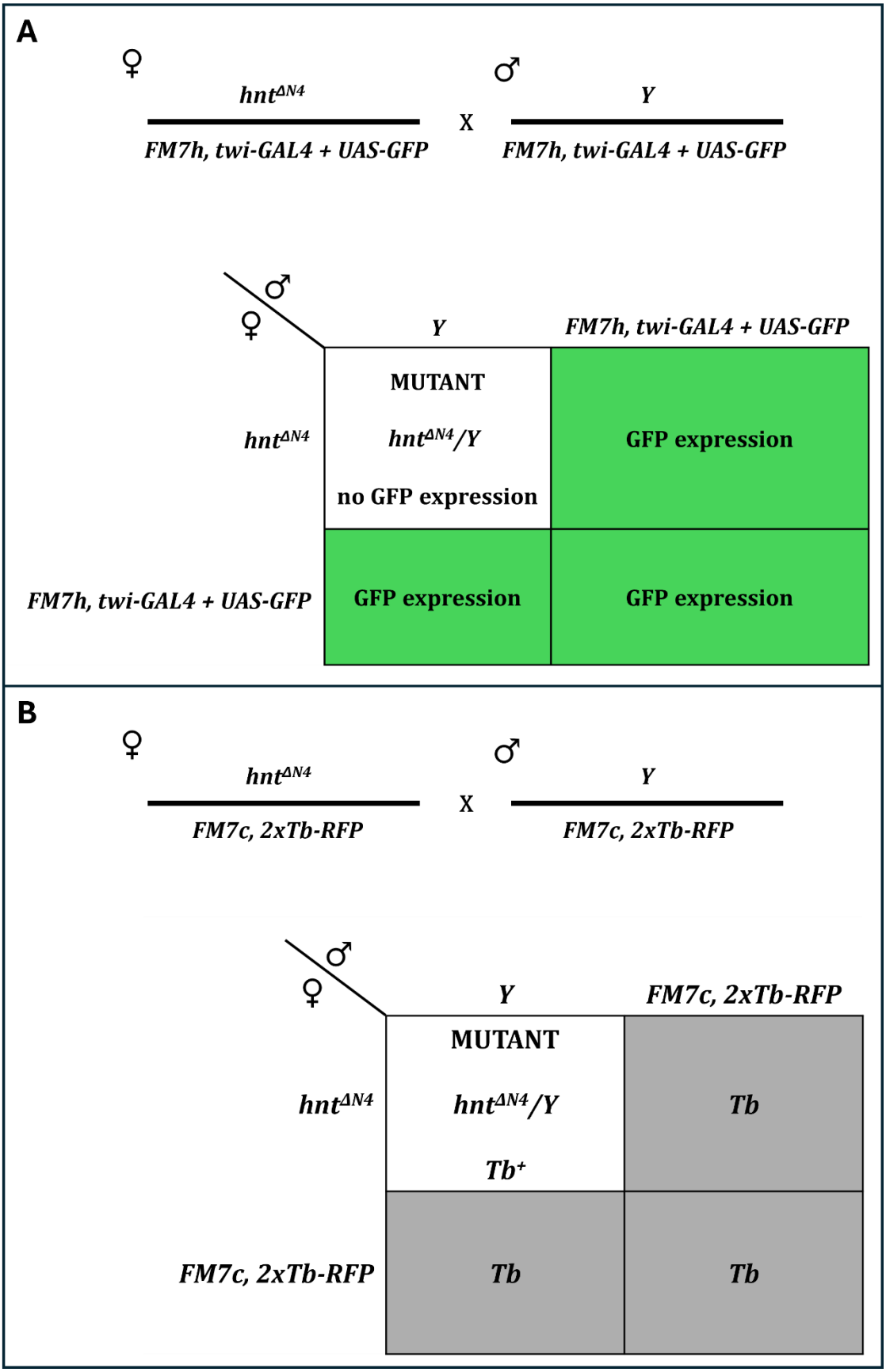

A
♀
hnt^ΔN4
FM7h, twi-GAL4 + UAS-GFP
X
♂
Y
FM7h, twi-GAL4 + UAS-GFP
♂
♀
Y
FM7h, twi-GAL4 + UAS-GFP
MUTANT
hnt^ΔN4/Y
no GFP expression
GFP expression
hnt^ΔN4
FM7h, twi-GAL4 + UAS-GFP
GFP expression
GFP expression
B
♀
hnt^ΔN4
FM7c, 2xTb-RFP
X
♂
Y
FM7c, 2xTb-RFP
♂
♀
Y
FM7c, 2xTb-RFP
MUTANT
hnt^ΔN4/Y
Tb+
Tb
hnt^ΔN4
FM7c, 2xTb-RFP
Tb
Tb

Figure 3.6 Punnett square diagrams of crosses used to identify *hnt$^{\Delta N4}$* mutants. (A) *hnt$^{\Delta N4}$/FM7i* was re-balanced using *FM7h, twi-GAL4 + UAS-GFP* to introduce a selectable embryonic screening marker. The *FM7h, twi-GAL4 + UAS-GFP* "green balancer" chromosome induces expression of *GFP* under regulatory control of the gene *twist,* which is strongly expressed in the developing mesoderm. Once the stock was established, *hnt$^{\Delta N4}$* mutant embryos were identified by the absence of strong mesodermal GFP expression in contrast to balancer sibs. (B) *hnt$^{\Delta N4}$/FM7i* was re-balanced using *FM7c, 2xTb-RFP* to introduce the dominant and selectable larval stage marker, *Tb*. *hnt$^{\Delta N4}$* mutant larvae (*Tb^{+}*) were readily identified by wildtype body shape while sibling progeny exhibited the *Tb* marker phenotype, possessing shorter and stockier larval and pupal body shape.

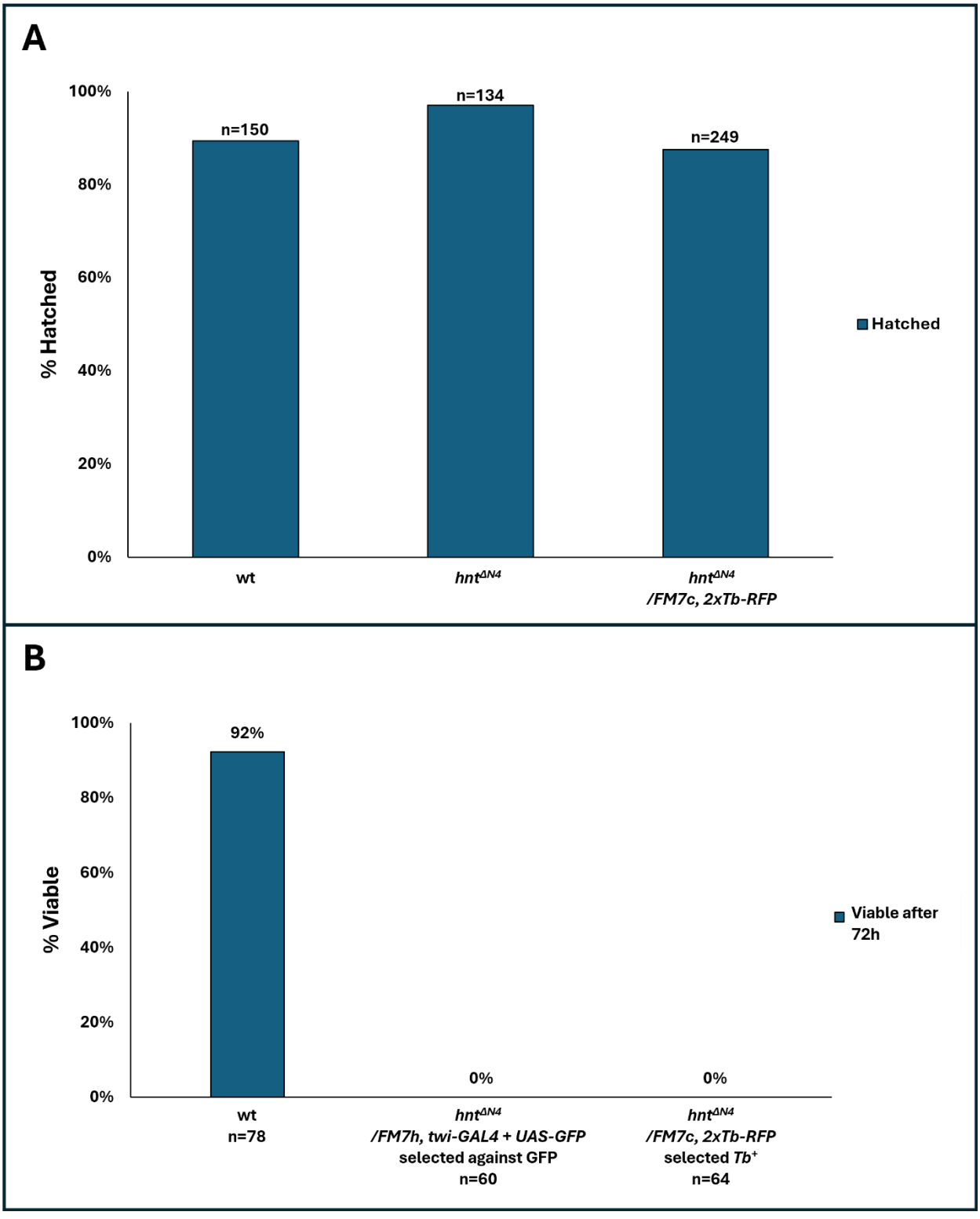

A
100%
80%
60%
40%
20%
0%
% Hatched
n=150
n=134
n=249
wt
hntΔN4
hntΔN4
/FM7c, 2xTb-RFP
Hatched
B
100%
80%
60%
40%
20%
0%
% Viable
92%
0%
0%
wt
n=78
hntΔN4
/FM7h, twi-GAL4 + UAS-GFP
selected against GFP
n=60
hntΔN4
/FM7c, 2xTb-RFP
selected Tb+
n=64
Viable after
72h

Figure 3.7 Embryonic Lethality and Viability Assay of CRISPR/Cas9 induced mutants. (A) Bar graph showing embryonic lethality assay data of $hnt^{\Delta N4}$ genotypes. Embryos were collected over a two-hour period, incubated at 25°C for 48 hours and scored for failed embryos. Embryonic lethality percentages of control wildtype, $hnt^{\Delta N4}$, and $hnt^{\Delta N4}$*/FM7c, 2xTb-RFP*, are represented in navy. ΔNRE-4 deletion did not negatively affect embryonic viability rates compared to controls. (B) Bar graph indicating the viability of selected $hnt^{\Delta N4}$ mutants, showing the lethality of $hnt^{\Delta N4}$ phenotypes was fully penetrant and demonstrated that the mutant phenotype can be selected. Mutant $hnt^{\Delta N4}$ embryos were identified by the absence of late-stage GFP expression and mutant $hnt^{\Delta N4}$ larvae were selected for Tb^{+}. Control wildtype embryo and larvae of similar stages were collected in matching conditions. The selected mutant and control individuals were scored for lethality approximately 72 hours after egg-laying and in both selected mutant groups, 0% of the selected mutants were found alive 72 hours after egg-laying (navy).

3.2.7 *hnt*$^{\Delta N4}$ mutants exhibit lethal larval tracheal phenotypes

hnt$^{\Delta N4}$ mutants can be selected based on symptomatic hypoxic behaviours in larvae or by screening for the absence of dominant markers as described above (Fig. 3.7B) (Wingrove & O'Farrell, 1999). As such, I performed a preliminary investigation of first instar mutant larvae using DIC imaging to identify visible phenotypes (Fig. 3.8). The most prominent phenotype of L1 *hnt*$^{\Delta N4}$ mutant larvae was the complete collapse of all tracheal branches shortly after hatching, which displayed a relatively high penetrance, being observed in the majority of *hnt*$^{\Delta N4}$ mutants (81.7%, Fig. 3.8F). DIC imaging of these larvae revealed areas along the collapsed dorsal trunk (DT) where the taenidia were crushed and warped (yellow arrows, Fig. 3.8B). These crushed taenidial fold zones were observed more frequently towards the posterior and were often, but not always, located at the junctions between the DT and dorsal branches (DB) or transverse connective (TC) branches (Fig. 3.8B-D). The taenidial folds of *hnt*$^{\Delta N4}$ mutants were also observed to be disorganized (Fig. 3.8C), and not conforming to parallel rings as is observed in wildtype larvae. Mutants with a completely collapsed tracheal system were not observed beyond the L1 stage (Fig. 3.8F).

Some *hnt*$^{\Delta N4}$ mutants (18.3%, Fig. 3.8F) were observed to display a phenotype of partial collapse of their tracheal system; such individual mutants were able to survive and were observed to progress to the L2 (second larval instar) stage (Fig. 3.8E). The inflated regions of the L2 escapers were found to be inconsistent and randomly distributed. However, the shape of the cuticle in adjacent deflated airways suggested that the collapse had "pinched" off the airway, allowing for partial tracheal inflation. These L2 larvae were observed to display defective cuticle shedding, often resulting in the molted cuticle becoming trapped near the mouthhooks at lateral spiracles (sometimes referred to as the

spiracular branch) (cyan arrowhead, Fig. 3.8E). These L2 mutant escapers were never observed as L3 stage larvae.

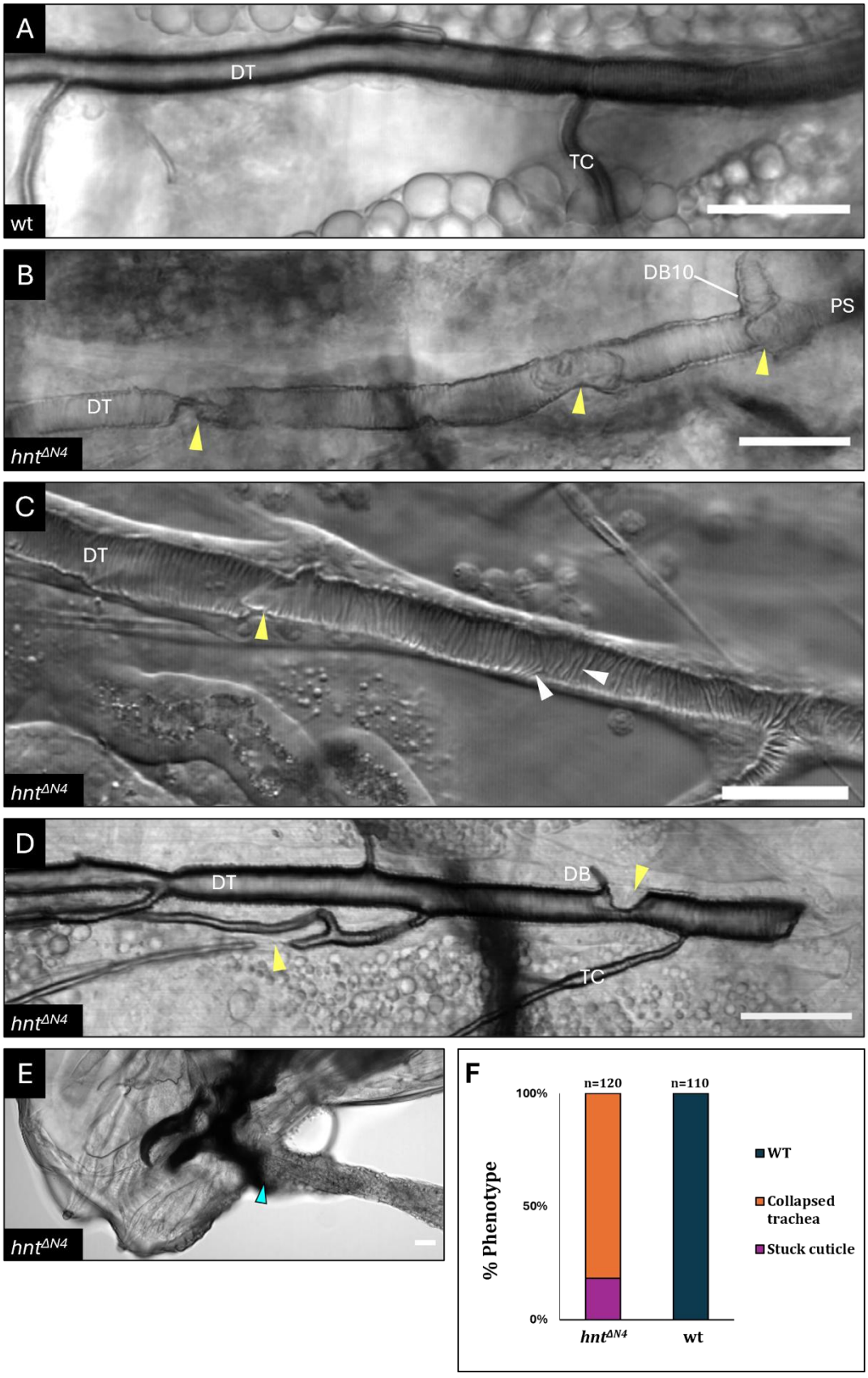

A
DT
TC
wt
B
DB10
PS
DT
hntΔN4
C
DT
hntΔN4
D
DT
DB
TC
hntΔN4
E
hntΔN4
F
100%
50%
0%
% Phenotype
n=120
n=110
WT
Collapsed trachea
Stuck cuticle
hntΔN4
wt

Figure 3.8 *hnt*$^{\Delta N4}$ mutants exhibit lethal tracheal phenotypes. DIC brightfield projection imaging of *hnt*$^{\Delta N4}$ larvae revealed tracheal phenotypes. (A) Lateral view of control wildtype L1 larva showing an intact and inflated tracheal system. (B) Dorsal view of a L1 *hnt*$^{\Delta N4}$ mutant larva showing a completely collapsed tracheal system and several broken or warped sections of the dorsal trunk (DT) (yellow arrowheads). Broken sections were more frequent and severe towards the posterior near the intersection between DB10 and the DT, and at transverse connective (TC) or dorsal branch (DB) junctions. DB10 is the most posterior dorsal branch and uniquely larger than other dorsal branches. The posterior spiracle (PS) connects to the DT and serves as a site for gas exchange. (C) DIC imaging of the apical taenidial folds in deflated DT segments of *hnt*$^{\Delta N4}$ L1 larvae revealed an uncharacteristic warping and general disorganization (white arrowheads). (D) Lateral view of L1 *hnt*$^{\Delta N4}$ mutant tracheal system shortly after hatching showing early breaks in the tracheal system (yellow arrowhead), leading to gas escaping through broken segments. (E) DIC imaging of an L2 *hnt*$^{\Delta N4}$ mutant with a molted cuticle that remained attached near the mouthhooks at a lateral spiracle (cyan arrowhead) instead of being properly shed. (F) Stacked bar graph indicating the tracheal phenotype penetrance in both *hnt*$^{\Delta N4}$ mutants and control wildtypes. Approximately 81.7% of mutant L1 larvae exhibited completely collapsed trachea (orange) while the other 18.3% of larvae progressed to the L2 stage and possessed only partially collapsed trachea and stuck cuticle (magenta). Control wildtype larvae did not exhibit any of the tracheal phenotypes described above (navy). All scale bars represent 20 μm.

Chapter Four:

In the Context of the Developing Tracheal System, Hnt is Required for Subcellular Organization of Actin and is Downstream of Notch Signalling

4.1 Overview

In the previous chapter, initial characterization of the CRISPR/Cas9 induced deletion alleles revealed that *hnt*$^{\Delta N4}$ was the only recovered deletion allele associated with lethality and exhibited notable tracheal phenotypes. Since *hnt* has been previously associated with tracheal defects, this warranted a deeper analysis of the different components of the late embryonic tracheal system and how they might relate to Notch and Hnt interactions (Wilk et al., 2000). Given that apical F-actin in tracheal cells determines the future shape of taenidial folds (Matusek et al., 2006), *hnt*$^{\Delta N4}$ mutant embryos were analyzed for underlying F-actin organization defects. The subcellular F-actin was found to be generally disorganized and absent in several zones interspersed along the DT. This finding suggests the observed larval taenidial fold defects are a result of underlying F-actin organization defects in embryonic tracheal cells.

Analysis of the closely related *Peb1* gene reporter construct indicated that the NRE-4 DNA region of *hnt* drives expression in transverse connective junction (TCJ) cells, DT, and a unique row of ventral PNS cells. To assess if this observation correlates with a decrease in *hnt* expression these specific tissues, *hnt*$^{\Delta N4}$ mutant embryos were immunostained using a Hnt antibody. *hnt* expression was notably reduced in the DT and TCJ/PNS cells.

To assess if *hnt* expression is Notch-dependent in these novel contexts, I performed CRISPR/Cas9 mutagenesis and Notch knockdown experiments. Direct mutation of the NRE-4 Su(H) consensus sequence caused subtle and variable tracheal phenotypes and knockdown of Notch signalling using a temperature sensitive allele, *N*^{ts}, resulted in a

notable reduction of *hnt* expression in the TCJ cells. Together, these results reveal the tracheal TCJ cells as a novel context in which *hnt* expression is Notch regulated.

4.2 Results

4.2.1 *Peb1* gene reporter constructs are expressed in the developing tracheal system and a single cell type of the PNS

A *Peb1* reporter construct was previously developed and used to investigate the relationship between *hnt*, *lozenge*, and Notch signalling in hemocytes and crystal cells. While previous work using this reporter construct focused on *hnt* expression in the context of the larval lymph gland and the differentiation of crystal cells (Terriente-Felix et al., 2013), there has been no previous report of expression of this reporter construct in the developing embryonic tracheal system.

This *Peb1* reporter uses an ~1.9 kb fragment of *hnt* regulatory sequence that was amplified and cloned upstream of a fluorescent reporter gene (*Peb1-GFP* or *Peb1-mCherry*) (Fig. 4.1A) (Terriente-Felix et al., 2013; Zacharioudaki & Bray, 2014). This 1.9 kb sequence maps within the NRE-4 deletion and as such, reporter gene expression from this construct could reveal cells or tissues that are under regulatory control of enhancer elements associated with the NRE-4 region (Fig. 4.1A). Since the *Peb1* enhancer sequence includes the Su(H) consensus binding sequence that was targeted in this study, then any observed expression patterns are potentially Notch dependent (Fig. 4.1A).

I discovered the *Peb1*-reporter gene construct to be expressed in the developing trachea as early as embryonic stage 11 in the invaginating tracheal placodes (Fig. 4.1B). Expression of *Peb1* reporter constructs was also found to continue during primary branching and DT fusion. Furthermore, the *Peb1* reporter construct expression was strongest in the DT and TC branches with weaker expression in the neighbouring DBs and

lateral trunks (Fig. 4.1C-D). Beginning at stage 14/15, the *Peb1* reporter gene was found to be more strongly expressed in a specific set of tracheal cells found at the junction between the DT and TC branches – here referred to as transverse connective junction (TCJ) cells (Fig. 4.1E-F). The TCJ cells are located towards the posterior side of the TC and are in contact with the DT fusion cell (Fig. 4.1G). Towards the end of embryogenesis, robust *Peb1* expression was also detected in the DT where it connected to the posterior spiracles (Fig.4.1F).

At embryonic stage 15/16, *Peb1* reporter construct expression was also observed in a row of 7 PNS cells (Fig. 4.1E,H,I), and this very specific (but mysterious) expression pattern most likely corresponds not to cells of the tracheal system, but to part of the PNS v'esA cell cluster (Appendix, Fig. A2) based on approximate positioning (Brewster & Bodmer, 1995; Richter et al., 2025; Wilk et al., 2000). For example, during late embryonic and larval stages, the mystery PNS cells (Fig. 4.1H-I") were observed adjacent to the cuticle surface and the molting pore (white arrowhead, Fig. 4.1I"). Additionally, my interpretation of the mystery *Peb1* expressing cells in question as belonging to the PNS, and not being part of the tracheal system, was further supported by the observation that these cells enclose the dendritic body (white arrowhead, Fig. 4.1I') of the sensory organ neuron (yellow arrowhead, Fig. 4.1I") that extends to the molting pore structure, which provides mechanoreceptor functions (Richter et al., 2025). The observed position and morphology suggests that these cells are not components of the tracheal system and strongly suggests that some *Peb1* reporter construct expression is associated with cells of the developing PNS.

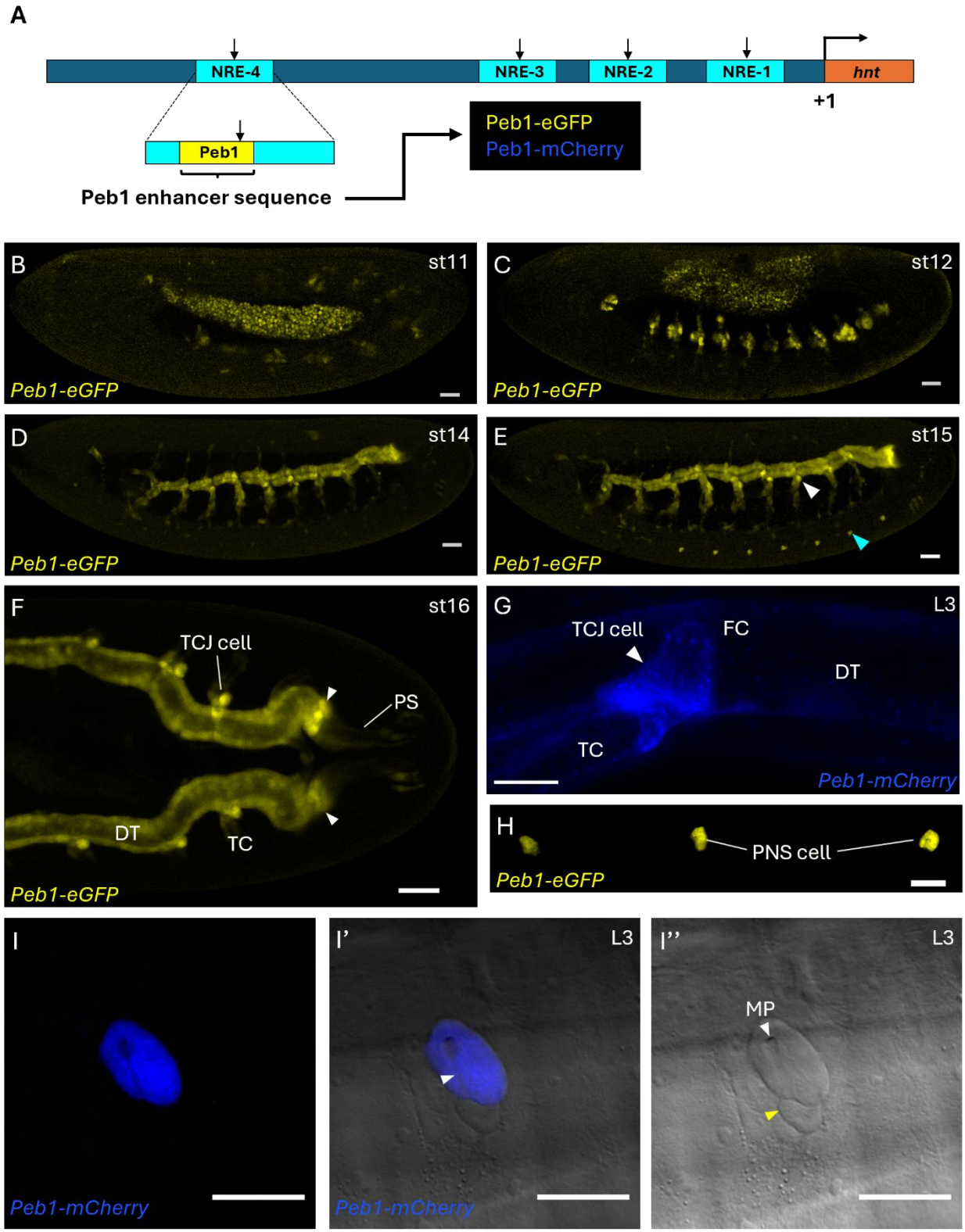

A
NRE-4
NRE-3
NRE-2
NRE-1
hnt
+1
Peb1
Peb1 enhancer sequence
Peb1-eGFP
Peb1-mCherry
B
st11
Peb1-eGFP
C
st12
Peb1-eGFP
D
st14
Peb1-eGFP
E
st15
Peb1-eGFP
F
st16
TCJ cell
PS
DT
TC
Peb1-eGFP
G
L3
TCJ cell
FC
DT
TC
Peb1-mCherry
H
PNS cell
Peb1-eGFP
I
Peb1-mCherry
I'
L3
Peb1-mCherry
I''
L3
MP

Figure 4.1 Embryonic expression of the *Peb1* reporter construct. (A) Schematic indicating the *hnt* regulatory sequence used to construct the *Peb1-eGFP* and *Peb1-mCherry* reporter constructs (Terriente-Felix, et al., 2013; Zacharioudaki & Bray, 2014). The *Peb1* sequence (yellow) maps to the NRE-4 sequence that was removed through CRISPR mutagenesis to generate the $hnt^{\Delta N4}$ allele. *Peb1* sequence also contains the NRE-4 Su(H) consensus binding sequence targeted for deletion (black arrows). (B-I") Confocal live-imaging microscopy was performed on embryos and larvae expressing the *Peb1* reporter construct. (B) Lateral view of embryonic stage 11 showing *Peb1* reporter expression in the invaginating tracheal placodes. Yolk autofluorescence was also evident at this stage. (C) *Peb1* reporter expression continued in the tracheal primordium as primary branching takes place, particularly in the nascent migrating DT branches. (D) Subsequent to DT fusion at embryonic stage 14, *Peb1* reporter expression was prominently detected in the DT and TC branches, and faintly in the lateral trunks and DBs. (E) At stage 15, as the tracheal lumen initiates expansion, strong *Peb1* expression was observed in TCJ cells (white arrowhead) and a row of ventral PNS cells (cyan arrowhead). (F) Dorsal view of stage 16 embryo showing high *Peb1* reporter expression where the DT connects to the posterior spiracles (PS) (arrowhead). (G) Lateral view of third instar DT/TC junction showing robust expression of the *Peb1* reporter in the TCJ cell (arrowhead), situated adjacent to the fusion cell (FC). (H) Single step image of three ventral PNS cells with strong *Peb1* reporter expression in an L2 larva showing an internal structure in the rightmost PNS cell. (I-I") Single step lateral view of a single v' eso PNS cell with robust *Peb1* reporter expression (blue, I) showing an internal structure interpreted as a sensory cell dendrite (white

arrowhead, I') extending to the molting pore (MP) (white arrowhead, I") from the associated neuron (yellow arrowhead, I"). All scale bars represent 20 μm.

4.2.2 *Peb1* and NRE-4 sequence contain specific tracheal enhancer elements

The *Peb1-eGFP* reporter construct is carried on the second chromosome and is independent of the native *hnt* gene locus.

In contrast, the $hnt^{\Delta N4}$ line carries a *3xP3-DsRed* enhancer trap at the NRE-4 deletion site and DsRed expression is being driven by putative *hnt* enhancer elements, not associated with NRE-4 DNA sequence, acting on the 3xP3 promoter (Fig. 3.3). As such, I decided to examine *Peb1-eGFP* reporter construct expression in the mutant $hnt^{\Delta N4}$ background for differences in expression (Fig. 4.2) and hypothesized that areas where the *Peb1* reporter is expressed, but lacked DsRed expression, would indicate cells or tissues that are under unique regulatory control of enhancer elements associated with the NRE-4 region of *hnt* and possibly Notch dependent.

In $hnt^{\Delta N4}$ mutants, *Peb1-eGFP* reporter gene expression was observed along the length of the DT, while DsRed enhancer trap expression was not detected in the anterior and posterior terminal regions of the DT (cyan arrows, Fig. 4.2A",B"). Additionally, DsRed expression was not detected in the TCJ cells (white arrow), nor the row of ventral cells (arrowheads), which are areas of strong and specific *Peb1-eGFP* expression (Fig. 4.2A",B"). This suggests that the deletion of NRE-4 associated with $hnt^{\Delta N4}$ has removed enhancer elements that promote *hnt* expression in the TCJ cells, the row of ventral PNS cells, as well as the anterior and posterior terminal sections of the DT.

The $hnt^{\Delta N3}$ mutant DsRed enhancer trap expression, however, did show co-expression with *Peb1-eGFP* in late-stage TCJ cells (Fig. 4.2C-C"). The NRE-3 deletion inserts DsRed ~ 20 kb upstream of *hnt* CDS and ~18 kb downstream of the NRE-4 site. Since the

DsRed is acting as an enhancer trap, then the faint expression of DsRed in *hnt*$^{\Delta N3}$ TCJ cells but not in the tracheal cells could suggest that the TCJ-specific enhancer element is closer in proximity to the *hnt*$^{\Delta N3}$ DsRed insertion than the general tracheal enhancer.

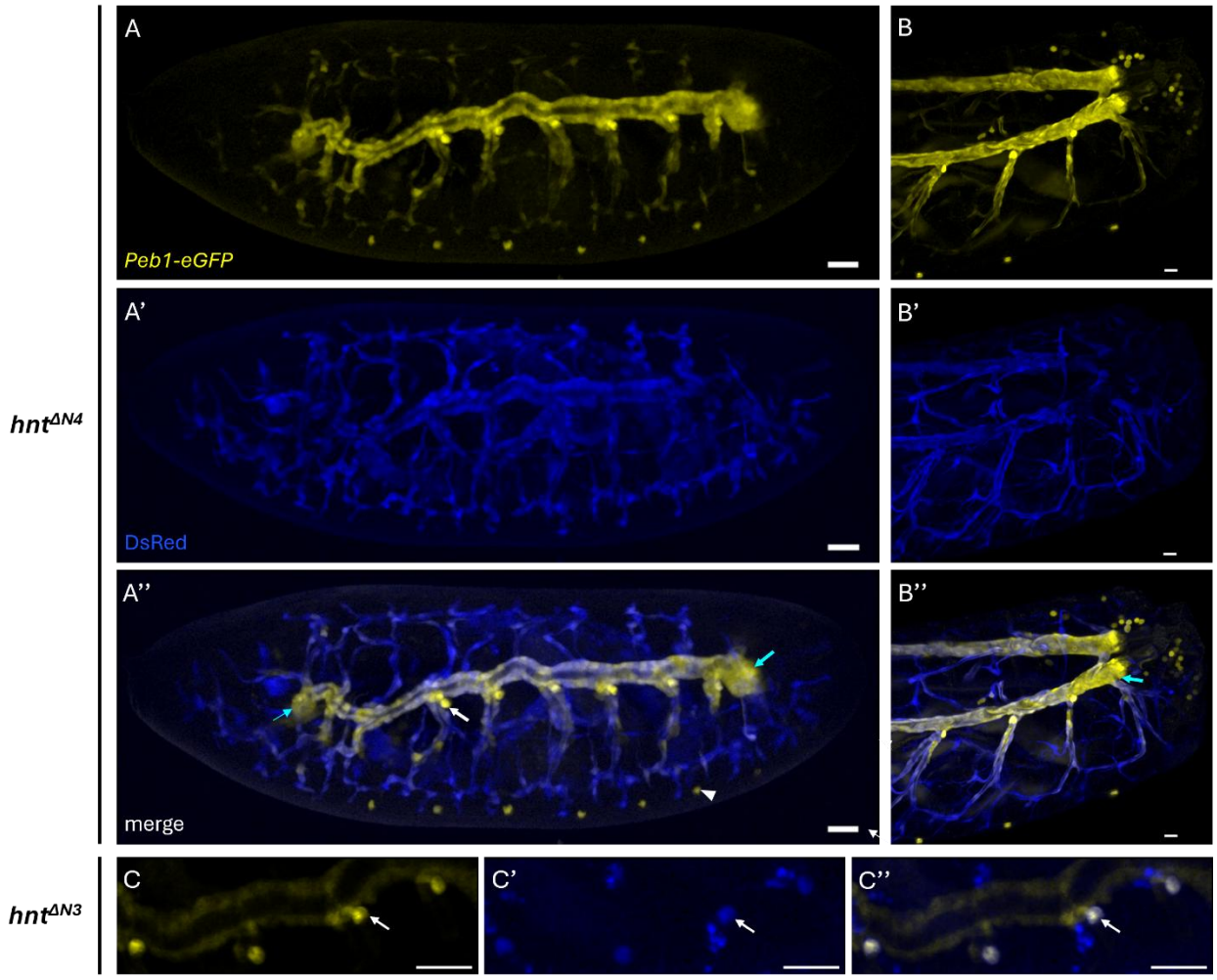

A
B
Peb1-eGFP
A'
B'
DsRed
A''
B''
merge
hnt^ΔN4
C
C'
C''
hnt^ΔN3

Figure 4.2 NRE-4 DsRed insert does not co-express with *Peb1-eGFP* in TCJ cells, single PNS cells, and the posterior DT. (A-B") Lateral view of (A) stage 17 embryo and (B) L2 larva showing *Peb1-eGFP* reporter expression in the $hnt^{\Delta N4}$ mutant background. (A-B) *Peb1-eGFP* expression was detected prominently in the DT, TCJ cells, and row of ventral PNS cells, and faintly detected in other tracheal branches such as the DBs and TCs. (A'-B') DsRed expression of $hnt^{\Delta N4}$ under the regulatory control of 3xP3 insect promoter and *hnt* regulatory elements. DsRed was expressed prominently in Bolwig's organ, the tracheal system, and PNS. (A"-B") Merged expression patterns of *Peb1-eGFP* and DsRed revealed exclusive *Peb1-GFP* expression in TCJ cells (white arrow), row of ventral PNS cells (white arrowhead), and both the anterior and posterior terminal ends of the DT (cyan arrow). (C-C") Magnified projection of *Peb1-eGFP* reporter expression in the $hnt^{\Delta N3}$ background. (C) *Peb1-eGFP* was expressed in the DT and TCJ cells (arrow). (C') $hnt^{\Delta N3}$ DsRed was detected in the TCJ cells as well, in contrast to $hnt^{\Delta N4}$. (C") Merged expression patterns showed co-expression of DsRed and *Peb1*-eGFP in $hnt^{\Delta N3}$ TCJ cells (arrow) but not in the DT. All scale bars represent 20 μm.

4.2.3 NRE-4 deletion reduces embryonic expression of Hnt in the developing trachea

Peb1 reporter analysis showed that the *Peb1/*NRE-4 sequence contains enhancers that drive expression in PNS cells, TCJ cells and the DT (Fig. 4.2), and given that $hnt^{\Delta N4}$ mutants are deficient for the NRE-4 enhancer region and exhibit tracheal phenotypes, I next assessed if $hnt^{\Delta N4}$ mutant embryos exhibited any changes in embryonic tracheal *hnt* expression. The rationale here being that changes in *hnt* expression could correlate with the observed tracheal phenotypes and deletion of the NRE-4 region. Both control wildtype and $hnt^{\Delta N4}$ mutant embryos of similar stages were immunostained using the anti-Hnt monoclonal antibody 1G9 (Fig. 4.3). Consistent with previously published work, I observed nuclear anti-Hnt immunostaining in all tracheal cells of control wildtype embryos (Fig. 4.3A,C,E) (Wilk et al., 2000; Yip et al., 1997). Anti-Hnt signal was readily detected in the DT (white arrows) and DBs (cyan arrows) of stage 13 wildtype embryos (Fig. 4.3A). By comparison, the anti-Hnt signal in the DT and DBs of $hnt^{\Delta N4}$ stage 13 mutants was significantly reduced, and this was especially evident in the Tr9 and Tr10 metameres (Fig. 4.3B). In stage 16 wildtype control embryos, anti-Hnt signal was observed as very strong in TCJ cells located along the DT (yellow arrows, Fig. 4.3C,E) and in PNS cells (arrowhead, Fig. 4.3G), but was reduced in $hnt^{\Delta N4}$ mutants at the same stage (Fig. 4.3F,H). Anti-Hnt signal at this stage was also found to be reduced or absent in the DT of the $hnt^{\Delta N4}$ mutants (white arrow, Tr9 and Tr10, Fig. 4.3D). Therefore, these data are consistent with the deletion of NRE-4 in $hnt^{\Delta N4}$ mutants being associated with reduced *hnt* expression in several cell subtypes of the developing embryonic tracheal system.

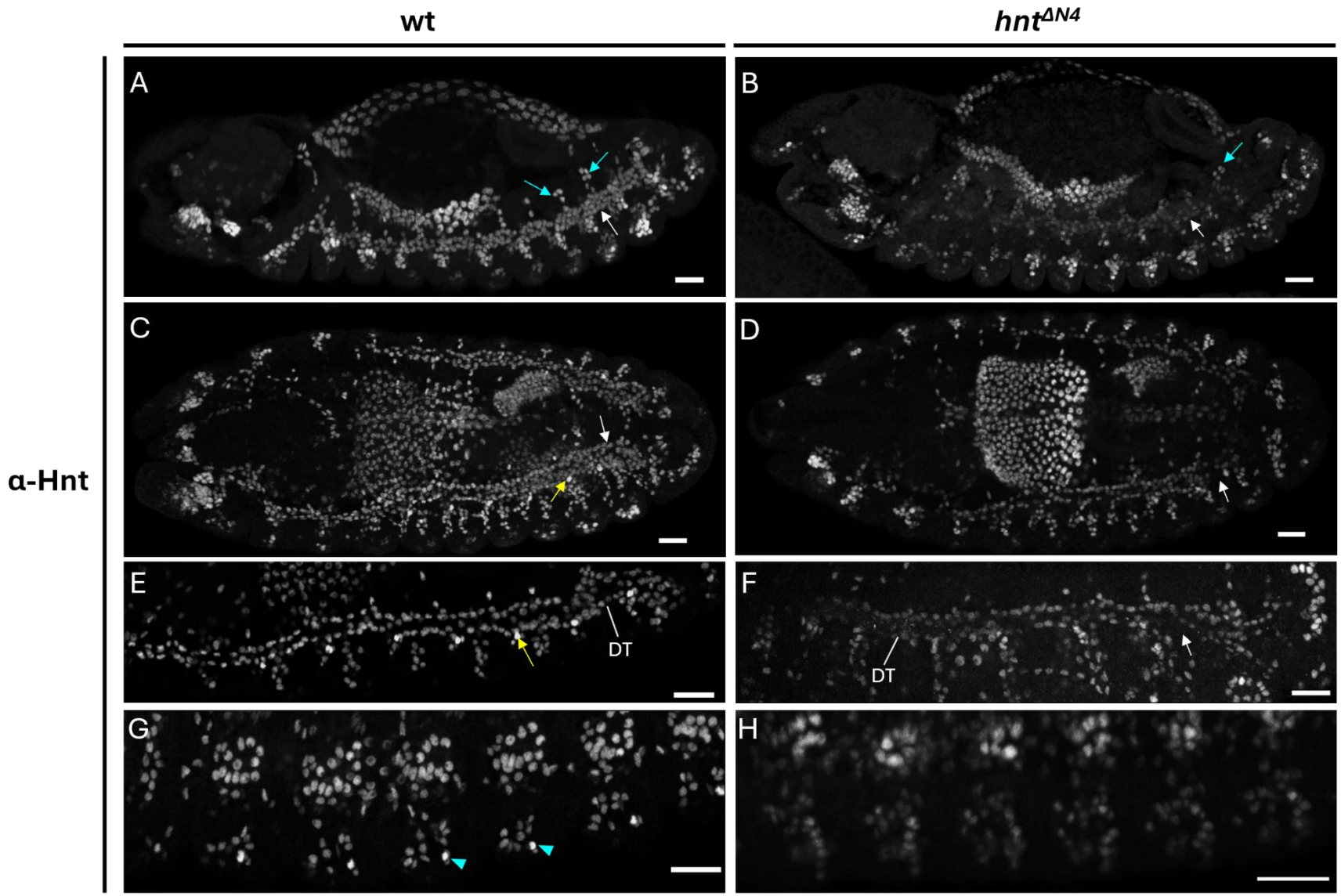

wt
hnt^ΔN4
α-Hnt
A
B
C
D
E
F
G
H
DT
DT

Figure 4.3 *hnt*$^{\Delta N4}$ embryos exhibit reduced expression levels of Hnt. Anti-Hnt immunostaining of *hnt*$^{\Delta N4}$ embryos (B,D,F,H) compared to wildtype (A,C,E,G). Hnt signal was detected in several tracheal branches during development, including the DT (white arrows), DB (cyan arrows), and TC. (A-B) Stage 13 *hnt*$^{\Delta N4}$ mutant embryos (B) exhibited reduced levels of *hnt* expression in the DT (white arrow) and DBs (cyan arrows) compared to the wildtype control (A). (C-D) Late-stage *hnt*$^{\Delta N4}$ mutant embryos (D) followed this trend, showing an increased reduction of Hnt signal in the posterior segments of the DT (white arrows) and TCJ cells (yellow arrows) compared to wildtype controls (C). (E-F) Magnified lateral view of late-stage DTs. Hnt signal in *hnt*$^{\Delta N4}$ mutant (F) tracheal system is very faint compared to the control (E), and TCJ *hnt* expression is abolished. (G-H) Lateral view of PNS cells (cyan arrowhead) with an elevated level of *hnt* expression positioned ventral to the oenocytes. Hnt signal is absent in *hnt*$^{\Delta N4}$ mutants (H) but strong in the control (G). All scale bars represent 20 μm.

4.2.4 *hnt* is required for apical organization of F-actin in the DT

Previous studies have shown that F-actin organization in the developing trachea serves as a template for the cuticle deposition that subsequently forms the taenidial folds (reviewed in Moussian, 2010; Matusek et al., 2006). F-actin is expressed in the DT of stage 14 embryos and displays apical parallel rings that span the circumference of the lumen across multiple cells (Matusek et al., 2006). To investigate if the $hnt^{\Delta N4}$ taenidial fold phenotype was a result of disrupted F-actin organization, I stained both late-stage $hnt^{\Delta N4}$ and control wildtype embryos with rhodamine phalloidin (Fig. 4.4). The rhodamine phalloidin staining of F-actin in DTs of control embryos was observed as continuous rings - typical of normal growth, reflecting the normal organization of F-actin in these cells (Fig. 4.4A). The fusion cells were also easily discernable, exhibiting typical actin accumulation in a punctate pattern (bracket, Fig. 4.4A) (Matusek et al., 2006). Strikingly, apical F-actin in mutant $hnt^{\Delta N4}$ DTs was found to be very disorganized (Fig. 4.4B-B'). Several areas along the DT were observed to be devoid of apical actin (dashed outline and asterisks, Fig. 4.4B-B') and numerous punctate actin bundles (arrows, Fig. 4.4B-B') were commonly found in the surrounding area. The punctate actin bundles observed near empty zones are likely the ends of actin cables that had failed to form a continuous ring, while other punctate actin forms observed in the fusion cells resembled previously reported phenotypes associated with actin disorganization (Morgani et al., 2021). The shape of the actin-free zones closely resembled the taenidial fold phenotypes observed in L1 $hnt^{\Delta N4}$ mutants (cyan arrowhead, Fig. 4.4C). Given that apical F-actin organization is a determiner of future taenidial fold deposition (Matusek et al., 2006), then the taenidial fold phenotypes of $hnt^{\Delta N4}$ mutants are most likely caused by a general paucity of organized F-actin.

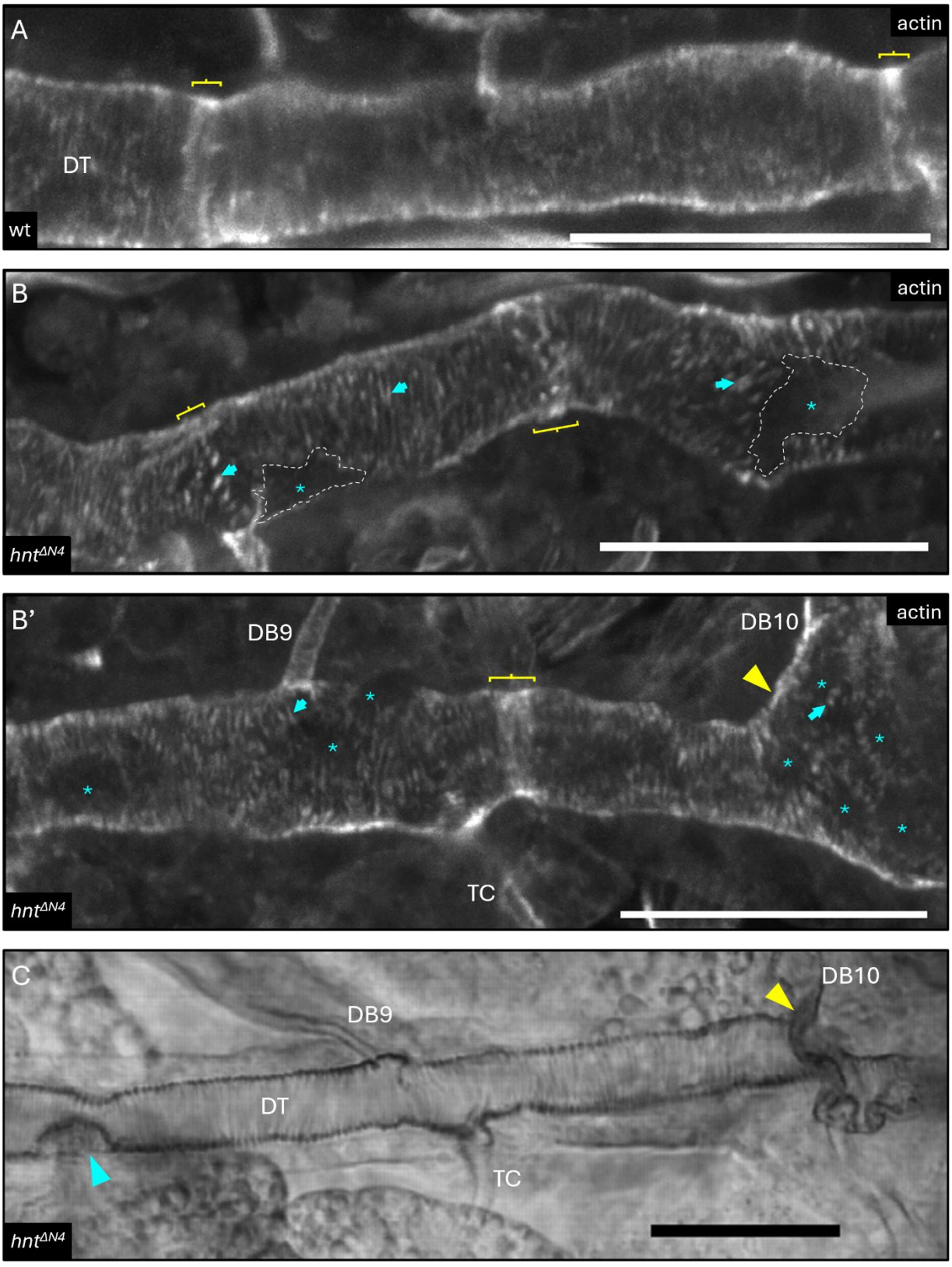

A
actin
DT
wt
B
actin
hntΔN4
B'
DB9
DB10
actin
TC
hntΔN4
C
DB10
DB9
DT
TC
hntΔN4

Figure 4.4 The late-stage 17 *hnt*$^{\Delta N4}$ mutant tracheal system displays a disorganized F-actin phenotype. (A) Rhodamine phalloidin staining of wildtype late-stage 17 embryo showing typical apical F-actin localization in the form of parallel rings spanning several tracheal cells of the DT. Fusion cells are outlined by brackets. (B) Rhodamine phalloidin stained *hnt*$^{\Delta N4}$ mutant DT segments showing disorganized apical F-actin that often formed into punctate bundles (cyan arrows) and were often found adjacent to zones completely void of F-actin (asterisks). Areas absent of actin are outlined in dashes. Fusion cells (brackets) also exhibited disorganized and punctate F-actin in *hnt*$^{\Delta N4}$ mutants. (B') Rhodamine phalloidin stained *hnt*$^{\Delta N4}$ mutant DT positioned with the DT/DB10 intersection (yellow arrowhead) on the right, showing the actin phenotype was stronger towards the posterior, indicated by a concentrated area of actin free zones surrounded by punctate F-actin bundled ends. (C) DIC projection of L1 *hnt*$^{\Delta N4}$ mutant larva trachea positioned with the DT/DB10 intersection on the right to match the position in (B'), showing crushed and warped taenidial folds as a result of missing cuticle. Areas of absent cuticle (cyan arrowhead) were similar in shape to actin-free zones revealed in rhodamine phalloidin staining. All scale bars represent 20 μm.

4.2.5 Increased actin expression partially rescues *hnt$^{\Delta N4}$* tracheal phenotypes

In contrast to phalloidin staining of F-actin, which is performed on fixed embryos, *btl-GAL4>UAS-Actin5C-GFP* expresses an Actin5C-GFP fusion protein in tracheal cells and can be used to live-image F-actin organization in tracheal cells during development. Following the observation of the F-actin phenotypes described above, I crossed the *btl-GAL4>UAS-Actin5C-GFP* into the *hnt$^{\Delta N4}$* mutant background to visualize and evaluate possible changes in actin organization in living embryos (Fig. 4.5). In the *hnt$^{\Delta N4}$* mutant background, the basolateral organization of actin was disorganized compared to wildtype controls (compare A-B, Fig. 4.5). Apical actin organization was also observed to be irregular; such irregularities included areas that lacked actin (arrows) and were associated with an apical disruption (compare brackets, Fig. 4.5C-D).

As previously mentioned (section 3.2.6), *hnt$^{\Delta N4}$* mutants were found to be early larval lethal, never surviving beyond the L2 stage to the wandering L3 and pupation stage. Interestingly, a rare few (~1 or 2 per vial, data not shown) *hnt$^{\Delta N4}$* mutants with *btl-GAL4>UAS-Actin5C-GFP* were found that had progressed to wandering L3 and pupal stages. The L3 larvae and pupae were thinner and smaller than wildtypes and ultimately failed during the larval-to-pupal transition and never eclosed as adults (data not shown). Therefore, the increased expression of actin5C-GFP can result in a partial rescue of the *hnt$^{\Delta N4}$* L1/L2 lethal phenotype.

I used DIC with brightfield confocal imaging to analyze the taenidial folds and DT of the wandering L3 escaper larvae (Fig. 4.5E-G). In general, the escaper L3 larvae, while less severe than *hnt$^{\Delta N4}$* mutants without *btl-GAL4>UAS-Actin5C-GFP*, proved to be more

amenable to analysis of taenidial fold defects. DIC imaging revealed that some taenidia do not form, leaving a gap (yellow arrows, Fig. 4.5F). Disrupted or incomplete taenidial folds not forming a complete ring were also observed, with some folds appearing more distinct and punctate than neighbouring folds (white arrows, Fig. 4.5G). Additionally, there were several smaller areas where the cuticle was devoid of taenidial folds and slightly compressed forming indentations (cyan arrows, Fig. 4.5F-G).

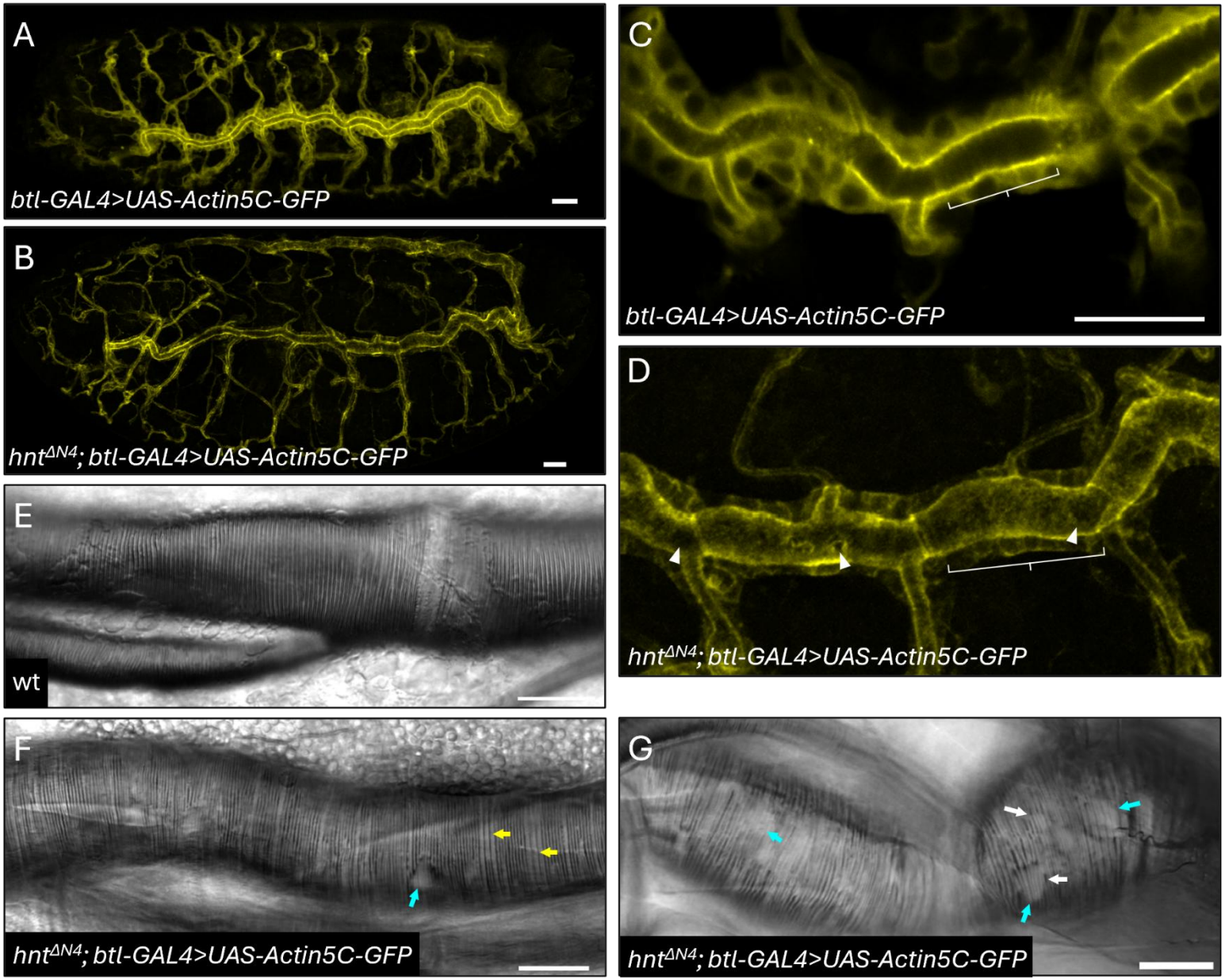

A
btl-GAL4>UAS-Actin5C-GFP
B
hntΔN4; btl-GAL4>UAS-Actin5C-GFP
C
btl-GAL4>UAS-Actin5C-GFP
D
hntΔN4; btl-GAL4>UAS-Actin5C-GFP
E
wt
F
hntΔN4; btl-GAL4>UAS-Actin5C-GFP
G
hntΔN4; btl-GAL4>UAS-Actin5C-GFP

Figure 4.5 Increased expression of actin5C partially rescues the *hnt$^{\Delta N4}$* phenotype.

Actin5C-GFP fusion protein was expressed in tracheal cells in both wildtype and *hnt $^{\Delta N4}$* mutant backgrounds to visualize *in vivo* actin arrangement. (A) Live imaging lateral view of control wildtype late-stage embryo showing actin5C-GFP fusion expression in the tracheal system. Actin5C strongly localizes to the apical side of tracheal cells. (B) Live imaging lateral view of similarly staged *hnt$^{\Delta N4}$* mutant embryo expressing actin5C-GFP showing a general disorganization of actin in the tracheal system in contrast to the wildtype. (C) Single step live imaging of the DT of wildtype background showing typical F-actin arrangement in parallel rings at cell apices (bracket). (D) Live imaging projection of DT in *hnt$^{\Delta N4}$* mutant background showing general disorganization and disruption of the apical F-actin in the form of actin-free zones (white arrowhead, compare brackets C-D). (E) DIC imaging of wildtype L3 larva DT showing typical corrugated taenidial fold patterning. Fusion cells feature a punctate cuticle pattern instead of folds. (F) DIC imaging of rescued L3 *hnt$^{\Delta N4}$* mutants expressing actin5C-GFP in the trachea showing DT taenidia with an abnormal composition. Some taenidial folds were absent or formed an incomplete ring around the circumference of the lumen (yellow arrows). Additionally, small depressions of the cuticle were found (cyan arrows) along the DT that featured weak taenidia that lacked the normal dark patterning. (G) Single step DIC image of rescued L3 *hnt$^{\Delta N4}$* DT showing discontinuous taenidia that appeared punctate and darker in contrast to neighbours (white arrows). All scale bars represent 20 μm.

4.2.6 NRE-4 Su(H) consensus binding sequence mutation causes tracheal phenotypes

While the engineered excision of NRE-4 deletes the Su(H) consensus binding sequence, it will also delete any other regulatory elements within this 5 kb region mapping ~38 kb upstream of the transcription start site (TSS) of the *hnt* gene. Therefore, following a reductionist approach, in order to investigate if the phenotypes in $hnt^{\Delta N4}$ are linked to modification of the Su(H) binding site specifically, I used a co-CRISPR technique to mutate the Su(H) binding site directly (Kane et al., 2017). I designed a single gRNA expression vector that would direct Cas9 to generate a single DSB in the NRE-4 Su(H) binding site. This was facilitated by the fortuitous finding of a PAM site (NGG) immediately adjacent to the Su(H) consensus binding sequence. Since no DNA repair template was provided, any Cas9-induced double stranded DNA break was expected to be repaired by error prone non-homologous end-joining (NHEJ), a process that would introduce small indels and mutate the target DNA sequence.

In tandem with the gRNA expression vector targeting the Su(H) site, an additional gRNA expression vector targeting *ebony* (pCFD3-ebony) was co-injected into *vas*-Cas9 stocks. Cas9 cleavage of *ebony*, located on the third chromosome, provides a screenable viable body color marker, which would indicate that a CRISPR-mutation event had taken place in specific individuals (Kane et al., 2017). The resulting G-0 adults, which are expected to harbour mutations in the target sites – these being the *ebony* gene and the Su(H) consensus sequence of NRE4 – were crossed to flies that carried both the *X*-balancer *FM7h* and the third chromosome marker *ebony* (*e*). As was done for the recovery of the NRE deletion lines, isogenic *X*-chromosome lines were established from single *FM7h/hnt? ;; e/e* female progeny. Maintaining only those lines that produced *ebony* mutants is an

established practice for increasing the chances of recovering CRISPR/Cas9 induced mutations in the second non-*ebony* target. These lines are known as "jackpot" lines and were subsequently analyzed by direct PCR sequencing for mutations of the NRE4-Su(H) target site (Kane et al., 2017).

The heterozygous *ebony* genotype (*e/e*$^{+}$) is associated with a semi-dominant phenotype that includes a darkened trident pattern on the adult thoracic segment (Takahashi et al., 2007), but this phenotype is not as easy to score as homozygous *ebony* mutants. Therefore, outcrossing the co-CRISPR adults to a line containing at least one copy of *ebony* allows for easier screening of the F1 population for *ebony* homozygotes. However, I wanted to investigate if screening the F1 generation for the heterozygous semi-dominant *ebony* phenotype was a viable approach to identify and isolate co-CRISPR mutation events. Therefore, a smaller population of injected G-0 adults were crossed to *FM7h;; e*$^{+}$ lines and F1 progeny were screened for the semi-dominant darkened trident phenotype and used to establish *X*-isogenic lines in parallel to the unambiguous homozygous *ebony* "jackpot" lines. The crossing schemes are further described in the appendix (Fig. A5, Fig. A6).

PCR analysis of these isogenic lines showed several unique modifications of the Su(H) consensus binding site (Fig. 4.7G). Indel mutations were observed in 30.1% (n = 71) of isogenic lines recovered through homozygous *ebony* screening methods, and in 37.5% (n = 16) of isogenic lines recovered through heterozygous *ebony* screening methods. This verified that screening for heterozygous *ebony* markers was a viable modification to the previously established co-CRISPR protocols, in the case a third-chromosome *e* marker is unavailable or undesirable, for G-0 adult crosses (Kane et al., 2017).

I next assessed if these indel mutations of the Su(H) consensus sequence caused changes in tracheal *hnt* expression during embryogenesis. Of the recovered mutants, the indel modifications in the $hnt^{N4\text{-}F42.2}$ and $hnt^{N4\text{-}F44.2}$mutant lines represented the greatest divergence from the native Su(H) consensus sequence (Fig. 1.1) and were therefore selected for further analysis.

As previously described, both control wildtype and $hnt^{N4\text{-}F42.2}$ mutant embryos of similar stage were immunostained using anti-Hnt monoclonal 1G9 (Fig. 4.6). In control wildtype embryos, *hnt* expression is readily found at the posterior and anterior ends of the DT (cyan arrows), and distinctly expressed in the TCJ (yellow arrow) and PNS cells (blue arrow) (Fig. 4.6A). Anti-Hnt signal patterning was variable in $hnt^{N4\text{-}F42.2}$ mutants, and identifiable changes in *hnt* expression were detected in 47% (n=37) of scored embryos. In contrast to the control wildtypes, anti-Hnt signal was found to be reduced or absent from entire metameres of the DT, often located at the terminal ends of the DT (asterisks, Fig. 4.6B-B"). Anti-Hnt signal was reduced in the TCJ cells of some individuals (Fig. 4.6B') but remained elevated in other embryos (Fig. 4.6B'-B"). Likewise, anti-Hnt signal was also found to be variable in the PNS cells (compare A with B-B", Fig. 4.6). Therefore, the data showed that mutation of the NRE-4 Su(H) consensus sequence is associated with variable and subtle changes to embryonic *hnt* expression in tracheal system.

In addition, I performed an embryonic lethality assay as described in section 3.2.6 (Fig. 3.7A) and found that 98.6% (n=213) of $hnt^{N4\text{-}F42.2}$ embryos successfully hatched into larvae, which indicated that the Su(H) site mutation was not associated with embryonic lethality.

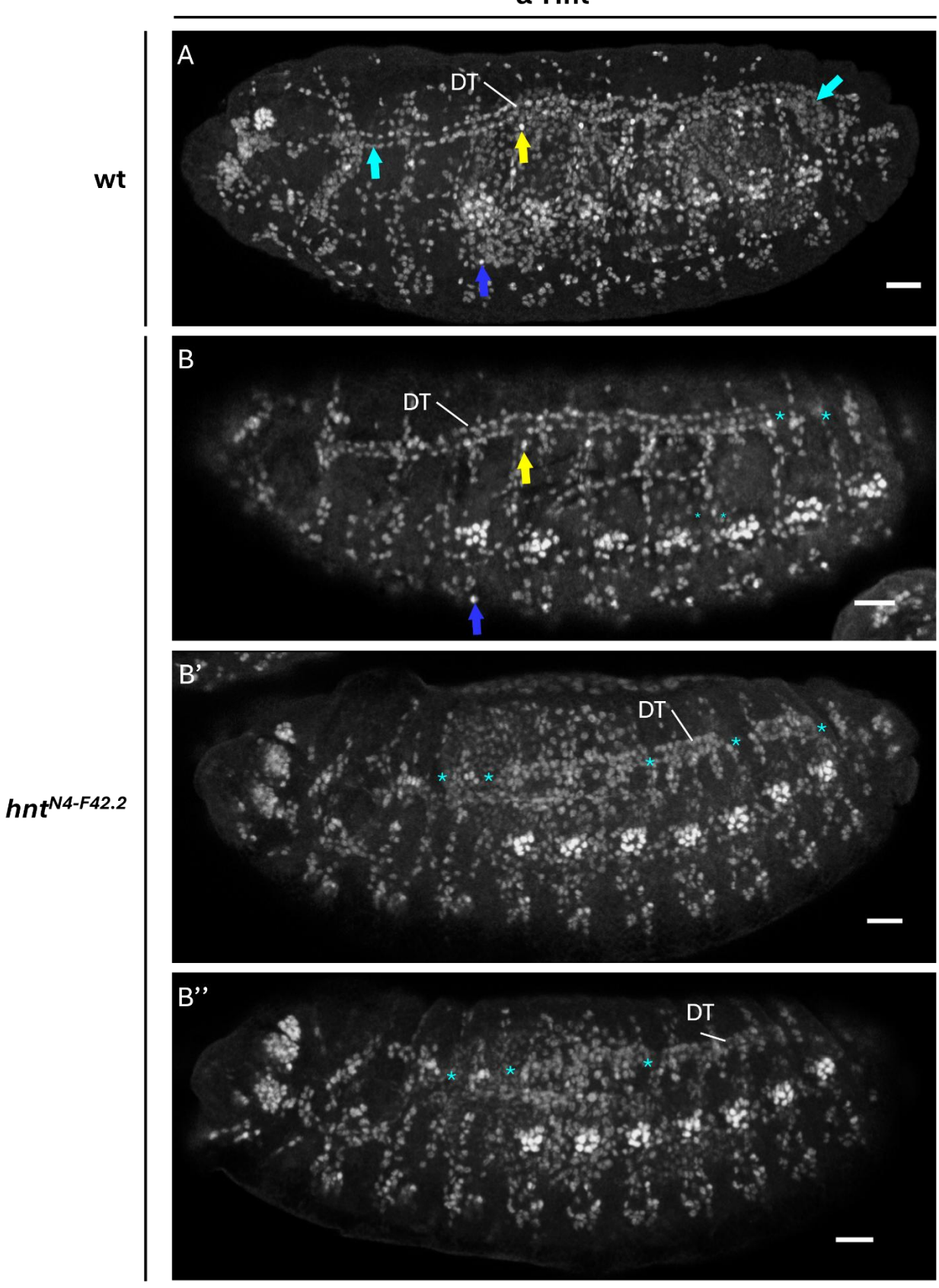

α-Hnt
wt
hntN4-F42.2
A
DT
B
DT
B'
DT
B''
DT

Figure 4.6 *hnt*$^{N4\text{-}F42.2}$ embryos exhibit variable levels of Hnt expression. (A) Lateral view of stage 15/16 control wildtype embryo immunostained with anti-Hnt showing normal *hnt* expression in the DT, TCJ cells (yellow arrow), and PNS cells (dark blue arrow). Hnt signal in the DT is continuous and extends almost the whole length of the embryo starting with the first metamere (Tr2, cyan arrow), approximately two segments anterior to the oenocytes, and ending with the last metamere (A8, cyan arrow) which extends posteriorly beyond the oenocytes and connects to the posterior spiracle. (B-B") Lateral view of *hnt*$^{N4\text{-}F42.2}$ embryos immunostained with anti-Hnt showing inconsistent and variable changes in Hnt signal at the terminal ends of the DT and TCJ cells. Changes in tracheal anti-Hnt signal was detected in only 47% (n=34) of observed embryos. Anti-Hnt immunostaining reveals differences in DT expression in contrast to the wildtype, exemplified by DT segments (asterisk) absent of Hnt, frequently located at the terminal ends of the DT. Anti-Hnt signal in TCJ and PNS cells was also inconsistent between individuals, where some individuals (B) retained a comparable level of anti-Hnt signal compared to controls (A) and other individuals (B'-B") exhibited reduced levels of anti-Hnt in TCJ and PNS cells.

None of the mutant lines recovered proved lethal and both *hnt*$^{N4\text{-}F42.2}$ and *hnt*$^{N4\text{-}F44.2}$ lines were further analyzed for tracheal phenotypes. Both *hnt*$^{N4\text{-}F42.2}$ and *hnt*$^{N4\text{-}F44.2}$ larvae were examined and revealed no tracheal collapse of any degree, but shared phenotypes were observed in both lines (Fig. 4.7).

These phenotypes were split into two distinct classes (class I DB defects; and class II DT defects – described below) and mutant larvae were scored as class I, class II, or the wildtype phenotype (Fig. 4.7F). Class I phenotypes primarily affected the DBs and were present in approximately 38.2% (n=136) of *hnt*$^{N4\text{-}F42.2}$ and 33.3% (n=110) of *hnt*$^{N4\text{-}F44.2}$ larvae (Fig. 4.7F). During the later stages of embryogenesis, the DBs migrate and fuse over the dorsal midline during dorsal closure, connecting the two DTs (Fig. 4.7C). In Class I defects observed, the DBs were disorganized, often displaying a failure to migrate and fuse properly (Fig. 4.7D-E). The most common Class I phenotype observed was DBs with free floating terminal branches in the body cavity that fail to migrate to local tissue (arrowheads, Fig. 4.7D). Other commonly observed phenotypes were DBs that failed to fuse over the dorsal midline, or occasionally, DBs that completed fusion but in the wrong conformation (Fig. 4.7E).

Class II defects observed consisted of DT phenotypes, the primary phenotype being severe constrictions and ectopic bending or creasing of the DT (Fig. 4.7B). Class II phenotypes were present in approximately 20.6% (n=136) of *hnt*$^{N4\text{-}F42.2}$ and 20.0% (n=110) of *hnt*$^{N4\text{-}F44.2}$ larvae and were not observed in wildtype controls (Fig. 4.7F). Most larvae that possessed Class II phenotypes also exhibited Class I phenotypes as well.

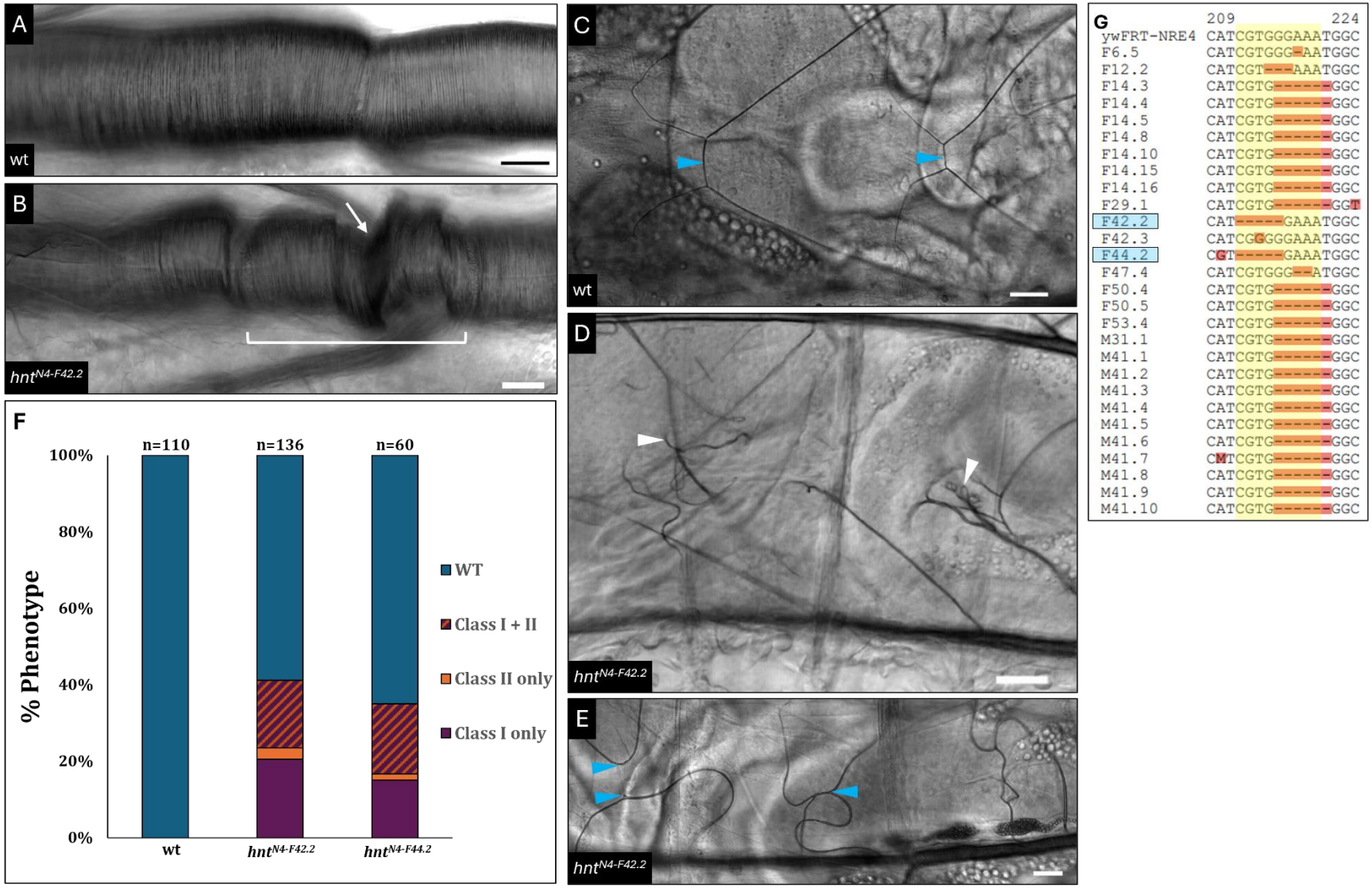

A
wt
B
hntN4-F42.2
C
wt
D
hntN4-F42.2
E
hntN4-F42.2
F
n=110
n=136
n=60
100%
80%
60%
40%
20%
0%
% Phenotype
WT
Class I + II
Class II only
Class I only
wt
hntN4-F42.2
hntN4-F44.2
G
209
224
ywFRT-NRE4 CATCGTGGGAAATGGC
F6.5 CATCGTGGG-AATGGC
F12.2 CATCGT---AAATGGC
F14.3 CATCGTG-----GGC
F14.4 CATCGTG-----GGC
F14.5 CATCGTG-----GGC
F14.8 CATCGTG-----GGC
F14.10 CATCGTG-----GGC
F14.15 CATCGTG-----GGC
F14.16 CATCGTG-----GGC
F29.1 CATCGTG-----GGT
F42.2 CAT-----GAAATGGC
F42.3 CATCGGGGGAAATGGC
F44.2 CGT-----GAAATGGC
F47.4 CATCGTGGG--ATGGC
F50.4 CATCGTG-----GGC
F50.5 CATCGTG-----GGC
F53.4 CATCGTG-----GGC
M31.1 CATCGTG-----GGC
M41.1 CATCGTG-----GGC
M41.2 CATCGTG-----GGC
M41.3 CATCGTG-----GGC
M41.4 CATCGTG-----GGC
M41.5 CATCGTG-----GGC
M41.6 CATCGTG-----GGC
M41.7 CMTCGTG-----GGC
M41.8 CATCGTG-----GGC
M41.9 CATCGTG-----GGC
M41.10 CATCGTG-----GGC

Figure 4.7 Direct mutation of NRE-4 causes visible tracheal phenotypes. DIC brightfield live imaging of wildtype and *hnt*$^{N4\text{-}F42.2}$ mutant larvae. (A) Single step dorsal view of wildtype L2 larvae posterior DT segment showing normal conformation. (B) *hnt*$^{N4\text{-}F42.2}$ mutant DT showing a representative Class II DT phenotype, exemplified by severe constrictions (white arrow) and irregular folding of a DT metamere (brackets) compared to the wildtype (A). (C) Dorsal view of wildtype DBs in L2 larvae showing the characteristic 'H' patterning at the fusion site over the dorsal midline (blue arrowhead). The thin anterior terminal branches migrate towards other tissues to facilitate oxygen delivery. (D) *hnt*$^{N4\text{-}F42.2}$ mutant DBs showing a representative Class I DB phenotype, exemplified by disorganized terminal branches (white arrowheads) floating in the body cavity. (E) *hnt*$^{N4\text{-}F42.2}$ mutant DBs showing another commonly observed Class I DB phenotype, demonstrated by DBs that have failed to fuse or have fused into an incorrect conformation (fusion sites marked by blue arrows) compared to the wildtype (C). (F) Stacked bar graph showing the penetrance of tracheal phenotypes in wildtype, *hnt*$^{N4\text{-}F42.2}$, and *hnt*$^{N4\text{-}F44.2}$ larvae. Embryos were collected over a two-hour period at room temperature and scored at early larval stages. Class I (purple) defects include disorganization of DBs, fusion failure over the dorsal midline, and ectopic branching. Class II (orange) defects include severe constrictions in the DT. A large portion of larvae that exhibit Class II phenotypes also exhibited Class I phenotypes (hatch pattern). Larvae with no observable phenotypes are represented in blue. Overall, tracheal defects were observed in 43.4% (n=136) of *hnt*$^{N4\text{-}F42.2}$and 35.0% (n=60) of *hnt*$^{N4\text{-}F44.2}$larvae. (G) Sequence alignments of the NRE-4 Su(H) consensus sequence (yellow box) to control wildtype sequence (ywFRT-NRE4) in CRISPR/Cas9 generated mutants. Indels are boxed in red and analyzed mutants are boxed in blue. All scale bars represent 20 μm.

4.2.7 Notch signalling regulates *hnt* expression in some cell types

To assess if *hnt* expression is responsive to Notch signalling in the developing embryonic tracheal system, I performed experiments using N^{55e11}, a loss of function allele, and N^{ts}, a temperature sensitive allele, as well as expression of a constitutively active construct, *UAS-*$N^{\Delta 34a}$. *Su(H)Gbe-GAL4* is a reporter construct that drives expression in areas of Notch activity (Furriols & Bray, 2000) and *Peb1-mCherry* drives expression in the trachea and TCJ cells using the *hnt* enhancer sequence associated with the NRE-4 region (see Fig. 4.1). I first analyzed the combined expression patterns of the *Peb1-mCherry* and *Su(H)Gbe-GAL4>UAS-*GFP^{nls} gene reporter constructs for candidate areas where the readouts for Notch activity and *hnt* expression might coincide (Fig. 4.8). The TCJ cells, PNS cells, and parts of the DT such as fusion cells, were found to be sites of co-expression between the Notch activity reporter and *Peb1-mCherry* reporter (Fig. 4.8A-B"). I also observed *Peb1-eGFP* and *hnt-GAL4>UAS-*$mCherry^{nls}$ co-expression to verify that TCJ cells and ventral cells are areas of *hnt* expression (Fig. 4.8C-D").

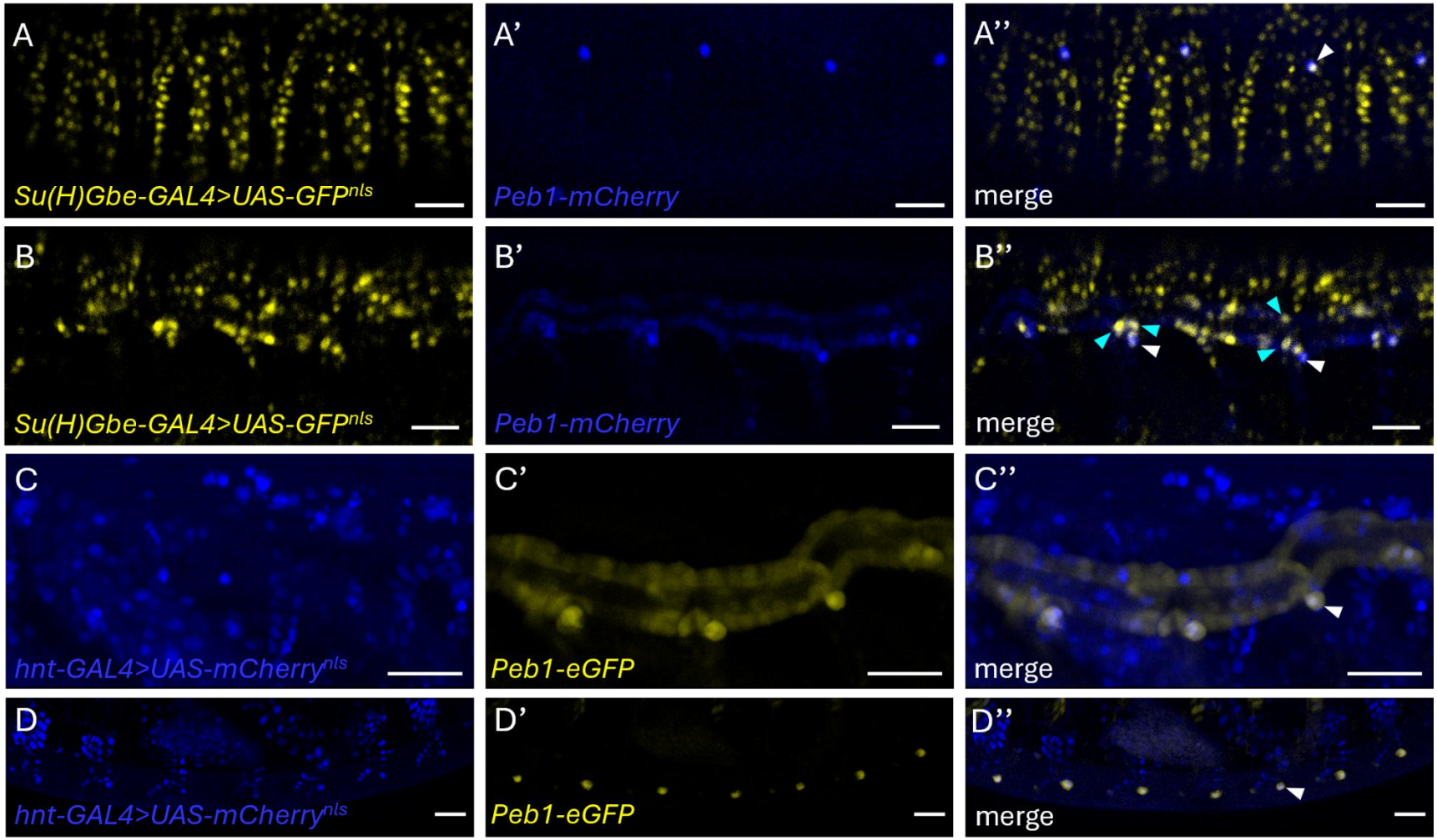

A
Su(H)Gbe-GAL4>UAS-GFPnls
A'
Peb1-mCherry
A''
merge
B
Su(H)Gbe-GAL4>UAS-GFPnls
B'
Peb1-mCherry
B''
merge
C
hnt-GAL4>UAS-mCherrynls
C'
Peb1-eGFP
C''
merge
D
hnt-GAL4>UAS-mCherrynls
D'
Peb1-eGFP
D''
merge

Figure 4.8 TCJ cells and PNS cells are sites of Notch activity. (A-B") Live imaging projections of wildtype embryo showing *UAS-GFP* expression driven by a Notch activity driver (*Su(H)Gbe-GAL4>UAS-GFP*) and *Peb1-mCherry* reporter expression. (A-A") Ventral view of PNS cells (white arrowhead, A") showing co-expression of both the Notch activity reporter (yellow, A) and *Peb1* (blue, A'). (B-B") Single step lateral view of the DT showing TCJ cells (white arrowhead, B") co-express both the Notch activity reporter (yellow, B) and *Peb1* (blue, B'). Paired fusion cells (cyan arrowheads, B") are also sites of Notch activity and found adjacent to the TCJ cells. (C-D") Live imaging projections of wildtype embryo showing *UAS-mCherry*^{nls} expression driven by a *hnt* driver (*NP 3312*), and *Peb1-eGFP* reporter expression. (C-C") Lateral projection of the DT revealed co-expression of both the *hnt* reporter (blue, C) and *Peb1* (yellow, C') in the TCJ cells (white arrowhead, C"). (D-D") Lateral projection of the PNS cells (white arrowhead, D") revealed co-expression of both the *hnt* reporter (blue, D) and *Peb1* (yellow, D'). All scale bars represent 20 μm.

Next, I observed the *Peb1-mCherry* reporter construct's expression in Notch-loss-of function and gain-of-function backgrounds (Fig. 4.9). In the N^{55e11} loss-of-function mutant background, the gene reporter expression was heavily disrupted, only expressing *mCherry* in the posterior and anterior ends of the DT (arrowheads, Fig. 4.9B). *Peb1-mCherry* reporter expression in the TCJ cells and ventral PNS cells was also completely abolished. Conversely, in the ubiquitous Notch gain-of-function background (*da-GAL4>UAS-*$N^{\Delta 34a}$) the *Peb1-mCherry* reporter showed strong expression in the DT and interestingly, ectopic expression of the reporter in the late amnioserosa (Fig. 4.9C). When taken together, these observations provide evidence that the TCJ cells, fusion cells, and ventral PNS cells are sites where Notch activity and *hnt* expression coincide and that the *Peb1* reporter expression responds to changes in Notch signalling, consistent with a direct relationship between Notch signalling and *hnt* expression.

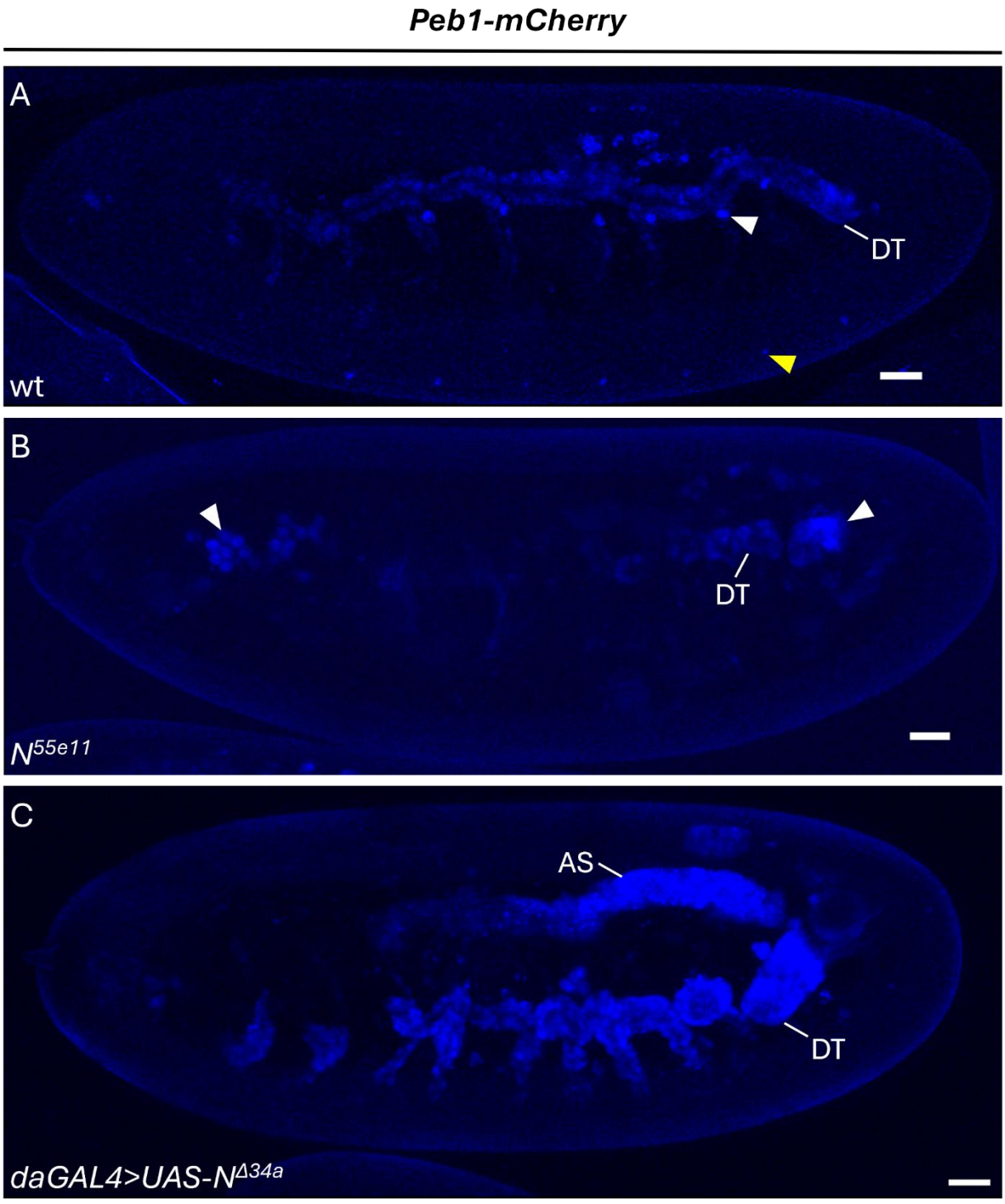

Peb1-mCherry
A
DT
wt
B
DT
N55e11
C
AS
DT
daGAL4>UAS-NΔ34a

Figure 4.9 *Peb1* reporter expression is reduced in a Notch loss-of-function background and is increased in a Notch gain-of-function condition. (A) Wildtype embryo expressing *Peb1-mCherry* reporter showing typical expression in the DT, TCJ cells (white arrowhead), and seven PNS cells (yellow arrowhead). (B) Notch loss of function allele (N^{55e11}) showing reduced expression of the *Peb1-mCherry* reporter. *Peb1* expression was revealed to be eliminated in TCJ cells, PNS cells, and the central DT, and was detected in the terminal ends of the DT (white arrowheads). (C) Lateral view of embryo expressing *Peb1-mCherry* reporter in Notch gain-of-function background associated with ubiquitous expression of an activated Notch construct (*daGAL4>UAS-*$N^{\Delta 34a}$) showing strong DT expression as well as persistent and ectopic reporter gene expression in the amnioserosa (AS). All scale bars represent 20 μm.

To assess if *hnt* is downstream of Notch signalling in TCJ cells, ventral cells, and trachea, I immunostained late-stage embryos using anti-Hnt in a Notch mutant background (Fig. 4.10A-F). Since Notch signalling is required for primary tracheal events such as fusion in the DT as well as DB patterning (Ikeya & Hayashi., 1999, Llimargas, 1999), and because both the TCJ cells and ventral cells display a high level of expression of *hnt* during late-stage embryogenesis, (see Fig. 4.4) I needed to disrupt Notch signalling at a later stage of development. Therefore, I used the temperature-sensitive allele N^{ts} to inactivate Notch at a later point following completion of these developmental events. Synchronous collections of embryos (collected over a period of 2 hours using the Flymax Automated Drosophila embryo collector) were left to develop at the permissive temperature of 18°C until late-stage 14 to ensure the DT had completed fusion, after which they were shifted to the restrictive temperature of 29°C to inactivate Notch. Embryo collections so treated were fixed and immunostained with anti-Hnt to observe any changes in Hnt levels (Fig. 4.10A-F). anti-Hnt signal levels were adjusted to the Hnt levels observed in the oenocytes. Hnt levels were found to be greatly reduced in both the TCJ cells (arrow) and PNS cells (cyan arrow) of the temperature shifted stage 16 N^{ts} embryos compared to the controls (Fig. 4.10A-F), suggesting that the high level of late-stage *hnt* expression in these cell types requires Notch signalling.

I also assessed if temperature-shifted N^{ts} L1 larvae display tracheal phenotypes. (Fig. 4.10G-H). Following the temperature shift regime as described above, N^{ts} mutant larvae were observed to die during the first instar larval stage and exhibited collapsed and discontinuous trachea (Fig. 4.10H) with breaks that were very similar to the phenotypes observed in $hnt^{\Delta N4}$ larvae (Fig. 4.10G). Thus, these results indicate that a disruption of

Notch signalling during late stages of embryonic development reduces the expression of *hnt* in TCJ cells and PNS cells, and results in a first instar larval lethal phenotype displaying tracheal collapse. The N^{ts} mutant under this temperature shift regime therefore appears to phenocopy the $hnt^{\Delta N4}$ mutants, and this observation supports the interpretation that Notch signalling regulates *hnt* expression in the context of specific cell types in the developing embryonic tracheal system.

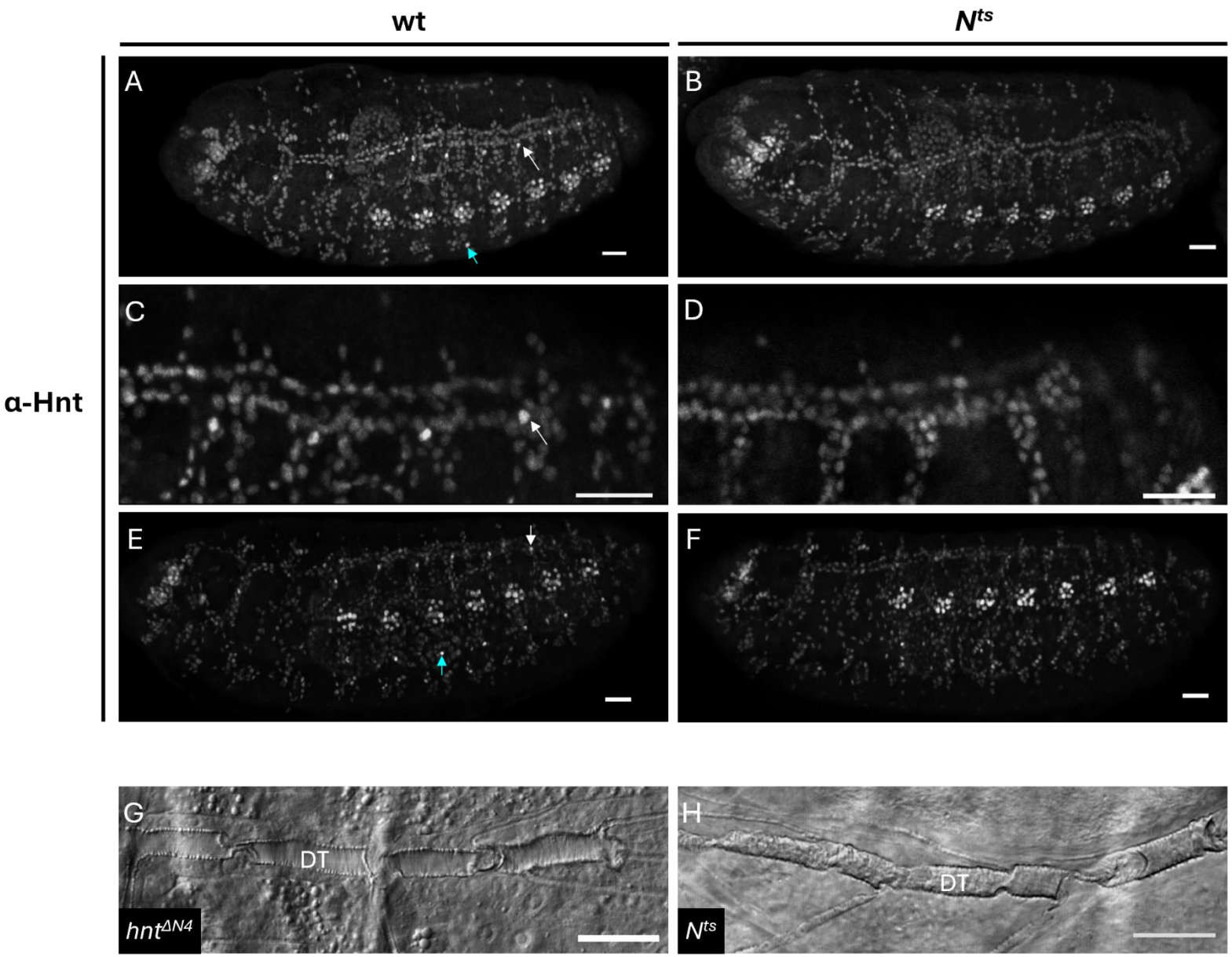

wt
Nts
α-Hnt
A
B
C
D
E
F
G
DT
hntΔN4
H
DT
Nts

Figure 4.10 A subset of embryonic expression of Hnt is downstream of Notch signalling. (A-F) Control wildtype and N^{ts} embryos were allowed to develop at permissive temperatures until DT fusion had completed, then shifted to non-permissive temperatures (29°C) for an additional two hours and immunostained with anti-Hnt. (A) Control late-stage wildtype embryo immunostained with anti-Hnt showing typical *hnt* expression in the DT, oenocytes, TCJ cells (white arrow) and PNS cells (cyan arrow). (B) N^{ts} embryo immunostained using anti-Hnt showing reduced expression of *hnt* in TCJ cells and ventral PNS cells. (C) anti-Hnt immunostained wildtype DT showing robust *hnt* expression in the TCJ cells (white arrow). (D) N^{ts} DT immunostained using anti-Hnt showing a reduction in *hnt* expression in TCJ cells. (E-F) Control wildtype (E) and N^{ts} (F) embryos were immunostained using anti-Hnt and equalized to match oenocyte *hnt* expression levels, further exemplifying a reduction in *hnt* expression in both PNS cells (cyan arrow) and TCJ cells (white arrow). (G-H) N^{ts} embryos were collected and allowed to develop following the regiment described above and then shifted to non-permissive temperatures until the first instar larval stage and imaged using DIC live imaging. (G) DIC live imaging of L1 $hnt^{\Delta N4}$ mutant trachea showing collapsed and broken DT, DB, and TC branches. (H) DIC live imaging of L1 N^{ts} trachea showing similarly collapsed and broken tracheal system that phenocopied $hnt^{\Delta N4}$. All scale bars represent 20 μm.

Chapter Five:

Discussion and Future Directions

5.1 Overview

hindsight is expressed in several embryonic tissues during development, including the amnioserosa, PNS, trachea, and oenocytes (Yip et al., 1997, Wilk et al., 2000, Reed et al., 2001) and has been previously identified as a target of Notch signalling in embryonic lymph gland crystal cells and follicle cells (Terriente-Felix et al., 2013; Sun & Deng, 2007). Previous *in vitro* analysis showed that following Notch activation, *hnt* is upregulated and that Su(H) is bound in the upstream regulatory region of *hnt* (Terriente-Felix et al., 2013). Given that *hnt* is expressed in such a broad range of developmental tissues, I hypothesized that there were unexplored contexts in which *hnt* responded to Notch activity. Therefore, I designed CRISPR-Cas9 deletion mutants with the intention of eliminating the *in vivo hnt* Notch response by individually deleting four Su(H) consensus binding sequences previously associated with Notch activity (Terriente-Felix et al., 2013). My research has successfully identified a novel developmental context in which *hnt* is required downstream of Notch signalling to organize actin in the developing Drosophila tracheal system.

In general, I expected that CRISPR/Cas9 mediated genome editing of the regulatory region of *hnt* would interrupt more developmental processes and it is interesting that only 1 of 4 deletions (NRE-4) produced a lethal phenotype. It is also curious that the three NRE deletions that did not produce phenotypes (NRE-1-3) exhibited similar ectopic expression patterns of the DsRed insert, which could indicate the presence of "shadow enhancers" (Hong et al., 2008). Shadow enhancers define redundant enhancer elements that contribute various levels of overlapping expression control over an associated gene. Notably, shadow enhancers do not necessarily map to the promoter region of a gene and can map to introns or even the far side of neighbouring genes (Hong et al., 2008; Barolo, 2012). As such, the

lack of observable phenotypes in the mutant *hnt*$^{\Delta N1\text{-}3}$ lines could be attributed to the presence of shadow enhancers, conveying redundant expression control over *hnt*. Given that *hnt*, as a transcription factor, controls downstream target gene expression and is required in a diverse range of developmental contexts, it would not be surprising if there were redundant systems in place to ensure gene expression (Yip et al., 1997; Wilk et al., 2000; Reed et al., 2001; Ming et al., 2013; Deady et al., 2017; Baechler et al., 2016). The lack of observable phenotypes is also not entirely unsurprising, since CRISPR/Cas9 mutagenesis techniques are typically used to modify the coding sequence of genes either by excision of whole genes or mutating specific exons (Gratz et al., 2013; Yu et al., 2014; Kane et al., 2017). As such, this atypical application of CRISPR/Cas9 genome editing, while successful, did not function ideally as a mutagenic screen for novel *in vivo* roles of *hnt* downstream of Notch signalling, but did lead to the interesting discovery of *3xP3-DsRed* insertions behaving as enhancer traps.

5.2 DsRed insertions into the regulatory region of *hnt* function as tissue specific enhancer traps

Here, I report an unintended and novel observation that the insertions of the *3xP3-DsRed* marker cassettes within the regulatory region of *hnt* function as enhancer traps. This was an unexpected observation. Traditional enhancer traps use a weak minimal synthetic promoter (Hartenstein & Jan, 1992; Furriols & Bray, 2001) having undetectable expression unless inserted in a site that is responsive to an enhancer element, whereas the 3xP3 promoter is associated with universal strong expression in the developing eyes of many different Orders of Insecta, including Diptera (flies and mosquitoes), Lepidoptera (butterflies and moths), Coleoptera (beetles), and Hymenoptera (crickets and sawflies) (Horn et al., 2000; Tsubota et al., 2014; Berghammer et al., 1999; Hatakeyama et al., 2016). In control *3xP3-GFP* lines, which carry an insert on the 3rd-chromosome and were not associated with *hnt* in any way, expression of the reporter GFP was observed in the embryonic structure known as Bolwig's organ, the developing larval light sensing organ, as well as a group of lateral bipolar neurons (Fig. 3.3E). It is curious that *hnt* is also endogenously expressed in these two embryonic cell types. During the initial DsRed screening of the CRISPR deletion mutants, I found that DsRed was expressed in several embryonic tissues in addition to Bolwig's organ that remarkably resemble subsets of Hnt expression patterns (Fig. 3.3) (Yip et al., 1997; Wilk et al., 2000). The DsRed expression patterns of $hnt^{\Delta N1}$, $hnt^{\Delta N2}$, $hnt^{\Delta N3}$ are similar but distinct from the expression pattern of $hnt^{\Delta N4}$ - and yet all the DsRed patterns observed were subsets of the known expression pattern of *hnt* (Yip et al., 1997). The ability of a particular promoter to function as an enhancer trap is indeed curious, and it would be of interest to determine if the 3xP3

promoter will always respond in this way, or if only certain genes, such as *hnt*, which share expression patterns with 3xP3, can acquire this enhancer trap function. As far as I am aware, this question has not been investigated by other Drosophila researchers using the same technique.

5.2.1 Spurious DsRed insertions are also expressed in *hnt* patterns

Two of the mutant deletion sibling lines, $hnt^{\Delta N1\text{-}5}$ and $hnt^{\Delta N4\text{-}1}$, did not pass the PCR confirmation test and yet curiously expressed DsRed so strongly as to be observable without the use of fluorescent microscopy (Fig. 3.4). As such, I used the same long-range PCR strategy used to verify the *bona fide* deletion mutants, to investigate the DsRed insertion sites of $hnt^{\Delta N1\text{-}5}$ and $hnt^{\Delta N4\text{-}1}$.

In the case of $hnt^{\Delta N1\text{-}5}$, I used the same primers that were used to investigate its sibling line, $hnt^{\Delta N1}$, to amplify a genomic DNA region that encompasses the NRE-1 site. The long-range PCR amplified an ~8 kb region in control wildtypes and a ~3.8 kb region in the *bona fide* $hnt^{\Delta N1}$ deletion mutant, as expected. However, the long-range PCR amplified an ~8 kb product in $hnt^{\Delta N1\text{-}5}$ mutants and sequencing showed it was a match to wildtype sequence and did not contain the DsRed cassette (appendix, Fig. A1). This data indicates that no CRISPR/Cas9 mutagenesis event occurred at the intended NRE-1 site and that DsRed was inserted off-target in the $hnt^{\Delta N1\text{-}5}$ mutant. A known caveat to CRISPR/Cas9-directed mutagenesis is the potential for off-site targeting (Gratz et al., 2014; Gratz et al., 2015; Jinek et al., 2012). This effect can be minimized through proper preparation by using tools such as flyCRISPR Optimal Target Tool to identify potential off-site targets against a reference

genome, and SNP sequencing of gRNA target sites, but cannot be completely eliminated as any DNA polymorphisms in the genome could cause off-site mutations (Gratz et al., 2015; Gratz et al., 2014). Since sequencing showed no DsRed integration at the NRE-1 site, the intense DsRed expression in the larval midgut could be interpreted as an off-site integration into a separate promoter/coding region of a strongly expressed midgut specific gene (Tsubota et al., 2014). However, the expression pattern is strikingly similar to that of *hnt* midgut expression, perhaps suggesting DsRed could be inserted elsewhere in the *hnt* gene locus (Baechler et al., 2016).

Long-range PCR and sequencing of the NRE-4 region of $hnt^{\Delta N4\text{-}1}$ was not conclusive but does indicate that the targeted NRE-4 DNA sequence had not been excised. Interestingly, elements of the HDR donor vector sequence, such as AmpR and 5S rRNA, were also detected in the sequence, which suggests that the vector backbone had been integrated into the gDNA target sites, and there are precedents for such events (Källstig et al., 2025, Yu et al., 2014). Donor vector backbone integration is a known by-product of HDR DNA repair mechanisms (Källstig et al., 2025, Yu et al., 2014) and studies have shown that this event occurs at a variable frequency depending on different factors such as the gene locus or design of the donor vector (Yu et al., 2014). This event can introduce two copies of the *3xP3-DsRed* gene cassette, as mentioned above, which could explain the intense DsRed expression in $hnt^{\Delta N4\text{-}1}$ adults (Fig. 3.4; Yu et al., 2014). Recently, new HDR donor vectors were designed to address this issue by incorporating a second screenable marker, such as *3xP3>ZsGreen*, outside of the homology arm cloning site to easily identify transformants with undesired vector backbone integration events (Källstig et al., 2025).

5.3 Specific enhancer elements map to NRE-4 sequence

Given that the sequence driving expression in the *Peb1* reporter construct maps to NRE-4 and is deleted in $hnt^{\Delta N4}$ mutants, I examined *Peb1* reporter construct expression in the mutant $hnt^{\Delta N4}$ background, taking advantage of the novel 3xP3 DsRed enhancer trap effect. This approach aimed to identify differences in expression between the *Peb1-eGFP* reporter construct and the $hnt^{\Delta N4}$ DsRed enhancer trap, where the rationale was that eGFP expression maintained by the *Peb1-eGFP* reporter, but not observed as part of the DsRed enhancer trap expression, would identify cell types where *hnt* expression was associated with the NRE-4 regulatory region (see Fig. 4.2).

I found several examples where *Peb1-eGFP* was distinctly expressed while $hnt^{\Delta N4}$ DsRed enhancer trap expression was not detected. These included the terminal regions of the DT, TCJ cells, and ventral PNS cells (Fig. 4.2A-B"), suggesting that the NRE-4 deletion associated with $hnt^{\Delta N4}$ deletes *hnt* enhancer elements that promote expression in these cell types. Further evidence to support this interpretation was the observation of *Peb1-eGFP* reporter construct expression in $hnt^{\Delta N3}$ mutant embryos. The $hnt^{\Delta N3}$ mutant carries a DsRed insertion ~20 kb upstream of *hnt* CDS and ~18 kb downstream of the NRE-4 site, leaving the NRE-4 site and any enhancers in this region intact. The $hnt^{\Delta N3}$ enhancer trap expression was found to co-express faintly with *Peb1-eGFP* in late-stage TCJ cells (Fig. 4.2C-C"). Taken together, these data indicate that a TCJ enhancer is present in $hnt^{\Delta N3}$ but not in $hnt^{\Delta N4}$ (NRE-4 deletion) mutants, further suggesting this TCJ enhancer maps to NRE-4 and can promote expression of the *3xP3-DsRed* enhancer trap effect associated with $hnt^{\Delta N3}$.

A tracheal system enhancer of *hnt* has been previously estimated to lie at ~20 kb upstream of the *hnt* TSS (Wilk et al., 2000; unpublished data B.H. Reed, I. Dawson, H.D. Lipshitz). This was based on the observation that *Df(1)rb*^{1} (3F6-4A1;4C7) lacks all *hnt* tracheal expression, fails to complement *hnt* mutants, including *hnt*^{XE81}, and whose proximal breakpoint is known to be 20-25 kb distal to the *hnt* TSS (Wilk et al., 2000). Cytology estimates *hnt* to be located at cytological position 4C10, consistent with the *Df(1)rb*^{1} deleting a large portion of the distal *hnt* upstream regulatory sequences while leaving the promoter and protein coding sequences intact. Observation data from *hnt*$^{\Delta N4}$ and *Peb1* reporters shows that *Peb1* drives expression strongly in the DT and faintly in TC and DBs (Fig. 4.2), whereas *hnt*$^{\Delta N4}$ expresses DsRed throughout the whole tracheal system (Fig. 3.3). When taken together, the data suggest the NRE-4/*Peb1* sequence contains a DT specific tracheal enhancer of *hnt*, and that redundant enhancers for the DT likely exist elsewhere, seeing as DT expression is not eliminated when NRE-4 is deleted in *hnt*$^{\Delta N4}$ mutants (Fig. 4.2). Therefore, the results presented here support the previous estimated position of a general *hnt* tracheal system enhancer (Wilk et al., 2000; unpublished data B.H. Reed, I. Dawson, H.D. Lipshitz) and narrows the location of a DT specific enhancer to ~38 kb upstream of the *hnt* TSS.

Using the same logic, my analyses of the co-expression patterns of both the *hnt*$^{\Delta N4}$ DsRed enhancer trap and *Peb1* reporter suggests that the NRE-4/*Peb1* reporter sequence contains unique enhancer elements for the TCJ cells, PNS cells, and the terminal ends of the DT that connect to the spiracles (Fig. 4.2).

5.4 Hnt is required for actin organization in the embryonic trachea

Some *hnt*$^{\Delta N4}$ larvae progressed to the second instar stage and showed a marked inability to properly shed their molted cuticles, which remained attached near the mouthhooks, likely at a lateral spiracle (Fig. 3.8E). Similar molting defects have been observed in *uninflatable* (Zhang & Ward, 2009) and *Mmp1* mutants (Page-McCaw et al., 2003). Larvae undergo ecdysis and molt their former cuticle during transitions to subsequent instar stages. The cuticle forming the taenidial folds is continuous with the outer cuticle and, during molts, is broken into smaller fragments at fusion cells by apically secreted Mmp1 (Glasheen et al., 2010). These cuticle fragments are then shed through the lateral spiracles, which only open at molts during larval stages to facilitate removal of tracheal cuticle (Manning & Krasnow, 1993). Taken together, the molting defects observed in *hnt*$^{\Delta N4}$ could be interpreted as an inability to digest the tracheal cuticle into appropriately sized fragments given the inconsistent and distorted structure of the mutant taenidial folds.

My results show that the majority of *hnt*$^{\Delta N4}$ mutants experience complete collapse of the tracheal system shortly after hatching (Fig. 3.8F). This failure in the development of the tracheal system, while somewhat subtle as a phenotype, results in classic hypoxic behaviours and phenotypes, including growth arrest, immobility, and lethality (Wingrove & O'Farrell, 1999). Tracheal collapse has been associated with defects in several tracheal functions, such as the inability to inflate the tracheal system (Kim et al., 2018; Zhang & Ward, 2009; Scholl et al., 2023), defects in epithelial integrity (Wilk et al., 2000), and faulty actin organization (Matusek et al., 2006). Tracheal inflation is easily observed using phase contrast bright field microscopy of live embryos; this event occurs at the end of embryogenesis and involves luminal clearance of extracellular matrix proteins followed by

gas filling (Liu et al., 2003). The trachea of *hnt*$^{\Delta N4}$ mutants inflate normally and have been observed to haemorrhage gas internally (as indicated in Fig. 3.8D) likely via the absence and warping of taenidial structures, and not through the posterior spiracles. This suggests that the tracheal collapse defects occur through a mechanism related to structural integrity and likely independent of tracheal inflation.

Late-stage *hnt*$^{\Delta N4}$ mutant embryos show a striking disorganization of apical F-actin in the developing tracheal system. The DTs of these mutants are populated by numerous zones completely devoid of F-actin, causing notable disruption to local F-actin composition (Fig. 4.4). Prior to tracheal cuticle deposition, F-actin is apically arranged into parallel rings, and in the case of the DT, is continuous across several tracheal cells (Matusek et al., 2006). During cuticle deposition, the tracheal cells corrugate at the apical cell surface, underlain by the F-actin cables and chitin synthase complexes, resulting in the hallmark taenidial fold pattern that directly corresponds to F-actin configuration (reviewed in Moussian, 2010; Matusek et al., 2006; Öztürk-Çolak, 2016b). Therefore, the distorted structure of mutant *hnt*$^{\Delta N4}$ taenidial folds can be interpreted as a consequence of the unusual F-actin arrangements observed in late-stage *hnt*$^{\Delta N4}$ mutant embryos. This interpretation is further supported by the observation of large cavities in both the mutant taenidia and F-actin that highly resemble one another (Fig. 4.4). This is consistent with previous reports that alterations in tracheal F-actin organization are reflected in taenidial fold patterning (Matusek et al., 2006; Öztürk-Çolak, 2016b).

One of the two Drosophila filamin homologs, *jbug*, is an actin crosslinking molecule and has been shown to be a transcriptional target of *hnt* during photoreceptor axon

guidance (Oliva et al., 2015). *hnt* is required to properly guide photoreceptor axons by regulating genes that regulate the organization of the actin cytoskeleton, such as *jbug*, and *hnt* mutants exhibit a decrease in polymerized actin in the R-cell axons in the developing pupal eye (Oliva & Sierralta, 2010). *jbug* is also expressed throughout the embryonic trachea, with a strong apical localization (Chung et al., 2021). Given the actin phenotypes of $hnt^{\Delta N4}$ and given that *hnt* has been shown to regulate actin polymerization though *jbug*, suggests a model whereby *hnt* could regulate tracheal actin organization through *jbug* downstream of Notch signalling.

5.4.1 Increased expression of actin partially rescues $hnt^{\Delta N4}$ actin phenotypes

An actin5C-GFP fusion protein was expressed in the trachea in $hnt^{\Delta N4}$ mutants to visualize the *in vivo* tracheal actin arrangement (Fig. 4.5). In the $hnt^{\Delta N4}$ mutant background, apical actin is disorganized, displaying several gaps in F-actin composition along the length of the DT. Interestingly, when actin is overexpressed in the $hnt^{\Delta N4}$ background, a few mutants escape the L2 lethal phase, progress through the L3 stage and eventually undergo pupation. This observation indicates that increased tracheal expression of actin can partially rescue the lethal phenotype associated with $hnt^{\Delta N4}$. Notably, these L3 “escaper” larvae and pupae are considerably shorter and thinner than their heterozygous siblings and do not survive to adulthood. However, the taenidial folds of these escaper L3 larvae are often indented in small patches, suggesting weak structural integrity, and some folds do not form complete rings, indicated by gaps where a taenidial fold was expected. Notably, some of the taenidia are more punctate than their neighbours, resemblant of the actin patterns

observed in late-stage $hnt^{\Delta N4}$embryos (Fig. 4.4). As such, it can be reasoned that the increased expression of actin5C in $hnt^{\Delta N4}$ mutants produces sufficiently organized intermediate actin structures that meet a threshold necessary to form an intact cuticle structure that seals in gas (Fig. 4.5).

hnt has been linked to cytoskeletal F-actin defects in several contexts, including the apical tips of photoreceptor precursor cells and axons as well as focal complexes at the epidermal leading edge during dorsal closure (Pickup et al., 2002; Oliva et al., 2015; Reed et al., 2001). *hnt* has also been identified as a putative target of the transcription factor Blimp-1 which regulates genes related to chitin deposition and F-actin organization (Öztürk-Çolak et al., 2018). In addition, a previous screen for possible genetic interactors of *hnt* identified several genes of interest related to F-actin polymerization and cytoskeletal organization (Wilk et al., 2004). Overall, my results describe a novel role for *hnt* in regulating F-actin organization, which is downstream of the Notch signalling pathway, in the context of the development of the tracheal system. These observations are consistent with what has been reported in the literature and support the view that a general role of *hnt* is to impact actin subcellular organization during development and morphogenesis.

5.5 Hnt operates downstream of Notch activity

Immunostaining of $hnt^{\Delta N4}$ mutant embryos shows a clear reduction in *hnt* expression levels in the DT, TCJ cells, and PNS cells (Fig. 4.4, Fig. 4.10) and mutants exhibit tracheal phenotypes during late embryogenesis and early larval stages (Fig. 3.8). These findings support the interpretation that the deleted NRE-4 sequence includes elements that promote *hnt* expression in those cell types, and that *hnt* expression is necessary for tracheal integrity and proper tubulogenesis. These observations also lay the groundwork for establishing *hnt* as a direct downstream responder of Notch signalling in the trachea through Su(H) regulation. A caveat to this interpretation is that, in addition to removal of the Su(H) consensus binding sequence, the NRE-4 deletion (which is ~5 kb in size) may also delete other additional regulatory elements, which could lead to compounding defects. To address this, I employed a reductionist approach and used CRISPR/Cas9 directed mutagenesis and NHEJ DNA repair to introduce indels into the NRE-4 Su(H) consensus sequence and recovered several unique mutant alleles, including $hnt^{N4\text{-}F42.2}$. The $hnt^{N4\text{-}F42.2}$ allele is not associated with lethality, but mutant larvae exhibit remarkable defects in both DBs and DTs (Fig. 4.7).

$hnt^{N4\text{-}F42.2}$ mutants show a unique DT phenotype, where posterior segments of the DT appear compressed and folded over itself (Fig. 4.7B). This observed phenotype is consistent with other observed tracheal constriction phenotypes that have been observed in genes that regulate and maintain tube expansion, such as *gnarled* and *megatrachea* (Beitel and Kransnow, 2000) and in chitin deficient mutants (Tonning et al., 2005). Notably, the compressions appear to correspond to individual DT metameres. Interestingly, anti-Hnt immunostainings of mutant $hnt^{N4\text{-}F42.2}$ embryos show a similar corresponding pattern, as

hnt signal is absent in whole DT segments yet remains expressed in the tracheal cells of neighbouring segments (Fig. 4.6). When taken together, these correlating patterns suggest that the DT constrictions observed in some larvae are caused by the absence of *hnt* in a DT metamere. Given that the DT phenotype appears to be limited to individual metameres and does not result in collapsed tracheal segments, suggests that mutation of the single Su(H) site produces a local and subtle effect, as evidenced by the contrasting complete tracheal collapse phenotype observed in $hnt^{\Delta N4}$ mutants (Fig. 3.8). Future studies would benefit from exploring if the DT compressions are related to underlying actin defects as observed in $hnt^{\Delta N4}$ mutants. However, given the low penetrance of the phenotype (~20%, Fig. 4.7F), such an analysis may not be tractable.

A particularly dramatic phenotype of $hnt^{N4\text{-}F42.2}$ larvae is complete disorder and fine ramification of the DBs into long and thin coiled extensions that closely resemble terminal branches. These branches are often unable to migrate properly to the dorsal midline and fuse, resulting in sporadic movement of the defective branches through the body cavity (Fig. 4.7D). I also observed subtler phenotypes, wherein DBs correctly form and migrate close to the dorsal midline but ultimately fail to complete fusion or fuse in an incorrect conformation (Fig. 4.7E). These observed phenotypes are remarkably similar to previously described fusion defects reported in Notch (Llimargas et al., 1999; Ikeya & Hayashi, 1999), *esg* (Tanaka-Matakatsu et al., 1996, Samakovlis et al., 1996b), and *dys* mutants (Jiang & Crews, 2003). In the developing trachea, Notch signalling is required to specify the tip cell of migrating branches. Following tracheal placode invagination, nascent primary branches process the Bnl ligand which promotes branch migration and upregulation of both *pointed* (*pnt*) and *Dl* in the presumptive tip cell. Notch signalling laterally inhibits adjacent stalk

cells, suppressing *Dl* expression and promoting the stalk cell identity (Ikeya & Hayashi, 1999; Llimargas, 1999). Tip cells later assume the fusion cell identity by expressing fusion cell markers such as *dysfusion* and *escargot* (Jiang & Crews, 2003, Samakovlis et al., 1996b; Tanaka-Matakatsu et al., 1996). Given this context and the observed DB phenotypes, my results suggest that mutation of the single Su(H) consensus sequence results in fusion defects that resemble Notch phenotypes and that these phenotypes occur downstream of *hnt* expression.

5.5.1 *hnt* mechanisms downstream of Notch signalling in the developing trachea

Through what mechanisms does *hnt* impact the fusion process downstream of Notch? Notch loss of function mutants have been shown to exhibit ectopic changes to cell identities, causing an increased number of fusion cells expressing *esg* and subsequently, both fusion failure and ectopic fusion (Llimargas, 1999; Ikeya & Hayashi, 1999). Given that Notch activity is well-known to regulate cell fate in this context, and given that *hnt* is functioning downstream of Notch signalling, then it would naturally fit that *hnt* is involved in fusion cell specification as well. However, previous studies have reported that *hnt* null mutants express *esg* properly in the DB (Wilk et al., 2000). Therefore, assuming this is also true in $hnt^{N4\text{-}F42.2}$ mutants, then through what alternative mechanisms does *hnt* disrupt the fusion process outside of classical Notch cell-fate specification?

Since *hnt* null mutants have been shown to express *esg* normally (Wilk et al., 2000), then another interpretation is that the observed fusion defects in $hnt^{N4\text{-}F42.2}$ occur downstream of *esg* expression. *dys* is a fusion marker that is expressed in fusion cells

downstream of *esg,* and *dys* mutants exhibit fusion defects (Jiang & Crews, 2003) similar to those described for both $hnt^{N4\text{-}F42.2}$ (Fig. 4.7) and *esg* mutants (Tanaka-Matakatsu et al., 1996; Samakovlis et al., 1996b). While previous studies have shown that *esg* expression is normal in *hnt* null mutants (Wilk et al., 2000), *dys* expression has not been investigated. Therefore, to test if the observed fusion defects in $hnt^{N4\text{-}F42.2}$ mutants are occurring downstream of *esg,* future studies would benefit from examining the expression of *esg* and *dys* in $hnt^{N4\text{-}F42.2}$ mutants.

Given that *hnt* was found to regulate F-actin in the DT (Fig. 4.4), one interpretation is that *hnt* is playing a similar actin associated role in the DB context, and that the observed DB fusion defects in $hnt^{N4\text{-}F42.2}$ mutants are a result of actin misregulation downstream of Notch activity. The Drosophila formin *DAAM* is required to organize apical actin into rings in tracheal cells and mutants exhibit disorganized actin defects (Matusek et al., 2006) similar to $hnt^{\Delta N4}$ mutants (Fig. 4.4). Fusion cell contacts require the accumulation of E-cadherin (*shg*) and assembly of an F-actin rich track (Kato et al., 2016; Tanaka-Matakatsu et al., 1996), a process that is mediated in part by *formin3* (*form3)*, another member of the formin family of proteins (Tanaka et al., 2004). Formins function in actin-related processes by nucleating actin bundles, and *form3* mutants have been shown to exhibit fusion defects (Tanaka et al., 2004) that resemble the observed phenotypes in *esg* mutants (Tanaka-Matakatsu et al., 1996, Samakovlis et al., 1996b) and $hnt^{N4\text{-}F42.2}$ mutants (Fig. 4.7). Notably, *form3* mutants express *esg* normally despite the fusion defects (Tanaka et al., 2004). When taken together, this precedent could suggest a similar scenario taking place in $hnt^{N4\text{-}F42.2}$ mutants, where the observed fusion defects are a result of actin-related defects.

5.5.2 Su(H) likely interacts with other enhancer elements to regulate *hnt* expression in the trachea

I have shown that deletion of the NRE-4 sequence results in a lethal tracheal phenotype (Fig. 3.8), but direct mutation of the singular Su(H) consensus sequence does not produce tracheal phenotypes associated with lethality (Fig. 4.7). My results have also shown that *hnt* likely functions downstream of Notch activity through Su(H) in those contexts. The differences in the observed mutant phenotypes of $hnt^{N4\text{-}F42.2}$ and $hnt^{\Delta N4}$, would suggest that Su(H) is not the sole regulatory element in the NRE-4 enhancer region that regulates tracheal *hnt* expression. Enhancer elements often integrate signals from multiple transcription factors that work in tandem to regulate the spatiotemporal expression of a gene (reviewed in Levine, 2010; Zinzen et al., 2009). The Su(H) motif is no exception, and in the gene *single-minded,* Su(H) consensus binding sites are clustered with the consensus binding sequences of *snail, twist, and dorsal*. This combination of transcription binding sites is thought to limit the Notch responsive expression of *single-minded* to a single row of cells in the developing mesectoderm (Morel & Schweisguth, 1999). In addition, the expression of *hnt* downstream of Notch activity in crystal cells has been shown to be influenced by Lozenge and Serpent enhancer motifs in proximity to the Su(H) motif, where notably, mutation of *lozenge* motifs abolishes *hnt* expression (Terriente-Felix et al., 2013). Therefore, the observed differences in tracheal phenotypes of $hnt^{N4\text{-}F42.2}$ and $hnt^{\Delta N4}$ could be attributed to different effects of mutating a singular Su(H) motif, versus excision of the ~5 kb NRE-4 enhancer region, which likely deletes additional enhancer elements that regulate tracheal *hnt* expression.

Additionally, previous work has illustrated that multiple Su(H) binding sites in close proximity to one another can amplify the suppressor and activation properties of Su(H) (Bailey & Posakonv, 1995; Furriols & Bray, 2001). In some *E(spl)* locus members, (*E(spl)m4, E(spl)m8, E(spl)mγ*), Su(H) motifs are found in conserved "paired" arrangements, thought to promote synergistic interactions between bound Su(H) monomers (Bailey & Posakonv, 1995). Furthermore, a synthetic lacZ reporter was constructed by combining a tandem Su(H) motif and three copies of *Grainyhead* binding sequence and it was shown that Su(H) co-operated with *Grainyhead* to amplify expression downstream of Notch activation (Furriols & Bray, 2001). While *hnt* does not have any "paired" Su(H) motifs in the regulatory region, there are three individual Su(H) motifs found in the NRE-4/*Peb1* sequence (data not shown). All three of these motifs are perfect matches to the core consensus sequence, but only the Su(H) motif that was targeted and mutated in these experiments ($hnt^{N4\text{-}F42.2}$) had matching flanking bps in addition to the core sequence. Since mutation of the singular Su(H) consensus sequence in $hnt^{N4\text{-}F42.2}$ mutants was not sufficient to phenocopy $hnt^{\Delta N4}$ deletion mutants, it could be interpreted that the activated Su(H) transcription complex operates in tandem with other nearby Su(H) motifs in response to Notch signalling, and that mutation of a singular Su(H) motif yields a comparatively subtle modification to Notch signalling.

5.5.3 N^{ts} disruption of Notch activity generates similar tracheal *hnt* phenotypes

Given the evidence that the developmental tracheal defects in $hnt^{\Delta N4}$ and $hnt^{N4\text{-}F42.2}$ are likely downstream of Notch signalling, I decided to examine the effect of disrupting Notch signalling on *hnt* expression in these contexts. Since Notch activity is required for early morphogenetic events, I used a well-characterized temperature sensitive allele of Notch, N^{ts}, to knockout Notch signalling later in development. Embryos were raised at the permissive temperature (18°C) until the completion of DT fusion, after which they were shifted to the restrictive temperature (29°C) to inactivate Notch signalling.

Strikingly, under the temperature shift regime employed, N^{ts} first instar larvae exhibit tracheal collapse defects that phenocopy the tracheal collapse observed in $hnt^{\Delta N4}$ mutants (Fig. 4.10G-H). Previous studies have used a similar approach, using N^{ts}, to study Notch interactions in the tracheal context, but either strictly investigated only embryos (Ikeya & Hayashi, 1999) or observed late-stage larvae by using a hemizygous condition (Furriols & Bray, 2001). As such, my observations that N^{ts} larvae exhibit tracheal collapse are both novel and consistent with tracheal phenotypes observed in both $hnt^{\Delta N4}$ (Fig. 3.8) and *hnt* null mutants (Wilk et al., 2000). Additionally, *hnt* immunostainings of N^{ts} embryos show clear reductions of *hnt* expression in the TCJ and PNS cells (Fig. 4.10), consistent with other studies that have identified the TCJ (Furriols & Bray, 2001; Rao et al., 2015) and embryonic PNS (Schweisguth & Posakony, 1992; Guo et al., 1996; Moore et al., 2004) as sites of Notch activity. When combined, this data strongly suggests that both tracheal integrity and *hnt* expression in TCJ/PNS cells is Notch dependent.

5.5.4 TCJ cells and PNS cells are sites of robust Notch-dependent *hnt* expression

My observations clearly show that the TCJ cells of the DT are sites of robust endogenous *hnt* expression (Fig. 4.4, Fig. 4.10) as well as Notch signalling activity (Fig. 4.9). These observations are consistent with previous reports that identified the TCJ junction as a site of elevated Notch activity (Furriols & Bray, 2001; Rao et al., 2015; Li et al., 2024). While *hnt* is well known to be expressed in the developing trachea (Yip et al., 1997; Wilk et al., 2000), the distinctly increased level of *hnt* expression I observed in TCJ cells has not been reported and represents a novel finding.

Given the strong expression of *hnt* in TCJ cells and given that this expression is reduced in $hnt^{\Delta N4}$ and N^{ts} mutants (Fig. 4.4, Fig. 4.10), suggests that there is a role for Notch at the TCJ. The activation of Notch signalling, which is classically described as juxtacrine signalling, requires interaction with either of its transmembrane ligands Dl or Ser, both of which are expressed in the DT. *Dl* is expressed first, shortly after tracheal pit invagination in tip/fusion cells and interacts with Notch to determine and maintain tip/fusion cell identity (Ikeya & Hayashi, 1999; Llimargas 1999). After the completion of DT fusion, *Dl* is then broadly expressed along the length of the embryonic DT (Ikeya & Hayashi, 1999). *Ser* is also broadly expressed along the DT, starting at stage 15, but a role has not been defined for *Ser* in the developing trachea (Ikeya & Hayashi, 1999; Haberman et al., 2003; Rao et al., 2015). In later larval stages where the tracheal cells are much larger, it has been shown that both expression of *Dl* and *Ser* in DT is distinctly cutoff at the TCJ cell (Rao et al., 2015). As such, the expression timings and spatial domains of the Notch ligands in the DT coincide with my observations showing strong expression levels of both *hnt* (Fig. 4.4) and the Notch activity reporter in the TCJ cells (Fig. 4.9). When taken together, it could be interpreted that *hnt* is

upregulated in response to Notch interactions with either Dl or Ser in the adjacent DT cells (Ikeya & Hayashi, 1999; Rao et al., 2015; Furriols & Bray, 2001; this work). *Dl* has been shown to generate Notch responses in adjacent cells when ectopically expressed in DB cells (Rao et al., 2015). In contrast, *Ser* has been briefly investigated in the tracheal context, but a tracheal Notch-*Ser* role has yet to be defined (Ikeya & Hayashi, 1999; Haberman et al., 2003; Rao et al., 2015). Interestingly, null alleles of *Ser* display larval lethality (Thomas et al., 1991). It would be valuable to investigate if *Ser* is providing the signal for Notch activation and the strong *hnt* expression observed in TCJ cells.

In other developmental contexts, Notch is known to play a role in mediating boundary formation, such as in the specification of imaginal ring cells of the salivary gland ducts (Haberman et al., 2003), as well as in the eye and wing imaginal discs (Cho & Choi, 1998; Couso et al., 1995; Panin et al., 1997). Given that the TCJ cell intersects two unique tracheal branches and is a site of Notch activity, then perhaps Notch is active at this junction to define a border from the DT to the TC branch. This interpretation is consistent with a previous study in third instar thoracic tracheal segments that identified both the TC junction and the DB junction as sites of Notch activity, acting to segregate the DT from other branches (Rao et al., 2015). If that context correlates to the abdominal segments where the *hnt* TCJ cells are located, then it could suggest a similar function where Notch activity acts to define a border to the TC branch and segregate the DT. However, given that I only observed strong *hnt* expression in the TC junction, and not the DB junction, could point to an additional function of *hnt* unique to the TC branch. Based on early preliminary data, I predict that this additional function could be related to cell adhesion, a function in which *hnt* and RREB-1 have been previously implicated (Melani et al., 2008; Morgani et al., 2021).

These primary observations, which are included in the appendix of this thesis (Fig. A3), warrant further investigation (see section 5.7 Future Directions).

5.5.4.1 PNS cell with strong expression of *hnt* is likely an extrasensory organ socket cell

In addition to prominent expression in the tracheal system, I also observed *Peb1* reporter expression in a row of seven ventral PNS cells, one per abdominal segment, spanning A1-A7 (Fig. 4.2). *hnt* expression in these PNS cells is notably distinct, indicated by immunostainings of wildtype embryos, and this robust expression is reduced in $hnt^{\Delta N4}$ and N^{ts} embryos (Fig. 4.4, Fig. 4.10). *hnt* is known to be expressed in the developing PNS system (Yip et al., 1997; Wilk et al., 2000) but a distinction between this particular cell and other *hnt* expressing PNS cells has not been reported.

The embryonic and larval PNS system is complex and consists of several different sensory organs, which in turn, are composed of several neurons and support cells, and as such, it was not immediately apparent which PNS cell is the one I observed in *hnt* immunostainings and *Peb1* reporter expression analysis. Here, I present my preliminary analysis into the identity of the PNS cell.

The PNS cell is first detected late into embryonic development (Fig. 4.2, Fig. 4.4). By this stage, the PNS has differentiated into the neuron and supporting cell identities (Brewster & Bodmer, 1995). The *Peb1* reporter did not co-express with a neuron specific driver (*elav-GAL4*) but did co-express with both a *DPax2* and Notch activity reporter (*Su(H)Gbe-GAL4*) (appendix, Fig. A2), therefore excluding the neuron identity and

indicating a support cell identity. This analysis is consistent with known PNS expression profiles of *DPax2* (Kavaler et al., 1999; Kim et al., 2020) and *Su(H)/*Notch activity (Barolo et al., 2000). Neurons and their three support cells are differentiated through a series of asymmetric divisions, a process that is mediated by Notch and Numb signalling (Guo et al., 1996; Kavaler et al., 1999). Notably, the socket support cell (tormogen) expresses high levels of Su(H) during development (Schweisguth & Posakony, 1992; Barolo et al., 2000). As such, since I observed *Peb1* reporter expression coincide with *Su(H)Gbe-GAL4* reporter expression (Fig. 4.8), I hypothesized the PNS cell is likely a tormogen support cell. Under this assumption, I analyzed the PNS cell in larval stages and observed an enclosed structure within the PNS cell that originated from an adjacent cell and extended to a molting pore (Fig. 4.2). This description is consistent with the structure of the v' extrasensory organ (Richter et al., 2015). Additionally, this PNS cell was found lateral to the second branch of the segmental nerve and adjacent to the cuticle surface (appendix, Fig. A2). Therefore, based on these observations, I surmise this particular PNS cell is a tormogen cell of the v'esA (extrasensory organ) cell cluster (Brewster & Bodmer, 1995).

5.6 Conclusions

This study has successfully described a novel context and role for *hnt* as a downstream responder of Notch signalling in the developing embryonic tracheal system. This was accomplished by designing and generating *hnt* deletion alleles using CRISPR/Cas9 genome editing that aimed to eliminate an *in vivo* Notch response. Of note, my data have identified the TCJ cells and PNS cells as particularly robust sites of *hnt* expression that have not been previously acknowledged. While the general expression of *hnt* within the developing tracheal system is likely not dependent on Notch signalling, a specific up-regulation in the TCJ cells does reflect a novel Notch-dependent response. In addition, and also representing a novel finding, I have shown that *hnt* is required for regulating F-actin organization in the developing tracheal system.

Furthermore, as an unexpected byproduct of my genome editing experiments, I discovered a capability for the *3xP3-DsRed* cassette to function as an enhancer trap. This enhancer trap effect has not been reported by any other Drosophila research group.

Overall, this work builds upon previously established knowledge of *hnt* regarding the location of tracheal specific enhancers, and introduces an additional context where *hnt* is likely a direct target of the Notch-signalling pathway. A key observation, and something that may be relevant to understanding *hnt* and its mammalian homolog, *RREB-1*, is perhaps that signalling pathways, such as Notch, likely operate to fine-tune the levels of expression of transcription factors such as *hnt*. The overall level of expression of transcription factors such as *hnt* may prove critical for certain developmental events as well as better understanding the progression of RAS-related pathologies.

5.7 Future Directions

My thesis represents an exploration of novel developmental contexts where *hnt* responds to Notch signalling. Given the results in my thesis, future studies could examine the role of *hnt* in tracheal development in further detail.

I have determined that specific cell types such as the TCJ cells and PNS cells are sites of robust *hnt* expression downstream of Notch activity. However, I have yet to determine specific functions associated with the observed increased expression levels of *hnt* in these contexts. Preliminary observations have indicated a striking accumulation of adhesion molecules at the lateral adherens junctions of TCJ cells. Since *hnt* has been previously shown to regulate cell adhesion in other contexts, this co-incidental localization could point toward a similar cell-adhesion related role for *hnt* in the TCJ cells. Further investigation is also warranted to investigate the role of *hnt* in the specific PNS cells, as *Peb1* reporter construct analyses has shown that there is a unique enhancer element for these PNS cells despite *hnt* being expressed in numerous PNS cells during development.

Although I have shown there is a general tracheal role of *hnt* in actin organization, I have not identified downstream targets of *hnt* in the trachea. Previous studies have shown that *hnt* interacts with different actin-related genes that include *karst*, which encodes β_H-Spectrin and *jbug* (Wilk et al., 2004; Oliva et al., 2015). Both of these genes encode proteins involved in actin-crosslinking and polymerization and apically localize in all tracheal cells and as such, it would be interesting to investigate if these genes are downstream targets of Hnt (Thomas & Kiehart, 1994; Chung et al., 2021).

In addition, I have yet to identify which Notch ligand is required to upregulate *hnt* expression in Notch responsive contexts such as the TCJ or PNS cells. It would be beneficial to perform similar temperature sensitive experiments described in section 2.8 using a temperature sensitive knockdown allele of Delta, dl^{6B}, given that Notch and Dl interactions are required for initial morphogenesis events (Giniger et al., 1993; Ikeya & Hayashi, 1999). *Ser* mutants have been reported to not impact overall tracheal morphology but Notch activity and downstream *hnt* expression in TCJ cells has not been investigated in that mutant background (Haberman et al., 2003; Ikeya & Hayashi, 1999).

Future experiments warrant investigation into a cell adhesion related function of *hnt* in the TCJ cells. *hnt* has been reported to regulate adhesion molecule levels in anterior follicle border cells and *hnt* clonal mutants exhibited an accumulation of cell adhesion proteins Armadillo (β-catenin) and DE-cadherin, and RREB-1 has been shown to regulate cadherin in embryonic mouse epiblast cells (Melani et al., 2008; Morgani et al., 2021). Preliminary observations of the TCJ cells using reporter constructs have shown a unique accumulation of both DE-cadherin (Fig. A3) and Armadillo (data not shown) at the ventral adherens junctions of TCJ cells. As such, it would be interesting to examine if *hnt* is playing a comparable cell adhesion role in the TCJ context as seen in the follicle cell context (Melani et al., 2008).

References

Artavanis-Tsakonas, S., Matsuno, K., & Fortini, M. E. (1995). Notch signaling. *Science*, *268*(5208), 225–232. https://doi.org/10.1126/science.7716513

Baechler, B. L., McKnight, C., Pruchnicki, P. C., Biro, N. A., & Reed, B. H. (2016). Hindsight/RREB-1 functions in both the specification and differentiation of stem cells in the adult midgut of Drosophila. *Biology Open*, *5*(1), 1–10. https://doi.org/10.1242/bio.015636

Bailey, A. M., & Posakony, J. W. (1995). Suppressor of hairless directly activates transcription of enhancer of split complex genes in response to Notch receptor activity. *Genes & development*, *9*(21), 2609–2622. https://doi.org/10.1101/gad.9.21.2609

Barolo, S. (2012). Shadow enhancers: Frequently asked questions about distributed cis-regulatory information and enhancer redundancy. *BioEssays*, *34*(2), 135–141. https://doi.org/10.1002/bies.201100121

Barolo, S., Walker, R. G., Polyanovsky, A. D., Freschi, G., Keil, T., & Posakony, J. W. (2000). A Notch-Independent Activity of Suppressor of Hairless Is Required for Normal Mechanoreceptor Physiology. *Cell*, *103*(6), 957–970. https://doi.org/https://doi.org/10.1016/S0092-8674(00)00198-7

Beitel, G. J., & Krasnow, M. A. (2000). Genetic control of epithelial tube size in the Drosophila tracheal system. *Development*, *127*(15), 3271–3282.

Berghammer, A. J., Klingler, M., & Wimmer, E. A. (1999). Genetic techniques: A universal marker for transgenic insects. *Nature, 402*(6760), 370-1. doi:https://doi.org/10.1038/46463

Bray, S. J. (2006). Notch signalling: A simple pathway becomes complex. *Nature Reviews Molecular Cell Biology*, *7*(9), 678–689. https://doi.org/10.1038/nrm2009

Brewster, R., & Bodmer, R. (1995). Origin and specification of type II sensory neurons in Drosophila. *Development*, *121*(9), 2923–2936. https://doi.org/10.1242/dev.121.9.2923

Brodu, V., & Casanova, J. (2006). The RhoGAP crossveinless-c links trachealess and EGFR signaling to cell shape remodeling in Drosophila tracheal invagination. *Genes and Development*, *20*(13), 1817–1828. https://doi.org/10.1101/gad.375706

Calhoun, V. C., Stathopoulos, A., & Levine, M. (2002). Promoter-proximal tethering elements regulate enhancer-promoter specificity in the Drosophila Antennapedia complex. *Proceedings of the National Academy of Sciences of the United States of America*, *99*(14), 9243–9247. https://doi.org/10.1073/pnas.142291299

Campos-Ortega, J.A. and V. Hartenstein. (1985). The embryonic development of Drosophila melanogaster. Springer Verlag, Berlin/Heidelberg, Germany.

Caviglia, S., & Luschnig, S. (2014). Tube fusion: Making connections in branched tubular networks. *Seminars in Cell and Developmental Biology*, *31*, 82–90. https://doi.org/10.1016/j.semcdb.2014.03.018

Chen, C.-K., Kühnlein, R. P., Eulenberg, K. G., Vincent, S., Affolter, M., & Schuh, R. (1998). The transcription factors KNIRPS and KNIRPS RELATED control cell migration and branch morphogenesis during Drosophila tracheal development. *Development*, *125*(24), 4959–4968. https://doi.org/10.1242/dev.125.24.4959

Chen, R.-L., Chou, Y.-C., Lan, Y.-J., Huang, T.-S., & Shen, C.-K. J. (2010). Developmental silencing of human ζ-globin gene expression is mediated by the transcriptional repressor RREB1. *Journal of Biological Chemistry*, *285*(14), 10189–10197. https://doi.org/10.1074/jbc.M109.049130

Chihara, T., & Hayashi, S. (2000). Control of tracheal tubulogenesis by Wingless signaling. *Development*, *127*(20), 4433–4442.

Cho, K. O., & Choi, K. W. (1998). Fringe is essential for mirror symmetry and morphogenesis in the Drosophila eye. *Nature*, *396*(6708), 272–276. https://doi.org/10.1038/24394

Chung, S. Y., Le, T. P., Vishwakarma, V., Cheng, Y. L., & Andrew, D. J. (2021). Isoform-specific roles of the Drosophila filamin-type protein Jitterbug (Jbug) during development. *Genetics*, *219*(2). https://doi.org/10.1093/genetics/iyab100

Cormier, O., Mohseni, N., Voytyuk, I., & Reed, B. H. (2012). Autophagy can promote but is not required for epithelial cell extrusion in the amnioserosa of the Drosophila embryo. *Autophagy*, *8*(2), 252–264. https://doi.org/10.4161/auto.8.2.18618

Couso, J. P., Knust, E., & Martinez Arias, A. (1995). Serrate and wingless cooperate to induce vestigial gene expression and wing formation in Drosophila. *Current biology : CB*, *5*(12), 1437–1448. https://doi.org/10.1016/s0960-9822(95)00281-8

Deady, L. D., Li, W., & Sun, J. (2017). The zinc-finger transcription factor hindsight regulates ovulation competency of Drosophila follicles. *ELife*, *6*. https://doi.org/10.7554/eLife.29887

Deng, Y. N., Xia, Z., Zhang, P., Ejaz, S., & Liang, S. (2020). Transcription factor RREB1: From target genes towards biological functions. *International Journal of Biological Sciences*, *16*(8), 1463–1473. https://doi.org/10.7150/ijbs.40834

Du, L., Zhou, A., Patel, A., Rao, M., Anderson, K., & Roy, S. (2017). Unique patterns of organization and migration of FGF-expressing cells during Drosophila morphogenesis. *Developmental Biology*, *427*(1), 35–48. https://doi.org/https://doi.org/10.1016/j.ydbio.2017.05.009

Ewen-Campen, B., Yang-Zhou, D., Fernandes, V. R., González, D. P., Liu, L.-P., Tao, R., Ren, X., Sun, J., Hu, Y., Zirin, J., Ni, J.-Q., & Perrimon, N. (2017). Optimized strategy for in vivo Cas9-activation in Drosophila. *Proceedings of the National Academy of Sciences of the United States of America*, *114*(35), 9409–9414. https://doi.org/10.1073/pnas.1707635114

Farley, J. E., Burdett, T. C., Barria, R., Neukomm, L. J., Kenna, K. P., Landers, J. E., & Freeman, M. R. (2018). Transcription factor Pebbled/RREB1 regulates injury-induced axon degeneration. *Proceedings of the National Academy of Sciences of the United States of America*, *115*(6), 1358–1363. https://doi.org/10.1073/pnas.1715837115

Fessler, J. H., & Fessler, L. I. (1989). Drosophila Extracellular Matrix. *Annual Review of Cell and Developmental Biology*, *5*(Volume 5, 1989), 309–339. https://doi.org/https://doi.org/10.1146/annurev.cb.05.110189.001521

Fortini, M. E., & Artavanis-Tsakonas, S. (1994). The suppressor of hairless protein participates in notch receptor signaling. *Cell*, *79*(2), 273–282. https://doi.org/10.1016/0092-8674(94)90196-1

Franch-Marro, X., & Casanova, J. (2002). Spalt-induced specification of distinct dorsal and ventral domains is required for Drosophila tracheal patterning. *Developmental Biology*, *250*(2), 374–382. https://doi.org/10.1006/dbio.2002.0799

Frank, L. H., & Rushlow, C. (1996). A group of genes required for maintenance of the amnioserosa tissue in Drosophila. *Development*, *122*(5), 1343–1352. https://doi.org/10.1242/dev.122.5.1343

Fuerstenberg, S., & Giniger, E. (1998). Multiple Roles for *Notch* in Drosophila *Myogenesis*. *Developmental Biology*, *201*(1), 66–77. https://doi.org/https://doi.org/10.1006/dbio.1998.8944

Giniger, E., Jan, L. Y., & Jan, Y. N. (1993). Specifying the path of the intersegmental nerve of the Drosophila embryo: a role for Delta and Notch. *Development*, *117*(2), 431–440. https://doi.org/10.1242/dev.117.2.431

Glasheen, B. M., Robbins, R. M., Piette, C., Beitel, G. J., & Page-McCaw, A. (2010). A matrix metalloproteinase mediates airway remodeling in Drosophila. *Developmental Biology*, *344*(2), 772–783. https://doi.org/10.1016/j.ydbio.2010.05.504

Gratz, S. J., Cummings, A. M., Nguyen, J. N., Hamm, D. C., Donohue, L. K., Harrison, M. M., Wildonger, J., & O'connor-Giles, K. M. (2013). Genome engineering of Drosophila with the CRISPR RNA-guided Cas9 nuclease. *Genetics*, *194*(4), 1029–1035. https://doi.org/10.1534/genetics.113.152710

Gratz, S. J., Harrison, M. M., Wildonger, J., & O'Connor-Giles, K. M. (2015). Precise Genome Editing of Drosophila with CRISPR RNA-Guided Cas9. In M. Lundgren, E. Charpentier, & P. C. Fineran (Eds.), *CRISPR: Methods and Protocols* (pp. 335–348). Springer New York. https://doi.org/10.1007/978-1-4939-2687-9_22

Gratz, S. J., Ukken, F. P., Rubinstein, C. D., Thiede, G., Donohue, L. K., Cummings, A. M., & Oconnor-Giles, K. M. (2014). Highly specific and efficient CRISPR/Cas9-catalyzed homology-directed repair in Drosophila. *Genetics*, *196*(4), 961–971. https://doi.org/10.1534/genetics.113.160713

Guan, X., Middlebrooks, B. W., Alexander, S., & Wasserman, S. A. (2006). Mutation of TweedleD, a member of an unconventional cuticle protein family, alters body shape in Drosophila. *Proceedings of the National Academy of Sciences of the United States of America*, *103*(45), 16794–16799. https://doi.org/10.1073/pnas.0607616103

Guo, M., Yeh Jan, L., & Nung Jan, Y. (1996). Control of Daughter Cell Fates during Asymmetric Division: Interaction of Numb and Notch. *Trends in Genetics*, *12*(10), 399. https://doi.org/https://doi.org/10.1016/0168-9525(96)90100-6

Haberman, A. S., Isaac, D. D., & Andrew, D. J. (2003). Specification of cell fates within the salivary gland primordium. *Developmental Biology*, *258*(2), 443–453. https://doi.org/10.1016/S0012-1606(03)00140-4

Hannezo, E., Dong, B., Recho, P., Joanny, J.-F., & Hayashi, S. (2015). Cortical instability drives periodic supracellular actin pattern formation in epithelial tubes. *Proceedings of the National Academy of Sciences of the United States of America*, *112*(28), 8620–8625. https://www.jstor.org/stable/26466011

Hartenstein, A. Y., Rugendorff, A., Tepass, U., & Hartenstein, V. (1992). The function of the neurogenic genes during epithelial development in the Drosophila embryo. *Development*, *116*(4), 1203–1220. https://doi.org/10.1242/dev.116.4.1203

Hartenstein, V., & Jan, Y. N. (1992). Studying Drosophila embryogenesis with P-lacZ enhancer trap lines. *Roux's Archives of Developmental Biology*, *201*(4), 194–220. https://doi.org/10.1007/BF00188752

Hatakeyama, M., Yatomi, J., Sumitani, M., Takasu, Y., Sekiné, K., Niimi, T., & Sezutsu, H. (2016). Knockout of a transgene by transcription activator-like effector nucleases (TALENs) in the sawfly, Athalia rosae (Hymenoptera) and the ladybird beetle, Harmonia axyridis (Coleoptera). *Insect Molecular Biology*, *25*(1), 24–31. https://doi.org/10.1111/imb.12195

Hong, J. W., Hendrix, D. A., & Levine, M. S. (2008). Shadow enhancers as a source of evolutionary novelty. In *Science* (Vol. 321, Issue 5894, p. 1314). https://doi.org/10.1126/science.1160631

Horn, C., Jaunich, B., & Wimmer, E. A. (2000). Highly sensitive, fluorescent transformation marker for Drosophila transgenesis. *Development Genes and Evolution*, *210*(12), 623–629. https://doi.org/10.1007/s004270000111

Hwang, W. Y., Fu, Y., Reyon, D., Maeder, M. L., Tsai, S. Q., Sander, J. D., Peterson, R. T., Yeh, J. R. J., & Joung, J. K. (2013). Efficient genome editing in zebrafish using a CRISPR-Cas system. *Nature Biotechnology*, *31*(3). https://doi.org/10.1038/nbt.2501

Ikeya, T., & Hayashi, S. (1999). Interplay of Notch and FGF signaling restricts cell fate and MAPK activation in the Drosophila trachea. *Development (Cambridge)*, *126*(20), 4455–4463. https://doi.org/10.1242/dev.126.20.4455

Jiang, L., & Crews, S. T. (2003). The Drosophila dysfusion Basic Helix-Loop-Helix (bHLH)–PAS Gene Controls Tracheal Fusion and Levels of the Trachealess bHLH-PAS Protein. *Molecular and Cellular Biology*, *23*(16), 5625–5637. https://doi.org/10.1128/mcb.23.16.5625-5637.2003

Jinek, M., Chylinski, K., Fonfara, I., Hauer, M., Doudna, J. A., & Charpentier, E. (2012). A programmable dual-RNA-guided DNA endonuclease in adaptive bacterial immunity. *Science*, *337*(6096), 816–821. https://doi.org/10.1126/science.1225829

Källstig, E., Ruchti, E., Raman, M., Asadzadeh, J., Schneider, B. L., & McCabe, B. D. (2025). Highly frequent undesired insertional mutagenesis during *Drosophila* genome editing. *bioRxiv*, 2025.08.11.669658. https://doi.org/10.1101/2025.08.11.669658

Kaltschmidt, J. A., Davidson, C. M., Brown, N. H., & Brand, A. H. (2000). Rotation and asymmetry of the mitotic spindle direct asymmetric cell division in the developing central nervous system. *Nature Cell Biology*, *2*(1), 7–12. https://doi.org/10.1038/71323

Kane, N. S., Vora, M., Varre, K. J., & Padgett, R. W. (2017). Efficient screening of CRISPR/Cas9-induced events in Drosophila using a Co-CRISPR strategy. *G3: Genes, Genomes, Genetics*, *7*(1). https://doi.org/10.1534/g3.116.036723

Kato, K., Chihara, T., & Hayashi, S. (2004). Hedgehog and Decapentaplegic instruct polarized growth of cell extensions in the Drosophila trachea. *Development*, *131*(21), 5253–5261. https://doi.org/10.1242/dev.01404

Kato, K., Dong, B., Wada, H., Tanaka-Matakatsu, M., Yagi, Y., & Hayashi, S. (2016). Microtubule-dependent balanced cell contraction and luminal-matrix modification accelerate epithelial tube fusion. *Nature Communications*, *7*. https://doi.org/10.1038/ncomms11141

Kavaler, J., Fu, W., Duan, H., Noll, M., & Posakony, J. W. (1999). An essential role for the Drosophila Pax2 homolog in the differentiation of adult sensory organs. *Development*, *126*(10), 2261–2272. https://doi.org/10.1242/dev.126.10.2261

Kent, O. A., Chivukula, R. R., Mullendore, M., Wentzel, E. A., Feldmann, G., Lee, K. H., Liu, S., Leach, S. D., Maitra, A., & Mendell, J. T. (2010). Repression of the miR-143/145 cluster by oncogenic Ras initiates a tumor-promoting feed-forward pathway. *Genes and Development*, *24*(24), 2754–2759. https://doi.org/10.1101/gad.1950610

Kent, O. A., Fox-Talbot, K., & Halushka, M. K. (2013). RREB1 repressed miR-143/145 modulates KRAS signaling through downregulation of multiple targets. *Oncogene*, *32*(20), 2576–2585. https://doi.org/10.1038/onc.2012.266

Kim, D.-H., Kim, Y.-J., & Adams, M. E. (2018). Endocrine regulation of airway clearance in Drosophila. *Proceedings of the National Academy of Sciences of the United States of America*, *115*(7), 1535–1540. https://doi.org/10.1073/pnas.1717257115

Kim, M., Du, O. Y., Whitney, R. J., Wilk, R., Hu, J., Krause, H. M., Kavaler, J., & Reed, B. H. (2020). A functional analysis of the drosophila gene hindsight: Evidence for positive regulation of EGFR signaling. *G3: Genes, Genomes, Genetics*, *10*(1), 117–127. https://doi.org/10.1534/g3.119.400829

Kooh, P. J., Fehon, R. G., & Muskavitch, M. A. T. (1993). Implications of dynamic patterns of Delta and Notch expression for cellular interactions during Drosophila development. *Development*, *117*(2), 493–507. https://doi.org/10.1242/dev.117.2.493

Krejcí, A., Bernard, F., Housden, B. E., Collins, S., & Bray, S. J. (2009). Direct response to Notch activation: signaling crosstalk and incoherent logic. *Science signaling*, *2*(55), ra1. https://doi.org/10.1126/scisignal.2000140

Levine, M. (2010). Transcriptional Enhancers in Animal Development and Evolution. *Current Biology*, *20*(17), R754–R763. https://doi.org/10.1016/j.cub.2010.06.070

Li, Y., Lu, T., Dong, P., Chen, J., Zhao, Q., Wang, Y., Xiao, T., Wu, H., Zhao, Q., & Huang, H. (2024). A single-cell atlas of Drosophila trachea reveals glycosylation-mediated Notch signaling in cell fate specification. *Nature Communications*, *15*(1). https://doi.org/10.1038/s41467-024-46455-w

Liu, H., Hew, H. C., Lu, Z.-G., Yamaguchi, T., Miki, Y., & Yoshida, K. (2009). DNA damage signalling recruits RREB-1 to the p53 tumour suppressor promoter. *Biochemical Journal*, *422*(3), 543–551. https://doi.org/10.1042/BJ20090342

Liu, L., Johnson, W. A., & Welsh, M. J. (2003). Drosophila DEG/ENaC Pickpocket Genes Are Expressed in the Tracheal System, Where They May Be Involved in Liquid Clearance. *Proceedings of the National Academy of Sciences of the United States of America*, *100*(4), 2128–2133.

Llimargas, M. (1999). The Notch pathway helps to pattern the tips of the Drosophila tracheal branches by selecting cell fates. *Development*, *126*(11), 2355–2364.

Llimargas, M. (2000). wingless and its signalling pathway have common and separable functions during tracheal development. *Development*, *127*(20), 4407–4417. https://doi.org/10.1242/dev.127.20.4407

Llimargas, M., & Casanova, J. (1999). EGF signalling regulates cell invagination as well as cell migration during formation of tracheal system in Drosophila. *Development Genes and Evolution*, *209*(3), 174–179. https://doi.org/10.1007/s004270050241

Manning, G., and Krasnow, M. A. (1993). Development of the Drosophila tracheal system. In "The Development of Drosophila melanogaster" (M. Bate and A. Martinez Arias, Eds.), Vol. 1, pp. 609–685. Cold Spring Harbor Laboratory Press, Cold Spring Harbor, N Y.

Matusek, T., Djiane, A., Jankovics, F., Brunner, D., Mlodzik, M., & Mihály, J. (2006). The Drosophila formin DAAM regulates the tracheal cuticle pattern through organizing the actin cytoskeleton. *Development*, *133*(5), 957–966. https://doi.org/10.1242/dev.02266

Melani, M., Simpson, K. J., Brugge, J. S., & Montell, D. (2008). Regulation of Cell Adhesion and Collective Cell Migration by Hindsight and Its Human Homolog RREB1. *Current Biology*, *18*(7), 532–537. https://doi.org/10.1016/j.cub.2008.03.024

Miao, G., & Hayashi, S. (2016). Escargot controls the sequential specification of two tracheal tip cell types by suppressing FGF signaling in Drosophila. *Development (Cambridge)*, *143*(22), 4261–4271. https://doi.org/10.1242/dev.133322

Ming, L., Wilk, R., Reed, B. H., & Lipshitz, H. D. (2013). Drosophila Hindsight and mammalian RREB-1 are evolutionarily conserved DNA-binding transcriptional attenuators. *Differentiation*, *86*(4–5), 159–170. https://doi.org/10.1016/j.diff.2013.12.001

Moore, A. W., Roegiers, F., Jan, L. Y., & Jan, Y. N. (2004). Conversion of neurons and glia to external-cell fates in the external sensory organs of Drosophila hamlet mutants by a cousin-cousin cell-type respecification. *Genes and Development*, *18*(6), 623–628. https://doi.org/10.1101/gad.1170904

Morgani, S. M., Su, J., Nichols, J., Massagué, J., & Hadjantonakis, A. K. (2021). The transcription factor Rreb1 regulates epithelial architecture, invasiveness and vasculogenesis in early mouse embryos. *ELife*, *10*. https://doi.org/10.7554/ELIFE.64811

Moussian, B. (2010). Recent advances in understanding mechanisms of insect cuticle differentiation. In *Insect Biochemistry and Molecular Biology* (Vol. 40, Issue 5, pp. 363–375). https://doi.org/10.1016/j.ibmb.2010.03.003

Ng, W. A., Ma, A., Chen, M., & Reed, B. H. (2020). A method for rapid selection of randomly induced mutations in a gene of interest using CRISPR/Cas9 mediated activation of gene expression. *G3: Genes, Genomes, Genetics*, *10*(6), 1893–1901. https://doi.org/10.1534/g3.120.401299

Ohshiro, T., Emori, Y., & Saigo, K. (2002). Ligand-dependent activation of breathless FGF receptor gene in Drosophila developing trachea. *Mechanisms of Development*, *114*(1), 3–11. https://doi.org/https://doi.org/10.1016/S0925-4773(02)00042-4

Oliva, C., & Sierralta, J. (2010). Regulation of axonal development by the nuclear protein hindsight (pebbled) in the Drosophila visual system. *Developmental Biology*, *344*(2), 911–921. https://doi.org/10.1016/j.ydbio.2010.06.007

Oliva, C., Molina-Fernandez, C., Maureira, M., Candia, N., López, E., Hassan, B., Aerts, S., Cánovas, J., Olguín, P., & Sierralta, J. (2015). Hindsight regulates photoreceptor axon targeting through transcriptional control of jitterbug/Filamin and multiple genes involved in axon guidance in Drosophila. *Developmental Neurobiology*, *75*(9), 1018–1032. https://doi.org/https://doi.org/10.1002/dneu.22271

Öztürk-Çolak, A., Marygold, S. J., Antonazzo, G., Attrill, H., Goutte-Gattat, D., Jenkins, V. K., Matthews, B. B., Millburn, G., dos Santos, G., Tabone, C. J., & Consortium, F. (2024). FlyBase: updates to the Drosophila genes and genomes database. *Genetics*, *227*(1), iyad211. https://doi.org/10.1093/genetics/iyad211

Öztürk-Çolak, A., Moussian, B., & Araújo, S. J. (2016). Drosophila chitinous aECM and its cellular interactions during tracheal development. *Developmental dynamics : an official publication of the American Association of Anatomists*, *245*(3), 259–267. https://doi.org/10.1002/dvdy.24356

Öztürk-Çolak, A., Moussian, B., Araújo, S. J., & Casanova, J. (2016). A feedback mechanism converts individual cell features into a supracellular ECM structure in Drosophila trachea. *eLife*, *5*, e09373. https://doi.org/10.7554/eLife.09373

Öztürk-Çolak, A., Stephan-Otto Attolini, C., Casanova, J., & Araújo, S. J. (2018). Blimp-1 Mediates Tracheal Lumen Maturation in Drosophila melanogaster. *Genetics*, *210*(2), 653–663.

Page-McCaw, A., Serano, J., Santé, J. M., & Rubin, G. M. (2003). Drosophila matrix metalloproteinases are required for tissue remodeling, but not embryonic development. *Developmental Cell*, *4*(1), 95–106. https://doi.org/10.1016/S1534-5807(02)00400-8

Panin, V. M., Papayannopoulos, V., Wilson, R., & Irvine, K. D. (1997). Fringe modulates notch-ligand interactions. *Nature, 387*(6636), 908-12. doi:https://doi.org/10.1038/43191

Pickup, A. T., Lamka, M. L., Sun, Q., Yip, M. L. R., & Lipshitz, H. D. (2002). Control of photoreceptor cell morphology, planar polarity and epithelial integrity during Drosophila eye development. *Development*, *129*(9), 2247–2258.

Pickup, A. T., Ming, L., & Lipshitz, H. D. (2009). Hindsight modulates Delta expression during Drosophila cone cell induction. *Development*, *136*(6), 975–982. https://doi.org/10.1242/dev.027318

Pitsouli, C., & Perrimon, N. (2010). Embryonic multipotent progenitors remodel the Drosophila airways during metamorphosis. *Development*, *137*(21), 3615–3624. https://doi.org/10.1242/dev.056408

Pitsouli, C., & Perrimon, N. (2013). The homeobox transcription factor cut coordinates patterning and growth during Drosophila airway remodeling. *Science signaling*, *6*(263), ra12. https://doi.org/10.1126/scisignal.2003424

Radtke, F., & Raj, K. (2003). The role of Notch in tumorigenesis: Oncogene or tumour suppressor. *Nature Reviews Cancer*, *3*(10), 756–767. https://doi.org/10.1038/nrc1186

Rao, P. R., Lin, L., Huang, H., Guha, A., Roy, S., & Kornberg, T. B. (2015). Developmental compartments in the larval trachea of Drosophila. *ELife*, *4*(OCTOBER2015). https://doi.org/10.7554/eLife.08666.001

Reed, B. H., McMillan, S. C., & Chaudhary, R. (2009). The preparation of Drosophila embryos for live-imaging using the hanging drop protocol. *Journal of visualized experiments : JoVE*, (25), 1206. https://doi.org/10.3791/1206

Reed, B. H., Wilk, R., & Lipshitz, H. D. (2001). Downregulation of Jun kinase signaling in the amnioserosa is essential for dorsal closure of the Drosophila embryo. *Current Biology*, *11*(14), 1098–1108. https://doi.org/10.1016/S0960-9822(01)00318-9

Reeves, N., & Posakony, J. W. (2005). Genetic Programs Activated by Proneural Proteins in the Developing Drosophila PNS. *Developmental Cell*, *8*(3), 413–425. https://doi.org/https://doi.org/10.1016/j.devcel.2005.01.020

Reichman-Fried, M., Dickson, B., Hafen, E., & Shilo, B. Z. (1994). Elucidation of the role of breathless, a Drosophila FGF receptor homolog, in tracheal cell migration. *Genes & development*, *8*(4), 428–439. https://doi.org/10.1101/gad.8.4.428

Ribeiro, C., Neumann, M., & Affolter, M. (2004). Genetic Control of Cell Intercalation during Tracheal Morphogenesis in Drosophila but during later stages, branch outgrowth stalls, and the. *Current Biology*, *14*. https://doi.org/10.1016/j

Richter, V., Rist, A., Kislinger, G., Laumann, M., Schoofs, A., Miroschnikow, A., Pankratz, M. J., Cardona, A., & Thum, A. S. (2025). Morphology and ultrastructure of external sense organs of Drosophila larvae. *ELife*, *12*. https://doi.org/10.7554/elife.91155

Samakovlis, C., Hacohen, N., Manning, G., Sutherland, D. C., Guillemin, K., & Krasnow, M. A. (1996). Development of the Drosophila tracheal system occurs by a series of morphologically distinct but genetically coupled branching events. *Development*, *122*(5), 1395–1407.

Samakovlis, C., Manning, G., Steneberg, P., Hacohen, N., Cantera, R., & Krasnow, M. A. (1996). Genetic control of epithelial tube fusion during Drosophila tracheal development. *Development*, *122*(11), 3531–3536. https://doi.org/10.1242/dev.122.11.3531

Schnakenberg, S. L., Matias, W. R., & Siegal, M. L. (2011). Sperm-storage defects and live birth in drosophila females lacking spermathecal secretory cells. *PLoS Biology*, *9*(11). https://doi.org/10.1371/journal.pbio.1001192

Scholl, A., Ndoja, I., Dhakal, N., Morante, D., Ivan, A., Newman, D., Mossington, T., Clemans, C., Surapaneni, S., Powers, M., & Jiang, L. (2023). The Osiris family genes function as novel regulators of the tube maturation process in the Drosophila trachea. *PLOS Genetics*, *19*(1), e1010571-. https://doi.org/10.1371/journal.pgen.1010571

Schweisguth, F., & Posakony, J. W. (1992). Suppressor of Hairless, the Drosophila Homolog of the Mouse Recombination Signal-Binding Protein Gene, Controls Sensory Organ Cell Fates. In *Cell* (Vol. 69).

Sun, J., & Deng, W.-M. (2007). Hindsight Mediates the Role of Notch in Suppressing Hedgehog Signaling and Cell Proliferation. *Developmental Cell*, *12*(3), 431–442. https://doi.org/10.1016/j.devcel.2007.02.003

Sun, J., & Spradling, A. C. (2013). Ovulation in Drosophila is controlled by secretory cells of the female reproductive tract. *eLife*, *2013*(2). https://doi.org/10.7554/eLife.00415

Sutherland, D., Samakovlis, C., & Krasnow, M. A. (1996). *branchless* Encodes a Drosophila FGF Homolog That Controls Tracheal Cell Migration and the Pattern of Branching. *Cell*, *87*(6), 1091–1101. https://doi.org/10.1016/S0092-8674(00)81803-6

Takahashi, A., Takahashi, K., Ueda, R., & Takano-Shimizu, T. (2007). Natural variation of ebony gene controlling thoracic pigmentation in Drosophila melanogaster. *Genetics*, *177*(2), 1233–1237. https://doi.org/10.1534/genetics.107.075283

Tanaka, H., Takasu, E., Aigaki, T., Kato, K., Hayashi, S., & Nose, A. (2004). Formin3 is required for assembly of the F-actin structure that mediates tracheal fusion in Drosophila. *Developmental Biology*, *274*(2), 413–425. https://doi.org/10.1016/j.ydbio.2004.07.035

Tanaka-Matakatsu, M., Uemura, T., Oda, H., Takeichi, M., & Hayashi, S. (1996). Cadherin-mediated cell adhesion and cell motility in Drosophila trachea regulated by the transcription factor escargot. *Development*, *122*(12), 3697–3705.

Tepass, U., & Hartenstein, V. (1994). The Development of Cellular Junctions in the Drosophila Embryo. *Developmental Biology*, *161*(2), 563–596. https://doi.org/https://doi.org/10.1006/dbio.1994.1054

Terriente-Felix, A., Li, J., Collins, S., Mulligan, A., Reekie, I., Bernard, F., Krejci, A., & Bray, S. (2013). Notch cooperates with Lozenge/Runx to lock haemocytes into a differentiation programme. *Development*, *140*(4), 926–937. https://doi.org/10.1242/dev.086785

Thiagalingam, A., De Bustros, A., Borges, M., Jasti, R., Compton, D., Diamond, L., Mabry, M., Ball, D. W., Baylin, S. B., & Nelkin, B. D. (1996). RREB-1, a novel zinc finger protein, is involved in the differentiation response to Ras in human medullary thyroid carcinomas. *Molecular and Cellular Biology*, *16*(10), 5335–5345. https://doi.org/10.1128/MCB.16.10.5335

Thomas, C. M., & Kiehart, D. P. (1994). βHeavy-spectrin has a restricted tissue and subcellular distribution during Drosophila embryogenesis. *Development*, *120*(7), 2039–2050. https://doi.org/10.1242/dev.120.7.2039

Thomas, U., Speicher, S. A., & Knust, E. (1991). The Drosophila gene Serrate encodes an EGF-like transmembrane protein with a complex expression pattern in embryos and wing discs. *Development*, *111*(3), 749–761. https://doi.org/10.1242/dev.111.3.749

Tonning, A., Hemphälä, J., Tång, E., Nannmark, U., Samakovlis, C., & Uv, A. (2005). A transient luminal chitinous matrix is required to model epithelial tube diameter in the Drosophila trachea. *Developmental Cell*, *9*(3), 423–430. https://doi.org/10.1016/j.devcel.2005.07.012

Tsubota, T., Uchino, K., Suzuki, T. K., Tanaka, H., Kayukawa, T., Shinoda, T., & Sezutsu, H. (2014). Identification of a novel strong and ubiquitous promoter/enhancer in the silkworm Bombyx mori. *G3: Genes, Genomes, Genetics*, *4*(7), 1347–1357. https://doi.org/10.1534/g3.114.011643

Uemura, T., Oda, H., Kraut, R., Hayashi, S., Kotaoka, Y., & Takeichi, M. (1996). Zygotic Drosophila E-cadherin expression is required for processes of dynamic epithelial cell rearrangement in the Drosophila embryo. *Genes & development*, *10*(6), 659–671. https://doi.org/10.1101/gad.10.6.659

Whitten, J. M. (1957). The Post-embryonic Development of the Tracheal System in Drosophila melanogaster. Quarterly Journal of Microscopical Science, 98, 123–150. https://doi.org/10.5281/zenodo.10773035

Wilk, R., Pickup, A. T., Hamilton, J. K., Reed, B. H., & Lipshitz, H. D. (2004). Dose-sensitive autosomal modifiers identify candidate genes for tissue autonomous and tissue nonautonomous regulation by the Drosophila nuclear zinc-finger protein, hindsight. *Genetics*, *168*(1), 281–300. https://doi.org/10.1534/genetics.104.031344

Wilk, R., Reed, B. H., Tepass, U., & Lipshitz, H. D. (2000). The hindsight gene is required for epithelial maintenance and differentiation of the tracheal system in Drosophila. *Developmental Biology*, *219*(2), 183–196. https://doi.org/10.1006/dbio.2000.9619

Wilk, R., Weizman, I., & Shilo, B. Z. (1996). trachealess encodes a bHLH-PAS protein that is an inducer of tracheal cell fates in Drosophila. *Genes & development*, *10*(1), 93–102. https://doi.org/10.1101/gad.10.1.93

Wingen, A., Carrera, P., Ekaterini Psathaki, O., Voelzmann, A., Paululat, A., & Hoch, M. (2017). Debris buster is a Drosophila scavenger receptor essential for airway physiology. *Developmental Biology*, *430*(1), 52–68. https://doi.org/10.1016/j.ydbio.2017.08.018

Wingrove, J. A., & O'Farrell, P. H. (1999). Nitric oxide contributes to behavioral, cellular, and developmental responses to low oxygen in Drosophila. *Cell*, *98*(1), 105–114. https://doi.org/10.1016/S0092-8674(00)80610-8

Wolf, C., Gerlach, N., & Schuh, R. (2002). Drosophila tracheal system formation involves FGF-dependent cell extensions contacting bridge-cells. *EMBO Reports*, *3*(6), 563–568. https://doi.org/10.1093/embo-reports/kvf115

Wolf, C., & Schuh, R. (2000). Single mesodermal cells guide outgrowth of ectodermal tubular structures in Drosophila. *Genes and Development*, *14*(17), 2140–2145. https://doi.org/10.1101/gad.180900

Yang, S. A., & Deng, W. M. (2018). Serrate/notch signaling regulates the size of the progenitor cell pool in Drosophila imaginal rings. *Genetics*, *209*(3), 829–843. https://doi.org/10.1534/genetics.118.300963

Yip, M. L. R., Lamka, M. L., & Lipshitz, H. D. (1997). Control of germ-band retraction in Drosophila by the zinc-finger protein Hindsight. *Development*, *124*(11), 2129–2141.

Yu, Z., Chen, H., Liu, J., Zhang, H., Yan, Y., Zhu, N., Guo, Y., Yang, B., Chang, Y., Dai, F., Li, C., & Jiao, R. (2014). Various applications of TALEN- and CRISPR/Cas9-mediated homologous recombination to modify the Drosophila genome. *Biology Open*, *3*(4), 271–280. https://doi.org/10.1242/bio.20147682

Zacharioudaki, E., & Bray, S. J. (2014). Tools and methods for studying Notch signaling in Drosophila melanogaster. *Methods*, *68*(1), 173–182. https://doi.org/10.1016/j.ymeth.2014.03.029

Zhang, L., & Ward IV, R. E. (2009). uninflatable encodes a novel ectodermal apical surface protein required for tracheal inflation in Drosophila. *Developmental Biology*, *336*(2), 201–212. https://doi.org/10.1016/j.ydbio.2009.09.040

Zhang, S., Qian, X., Redman, C., Bliskovski, V., Ramsay, E. S., Lowy, D. R., & Mock, B. A. (2003). $p16^{INK4a}$ gene promoter variation and differential binding of a repressor, the ras-responsive zinc-finger transcription factor, RREB. *Oncogene*, *22*(15), 2285–2295. https://doi.org/10.1038/sj.onc.1206257

Zhou, F., Qiang, K. M., & Beckingham, K. M. (2016). Failure to burrow and tunnel reveals roles for jim lovell in the growth and endoreplication of the drosophila larval tracheae. *PLoS ONE*, *11*(8). https://doi.org/10.1371/journal.pone.0160233

Zinzen, R. P., Girardot, C., Gagneur, J., Braun, M., & Furlong, E. E. M. (2009). Combinatorial binding predicts spatio-temporal cis-regulatory activity. *Nature*, *462*(7269), 65–70. https://doi.org/10.1038/nature08531

Zou, J., Milon, B. C., Desouki, M. M., Costello, L. C., & Franklin, R. B. (2011). HZIP1 zinc transporter down-regulation in prostate cancer involves the overexpression of ras responsive element binding protein-1 (RREB-1). *Prostate*, *71*(14), 1518–1524. https://doi.org/10.1002/pros.21368

Appendices

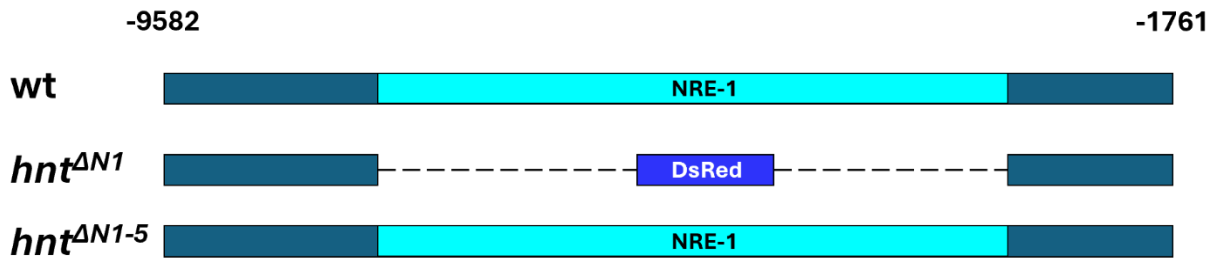


Figure A1 Long-range PCR sequence confirmation. Schematic representing example long-range PCR analyses used to confirm mutant sequences. Control wildtype sequence contains the designated ~5 kb NRE-1 sequence (cyan). *hnt*$^{\Delta N1}$ sequence showed complete excision of NRE-1 sequence and insertion of the DsRed gene cassette (blue). *hnt*$^{\Delta N1-5}$ sequence matches the wildtype sequence.

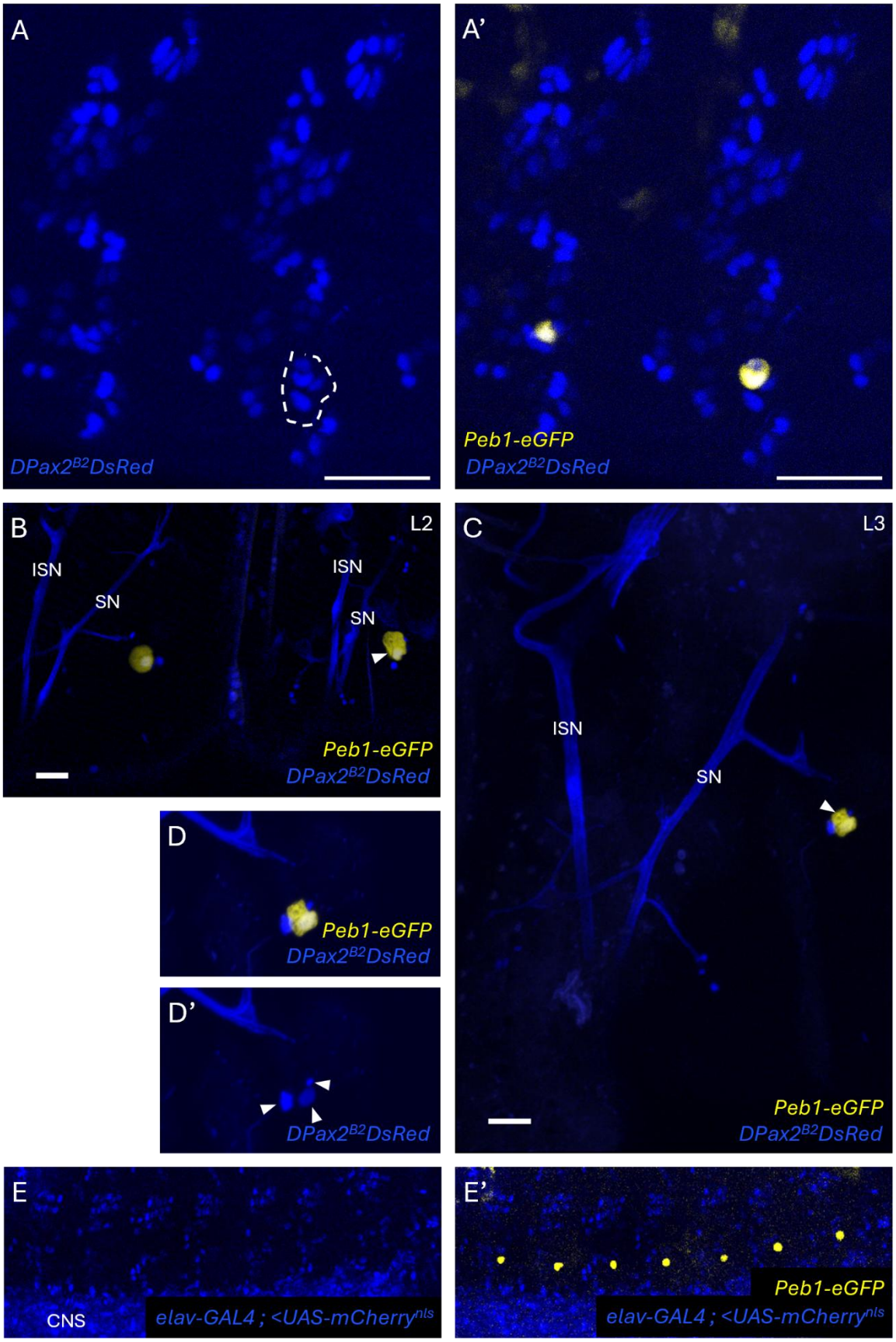

A
DPax2B2DsRed
A'
Peb1-eGFP
DPax2B2DsRed
B
L2
ISN
SN
ISN
SN
Peb1-eGFP
DPax2B2DsRed
C
L3
ISN
SN
Peb1-eGFP
DPax2B2DsRed
D
Peb1-eGFP
DPax2B2DsRed
D'
DPax2B2DsRed
E
CNS
elav-GAL4 ; <UAS-mCherrynls
E'
Peb1-eGFP
elav-GAL4 ; <UAS-mCherrynls

Figure A2 PNS cell with high expression of hindsight co-expresses with DPax2 during development. (A-A') Live imaging lateral view projection of two abdominal embryonic segments. *DPax2* reporter is expressed in shaft, sheath, and socket cells of extrasensory organ neuron clusters. The cell cluster in which *Peb1* hindsight reporter expresses strongly is outlined. (B) Single step image showing lateral view of two of the *Peb1* reporter PNS cells (arrowhead) positioned near the anterior segmental nerve (SN) and intersegmental nerve (ISN) in a second instar larva. (C) Live imaging lateral view projection of a single L3 larva abdominal segment. The PNS cell (arrowhead) is adjacent to the axon branch connected to the v' region of the PNS. (D-D') Magnified image of the PNS cell in (C), showing the PNS cell is one of three closely associated DPax2 cells (arrowhead). (E-E') Live imaging lateral view projection of ventral PNS and central nervous system (CNS). *Peb1* reporter PNS cell does not co-localize with neuronal nuclei expressing mCherry. All scale bars represent 20 μm.

Given that the taenidial fold disruptions observed in $hnt^{\Delta N4}$ embryonic trachea were commonly observed around fusion cells and given that *hnt* and *rreb-1* expression have been implicated in cell adhesion defects, I presumed that the taenidial fold phenotypes could be related to defects in cell adhesion (Melani et al., 2008; Morgani et al., 2021). Previous studies have shown that *hnt* plays a role in cell adhesion in the Drosophila follicle cells and attenuates the expression of cell adhesion proteins such as Armadillo and DE-cadherin (Melani et al., 2008). In tracheal fusion events, DE-cadherin, or *shotgun* (*shg*), is required, regulated by *esg*, and localizes to apical adherens junctions in fusion cells (Tanaka-Matakatsu et al., 1996). Therefore, I investigated the localization of *shg* in the developing trachea to assess if *hnt* could be associated with cell adhesion in this context.

I decided to observe the localization of *shg* in the developing trachea using a *shg-GFP* fusion protein that is expressed under endogenous regulatory control, in tandem with the *Peb1-mCherry* reporter construct to visualize the localization of *shg* relative to other *hnt* tracheal compartments. Observation of larvae revealed that *shg-GFP* fusion protein accumulated at the adherens junctions, outlining the tracheal cells in both the DT and TC (Fig. A3). *shg-GFP* also accumulates in high concentrations at the fusion cells (cyan arrowheads) of the DT, and in a ventral compartment of the TC branch (asterisk, Fig. A3). Interestingly, I have also observed Armadillo-GFP (*armGFParm*) fusion proteins accumulate in the same pattern, at the ventral adherens junction of the TCJ cell (data not shown). *Peb1-mCherry* reporter expression showed that the TCJ cell (white arrowhead) is localized between, and in contact with, the DT fusion cells and the ventral compartment of *shg*. The positioning of the TCJ cell between two points of concentrated E-cadherin is interesting, as it is a site of robust *hnt* expression (this work), shown to be a point of Notch

activity (this work; Furriols & Bray, 2001; Rao et al., 2015) and it is uniquely one of 1-2 TC cells that form autocellular adherens junctions (Ribeiro et al., 2004). As such, these observations could suggest another role of *hnt* in the tracheal TCJ cells related to cell adhesion.

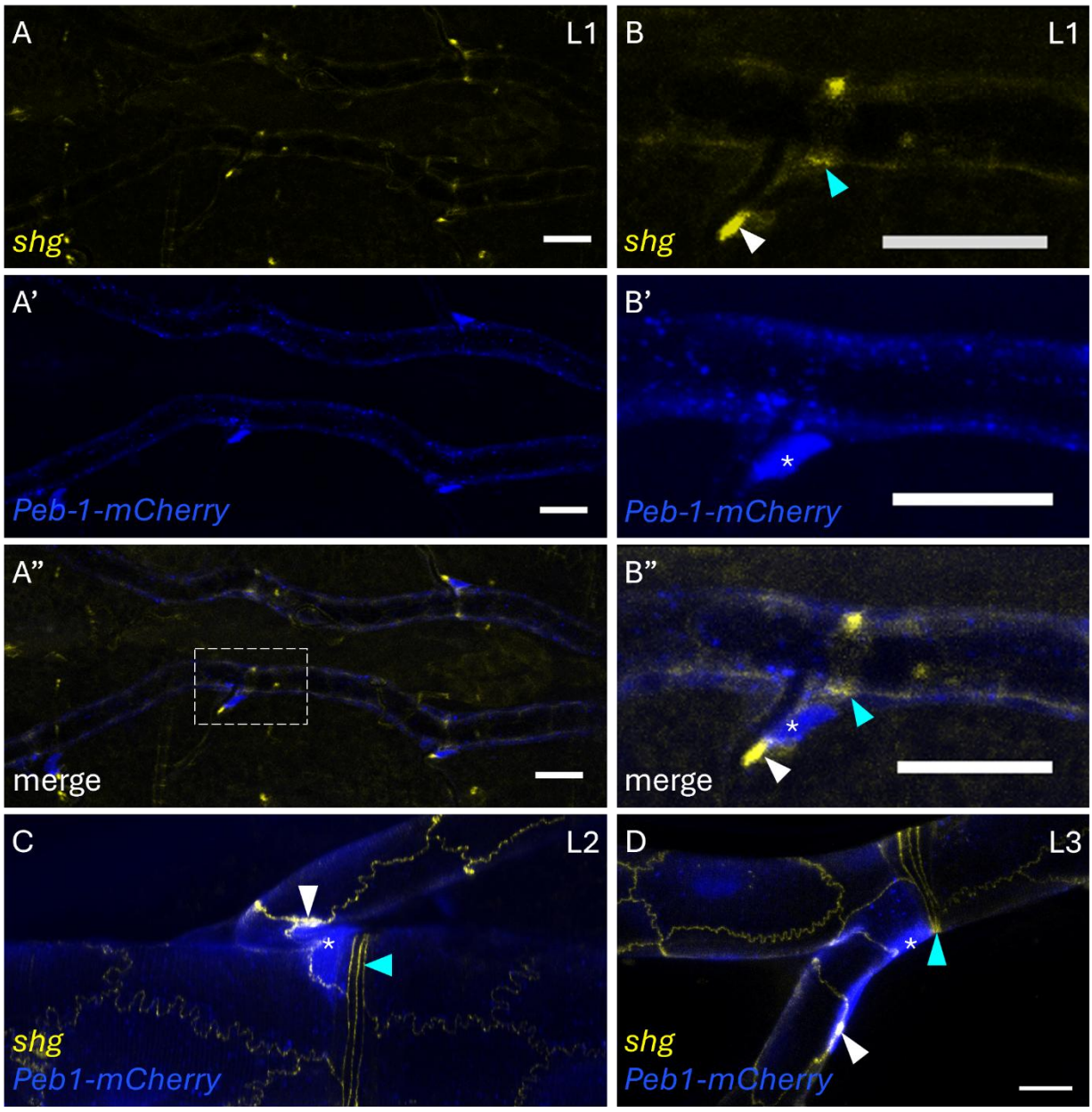

A
L1
shg
B
L1
shg
A'
Peb-1-mCherry
B'
Peb-1-mCherry
A"
merge
B"
merge
C
L2
shg
Peb1-mCherry
D
L3
shg
Peb1-mCherry

Figure A3 *Shg-GFP* localizes in compartments adjacent to TCJ cells. (A-B") Live imaging projections of DTs in first instar larvae expressing both *Shg-GFP* fusion proteins expressed under endogenous regulatory control and *Peb1-mCherry* reporter construct. (A-A") Both *Shg-GFP* fusion protein and *Peb1-mCherry* reporter expression was observed throughout the DT. (B-B") Magnified inset of (A") showing *shg-GFP* fusion protein and *Peb1-mCherry* reporter expression at a single DT/TC junction. (B) *Shg-GFP* fusion proteins localize to adherens junctions of tracheal cells and in high concentrations in fusion cells (cyan arrowhead) and ventrally (white arrowhead) to the TCJ cell. (B') *Peb1-mCherry* reporter is expressed in the tracheal cells and in the TCJ cell (asterisk). (B") Merged image showing the TCJ cell (asterisk) is contact with both the fusion cells (cyan arrowhead) and the ventral accumulation of *shg-GFP* (white arrowhead). (C-D) This notable localization pattern is observed in L2(C) and L3(D) larval stages as well. All scale bars represent 20 μm.

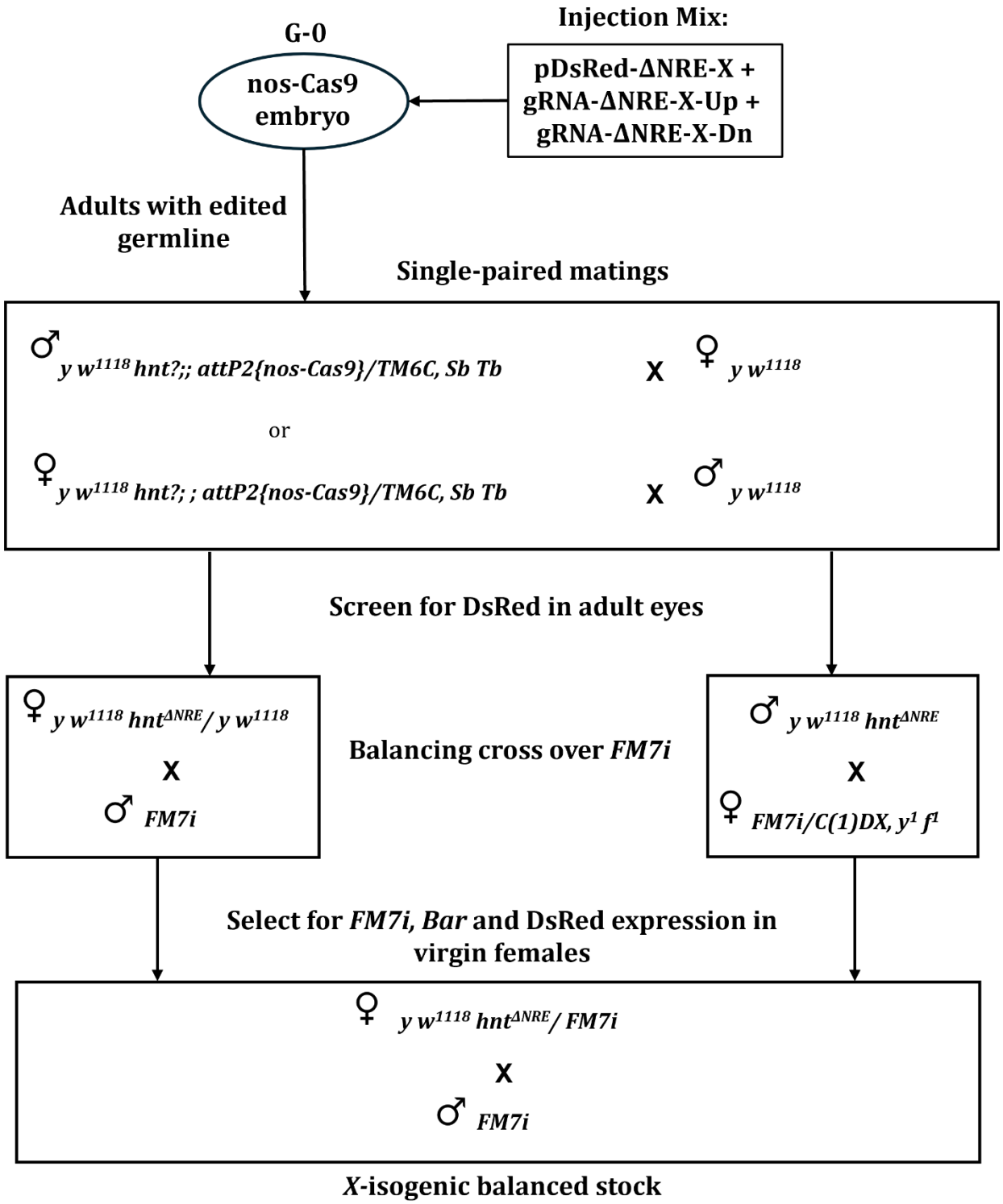

G-0
nos-Cas9 embryo
Injection Mix:
pDsRed-ΔNRE-X + gRNA-ΔNRE-X-Up + gRNA-ΔNRE-X-Dn
Adults with edited germline
Single-paired matings
♂ y w1118 hnt?;; attP2{nos-Cas9}/TM6C, Sb Tb
X
♀ y w1118
or
♀ y w1118 hnt?; ; attP2{nos-Cas9}/TM6C, Sb Tb
X
♂ y w1118
Screen for DsRed in adult eyes
♀ y w1118 hntΔNRE/ y w1118
X
♂ FM7i
Balancing cross over FM7i
♂ y w1118 hntΔNRE
X
♀ FM7i/C(1)DX, y1 f1
Select for FM7i, Bar and DsRed expression in virgin females
♀ y w1118 hntΔNRE/ FM7i
X
♂ FM7i
X-isogenic balanced stock

Figure A4 Crossing scheme for screening *hnt*$^{\Delta NRE}$ mutants generated by CRISPR/Cas9 genome editing. *nos-Cas9* embryos were injected with a mix of two gRNA expression vectors that target sites both upstream and downstream of an NRE Su(H) consensus sequence, and a complementary pDsRed-ΔNRE HDR donor vector. Injected virgin females and males were crossed to a *y w* background. Progeny were scored for DsRed expression in the adult eye and crossed to *FM7i* balancers. *FM7i* balanced virgin females that expressed DsRed were then backcrossed to *FM7i* males to generate *X*-isogenic balanced stocks that carry a potential ΔNRE deletion which were further evaluated using PCR analysis.

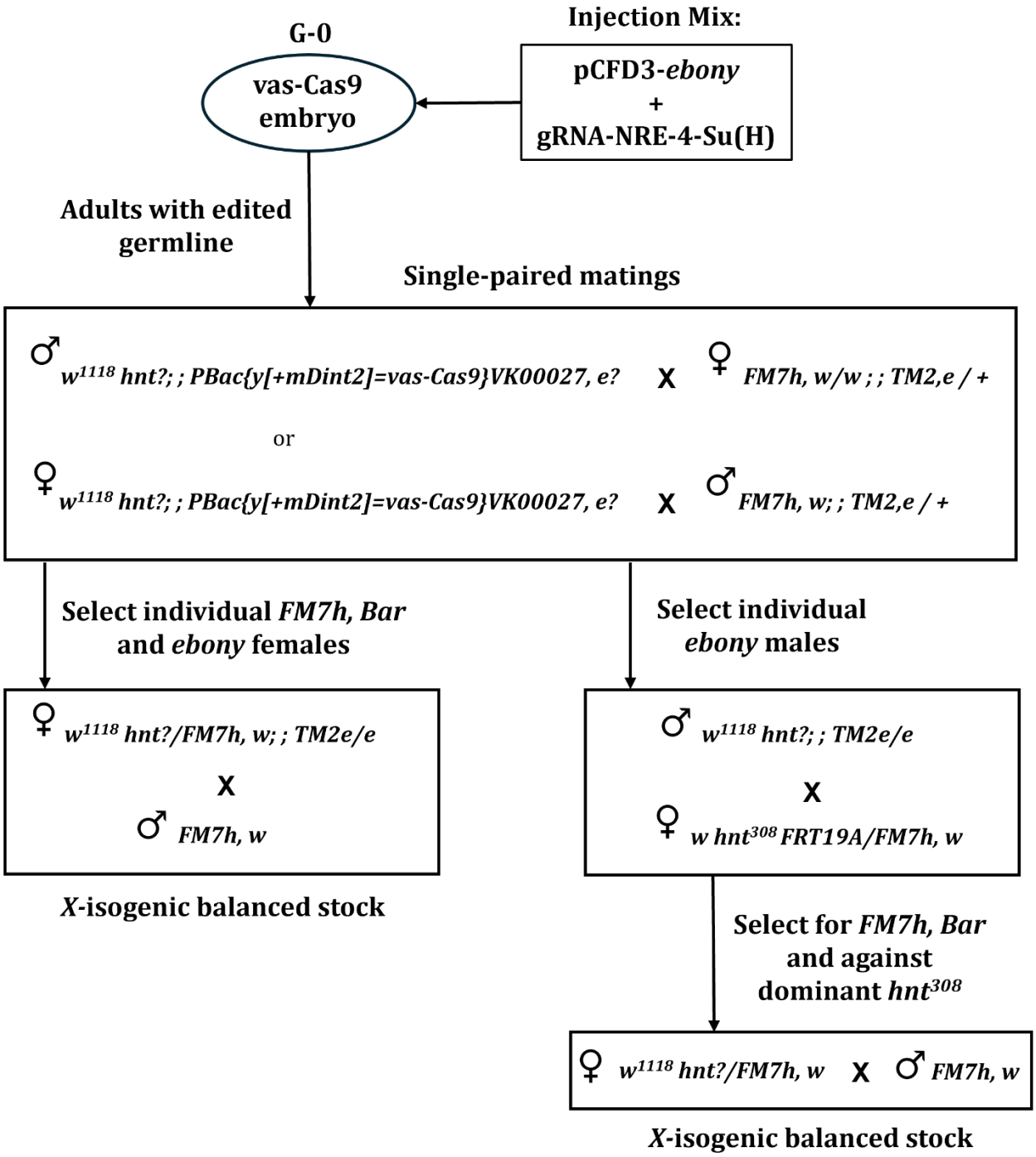

G-0
vas-Cas9 embryo
Injection Mix:
pCFD3-ebony + gRNA-NRE-4-Su(H)
Adults with edited germline
Single-paired matings
♂ w1118 hnt?; ; PBac{y[+mDint2]=vas-Cas9}VK00027, e? X ♀ FM7h, w/w ; ; TM2,e / +
or
♀ w1118 hnt?; ; PBac{y[+mDint2]=vas-Cas9}VK00027, e? X ♂ FM7h, w; ; TM2,e / +
Select individual FM7h, Bar and ebony females
Select individual ebony males
♀ w1118 hnt?/FM7h, w; ; TM2e/e
X
♂ FM7h, w
X-isogenic balanced stock
♂ w1118 hnt?; ; TM2e/e
X
♀ w hnt308 FRT19A/FM7h, w
Select for FM7h, Bar and against dominant hnt308
♀ w1118 hnt?/FM7h, w X ♂ FM7h, w
X-isogenic balanced stock

Figure A5 Crossing scheme for screening homozygous *ebony* and NRE-4 Su(H) mutants generated with co-CRISPR injections. Crossing scheme used to generate balanced *X*-isogenic lines following co-CRISPR injection into *vas-Cas9* embryos. *vas-Cas9* embryos were injected with a mix of *ebony* targeting gRNA expression vector, pCFD3-*ebony*, and gRNA-NRE-4-Su(H) expression vector. Injected virgin females and males were crossed to the *FM7h, Bar;; TM2e/+* double balancer lines. "Jackpot" progeny that likely harbor a mutation event at the NRE-4 Su(H) consensus sequence were identified by homozygous *ebony* body color in males and both *ebony* body color + *FM7h, Bar* in females. These "jackpot" progeny were crossed to *FM7h* balancer stocks to generate *X*-isogenic balanced stocks that potentially carry an NRE-4-Su(H) mutation and further evaluated using PCR analysis.

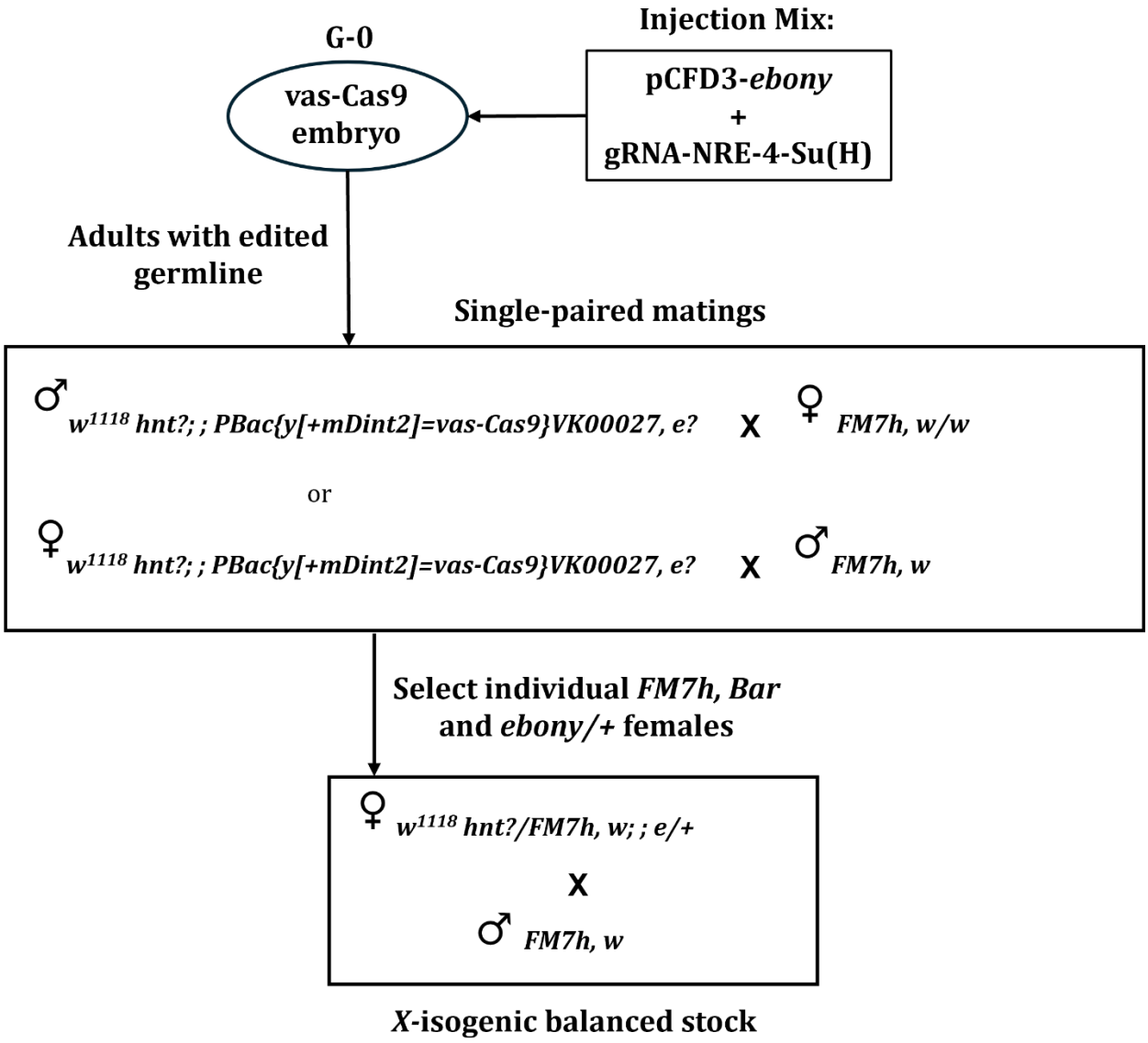

G-0
vas-Cas9 embryo
Injection Mix:
pCFD3-ebony + gRNA-NRE-4-Su(H)
Adults with edited germline
Single-paired matings
♂ w1118 hnt?; ; PBac{y[+mDint2]=vas-Cas9}VK00027, e? X ♀ FM7h, w/w
or
♀ w1118 hnt?; ; PBac{y[+mDint2]=vas-Cas9}VK00027, e? X ♂ FM7h, w
Select individual FM7h, Bar and ebony/+ females
♀ w1118 hnt?/FM7h, w; ; e/+
X
♂ FM7h, w
X-isogenic balanced stock

Figure A6 Crossing scheme for screening heterozygous *ebony* and NRE-4 Su(H) mutations generated with co-CRISPR injections. *vas-Cas9* embryos were injected with a mix of *ebony* targeting gRNA expression vector, pCFD3-*ebony*, and gRNA-NRE-4-Su(H) expression vector. Injected virgin females and males were crossed to a *FM7h, Bar* balancer. Virgin female progeny that likely harbor a mutation event at the NRE-4 Su(H) consensus sequence were identified by the semi-dominant darkened trident phenotype that manifests in (e^{+}/e) heterozygotes. These selected virgin females were crossed to *FM7h* balancer stocks to generate *X*-isogenic balanced stocks that potentially carry an NRE-4-Su(H) mutation and further evaluated using PCR analysis.